Collisions of slow electrons with molecules

Mgr. Michal Tarana
Institute of Theoretical Physics

Institute of Theoretical Physics
Faculty of Mathematics and Physics
Charles University Prague

Ph.D. thesis supervisor: Prof. RNDr. Jiří Horáček, DrSc.

Results of this work are contained in:

- M. Tarana, and J. Horáček. *Correlation effects in R-matrix calculations of electron-F_2 elastic scattering cross sections*, J. Chem. Phys. **127**, 154319 (2007).
- M. Tarana, and J. Tennyson. *Polarisation effects in electron collisions with Li_2: Application of the molecular R-matrix method with pseudostates*, J. Phys. B: At. Mol. Opt. Phys. **41**, 205204 (2008).
- M. Tarana, B.M. Nestmann, and J. Horáček. *R-matrix calculations of the elastic electron scattering off the Li_2 molecule*, Phys. Rev. A., **79**, 012716 (2009)
- M. Tarana, P. Wielgus, S. Roszak, and I.I. Fabrikant. *Effects of two vibrational modes in the dissociative electron attachment to CF_3Cl*, Phys. Rev. A., **79**, 052712 (2009).

Declaration

This dissertation is the result of my own work, except where explicit reference is made to the work of others, and has not been submitted for another qualification to this or any other university.

Mgr. Michal Tarana

Acknowledgements

Of the many people who deserve thanks, some are particularly prominent. I would like to express my gratitude to Jiří Horáček his supervision of my studies, for his personal support and time spent with inspirational discussions.

I would like to thank Bernd M. Nestmann for his invaluable guidance during my exploration of the subject of the scattering theory and R-matrix methods. I was very pleased by his hospitality during my stay in Bonn.

I wish to acknowledge Jonathan Tennyson for the time spent in discussions with me and for his guidance during my work on the MRMPS calculations during my stay at UCL in London as well as for other inspirational suggestions.

I want to thank Ilya Fabrikant and his family for their hospitality during my stay in Lincoln, USA. Ilya Fabrikant spent a lot of time with me and I am very thankful for his supervision of my research in field of the nuclear dynamics of the non elastic electron-molecule collisions.

I want to express my gratitude to the members of the group dealing with quantum mechanics at the Institute of Theoretical Physics at the Charles University. Přemysl Kolorenč, Karel Houfek and Martin Čížek helped me to understand many physical and technical aspects of the electron-molecule scattering, stimulated my research and granted me substantial personal support.

Contents

Chapter 1

Introduction

In this chapter we introduce the topic of this thesis – collisions of the slow electrons with molecules. We will show the physical processes of interest and mention some methods enabling their theoretical treatment. We will restrict our considerations to the resonant processes. Finally, the main objectives of the thesis will be outlined.

Main subject of this work is the investigation of the low-energy resonant processes occurring in electron-molecule collisions, namely vibrational excitation (VE) of the molecule by electron impact and dissociative electron attachment (DEA) to the molecule. We will restrict our considerations of the DEA to such processes, where at least the anionic fragment is a single atom which does not have any vibrational degrees of freedom. General scheme for such process is

$$\mathrm{e}^- + AB(\nu) \rightarrow (AB)^- \rightarrow \begin{array}{ll} & \mathrm{e}^- + AB(\nu') \\ \text{or} & A(\nu'') + B^- \end{array} ,$$

where $AB(\nu)$ is the target neutral molecule in its initial vibrational state described by set of quantum numbers ν, $A(\nu'')$ is the final neutral fragment of DEA in the vibrational state described by set of quantum numbers ν'' and B^- substitutes the corresponding final anionic atomic fragment, ν' denotes the set of quantum numbers describing the final vibrational state of the molecule after the VE by electron impact. Formation of the metastable anionic complex AB^- is responsible for the resonant nature of these processes.

The above scheme contains a broad variety of processes of great practical interest.

Such collisional reactions are often encountered in plasma physics both in laboratory and nature including physics of ionosphere, stellar atmospheres and nebulae in the outer space. The cross sections determine the equilibrium densities of electrons, ions, atoms and molecules in such environments. Dissociative attachment processes may serve as sources for negative ion beams used for loading of thermonuclear devices or for electromagnetic propulsion of space vehicles. DEA is found to be of importance in the chemistry of flames and play important role in gas lasers (see [1] and references therein). In addition, the reactions are of considerable interest as destruction mechanism of halogen ions of anthropogenic origin in the ionosphere. More about applications of DEA to molecules including radiocarbon dating and very sensitive detection of explosives or drugs can be found in the review paper [2].

Cross sections of the resonant processes often exhibit pronounced features interesting from the theoretical point of view. For some molecules, the cross sections for VE attain high values in a very vicinity of the threshold. Such a phenomenon is called threshold peak and was observed for the first time by Rohr and Linder [3]. The cross sections for DEA and VE are not smooth functions of the collision energy and abrupt changes of a slope called Wigner cusps are often encountered near opening of a new channel in the reaction. In spite of almost three decades of theoretical study these phenomena are still not fully comprehended. The most successful approach which describes qualitatively well all the observed features, is the nonlocal resonance model (NRM) reviewed by Domcke [4].

As we are dealing with resonant vibrationally non-elastic electron-molecule collisions throughout this work, it is worth to mention that in these processes the electron motion is strongly coupled with the nuclear motion and the Born – Oppenheimer approximation is not valid. In other words, the incoming electron is captured into the metastable electronic-resonance state. The electronic cloud in this temporal anionic complex allows the nuclear motion leading to VE or DEA.

The usual theoretical treatment of the resonant processes like VE or DEA consists of two parts:

- **The fixed-nuclei scattering calculation** performed for a set of nuclear geometries relevant for the process in question. It enables us to obtain properties of the electronic resonance which can be used in the subsequent nuclear dynamics calculation. It can directly give the diabatic potential energy surfaces for geometries where the temporal negative ion is not bound and these can be used in the local

complex potential (LCP) calculation. Alternatively, the fixed-nuclei results can be used to fit the NRM [4].

- **The calculation of the nuclear dynamics** using either the NRM or the LCP approximation [4–6] which allow for calculation of the VE and DEA cross sections from the data extracted from the fixed-nuclei calculations. Although the NRM represents a more exact approach to the nuclear dynamics of VE and DEA than the LCP approximation (it can describe the Wigner cusps and other non-local phenomena), it is very difficult to implement it even for diatomic molecules [7]. It has not been implemented successfully for any larger molecule than diatomic so far. We will not deal with NRM itself in the present work, although in Section 2.1 we test a method designed to obtain the data necessary for construction of the NRM from the fixed-nuclei scattering calculations. On the other hand, the LCP approximation represents a simpler approach which has several restrictions. It treats the nuclear dynamics as the motion of the nuclei on the LCP surface. This is used to calculate the nuclear scattering wave function and cross sections of VE and DEA. The imaginary part of the LCP surface represents the probability of the autodetachment of the electron in the region of nuclear geometries where the anion is not bound.

This work is dealing with both types of calculations mentioned above. Each of them has its own complications and bottlenecks. We present the fixed-nuclei R-matrix calculations of the electron collisions with molecules F_2 and Li_2 which represent a challenge for the method used. In the next chapter, this work is dealing with the LCP calculations of the DEA and VE of the molecule CF_3Cl with emphasis on the effects of two vibrational modes in these processes.

Chapter 2

Scattering calculations in the fixed-nuclei approximation

The development of *ab initio* quantum chemical methods in recent decades stimulated the progress in development of fixed-nuclei electron-molecule scattering methods. Therefore, nowadays there is variety of approaches available, the most successful include the R-matrix theory [8, 9], complex Kohn variational principle [10] and Schwinger variational method [11, 12]. In this chapter we are dealing with the R-matrix theory and its application to electron scattering off small molecules in the fixed-nuclei approximation with emphasis on the correlation and polarization effects.

2.1 Correlation treatment

The R-matrix method is based on dividing coordinate space into two regions using a spherical boundary centred on the center-of-mass of the target molecule [8, 13]. The radius of the boundary, a, is chosen so that the inner region Ω contains all the electronic charge cloud of the target molecular states included in the calculation. The accuracy of this method is strongly dependent on the representation of the problem in the inner region where it is necessary to consider all short-range interactions between the N target electrons and the scattering one. As the correlation and exchange interaction between the scattered and target electrons can be neglected in the outer region, the projectile is considered to move in a local potential obtained from the multipole moments of the target outside the sphere.

In standard R-matrix calculations, the eigenfunctions Ψ_k of the $(N+1)$-electron Hamiltonian restricted to the inner region H_Ω [14] are given by the following close-coupling (CC) expansion [13, 14]:

$$\Psi_k(\boldsymbol{x}_1, \ldots, \boldsymbol{x}_{N+1}) = \sum_i c_{ik} A \left[\Phi_i(\boldsymbol{x}_1, \ldots, \boldsymbol{x}_N) f_{ik}(\boldsymbol{x}_{N+1})\right] + \sum_i b_{ik} \chi_i(\boldsymbol{x}_1, \ldots, \boldsymbol{x}_{N+1}). \tag{2.1}$$

The index k specifies the eigenstate of the inner Hamiltonian. Φ_i is the wave function of the ith target state given as a linear combination of configuration state functions (CSFs). $\boldsymbol{x}_n$ are the spatial and spin coordinates of nth electron, $f_{ik}(\boldsymbol{x}_{N+1})$ describe the wave function of the scattered electron, A is the antisymmetrization operator. c_{ik} and b_{ik} are the variational coefficients and χ_i are L^2 functions constructed from the molecular orbitals (MOs).

In order to calculate the R-matrix it is necessary to calculate the $(N+1)$-electron eigenfunctions Ψ_k as well as the target N-electron wave functions Φ_i. Treatment of the correlation in these calculations is one of the major complications in the present implementations of the molecular R-matrix method. In all the scattering calculations based on the CC expansion it is important to keep the correlation balanced between the target states Φ_i and the $(N+1)$-electron wave function expansion. The first work presented in this chapter as well as the recent work by Cooper et al. [15], actually on positron scattering using a Kohn variational method, emphasize the pitfalls of an unbalanced treatment. An unbalanced calculations will give unpredictable results with, for example, resonances potentially becoming bound, or weakly bound states appearing in the calculation as resonances. "Improving" the R-matrix pole energies in a variational sense which means lowering them will cause any resonance feature associated with a particular pole to also move to lower energy and potentially become bound. Conversely improving the target representation will cause the energy of the target (with respect to which the R-matrix poles are taken) to be lowered and hence the pole positions to effectively rise with converse effect associated properties. If the aim of a calculation is to compute resonance or bound state energies, then reliable results will only be obtained if the target and scattering calculations are performed at a similar level of approximation.

At present, two independent implementations of the molecular R-matrix method are widely used. The way how each of them deals with the electron correlation, is the principal difference between them:

- In the **UK *R*-matrix Codes** [16] the hand specification of the configurations is used. The configurations used in the calculation of electronic target states Φ_i and in the calculation of Ψ_k are used so that they are explicitly consistent with each other. The favored approach for doing this is to use a complete active space configuration interaction (CAS-CI) method [17]. This approach is size consistent, however the number of active electrons as well as the size of the active space, are limited. The reason is that every configuration added to the target states calculation requires addition of corresponding configurations to the $(N+1)$-electron calculation. This number increases rapidly with number of continuum orbitals (COs) used. Therefore, the extension of the active space beyond the valence orbitals dramatically complicates the computational tractability of this approach. On the other hand, in most cases the correlation of valence electrons plays more important role in the electron scattering and the employment of the CAS-CI method was proved reasonable and sufficient by many successful applications. In addition, construction of the $(N+1)$-electron Hamiltonian H_Ω is not independent of the target eigenstates, what makes the construction more efficient. Taking into account the CC-expansion structure of Ψ_k (see equation (2.1)), the matrix elements are constructed more efficiently using the neutral target eigenstates Φ_i calculated previously [18].

- The **Bonn *R*-matrix Codes** [14] are based on the single and double multireference configuration method (SD-MRCI) [17, 19–21]. This suite uses the SD-MRCI program DIESEL due to Hanrath and Engels [22]. The SD-MRCI is a well used quantum chemistry procedure for target electronic structure calculations which considers single and double excitations from a multireference state of the target. A particular feature of Buenker and Peyerimhoff's approach is the use truncation of the configuration space at some threshold. Balance mentioned above is obtained in the Bonn codes by using this procedure with the same threshold parameters simultaneously for both the target and scattering wave function, see [14] and the work presented here for more details. It should be noted that this procedure allows for the inclusion of a high level of correlation in the target wave functions Φ_i, although it definitely runs the risk of over-correlation.

The issue of how to further improve the representation of target and scattering wave functions in a balanced fashion remains one of active research. One approach which appears particularly promising, albeit computationally expensive, is the use of pseudostates. This approach is discussed in the next section.

The problem of electron correlation effects in the fixed-nuclei calculations is addressed in the article included in this section. We compare several standard and widely used scattering models (static exchange, static exchange with polarization and CC model), where we study the correlation effects on the position and width of the electronic resonance in the F_2 molecule. It is well known that the DEA and VE cross sections for F_2 strongly depend on the correlation included in the fixed-nuclei calculation [23]. The reason is that the geometry at which the negative ion becomes stable against autodetachment is very close to the equilibrium internuclear separation [23, 24]. Particularly, using the SE model and CC CI model, the resonance appears at the equilibrium internuclear separation of the target, while in the SEP approximation this resonance turns into bound state at the same geometry.

All the calculations were performed using the Bonn codes as it is difficult to treat the electron correlation in F_2 using CAS CI only. Another aim of the work presented here was to test the CC CI approach introduced in the Bonn codes and to compare our results with previously published calculations of the electron collisions wit F_2. In addition, we wanted to calculate all the input data required for construction of the NRM and subsequent calculation of DEA and VE using the CC CI model of the electron correlation. To this end we used the Feshbach-Fano R-matrix (FFR) method due to Nestmann [25] and constructed the discrete state corresponding to the electronic resonance and corresponding coupling with the continuum background. This separation allowed for explicit calculation of the resonance and background eigenphases and elastic scattering cross sections.

THE JOURNAL OF CHEMICAL PHYSICS **127**, 154319 (2007)

Correlation effects in *R*-matrix calculations of electron-F_2 elastic scattering cross sections

Michal Tarana[a)] and Jiří Horáček
Institute of Theoretical Physics, Charles University in Prague, V Holešovičkách 2, CZ-180 00 Prague, Czech Republic

(Received 12 July 2007; accepted 30 August 2007; published online 19 October 2007)

Correlation effects are studied in electron scattering off the fluorine molecule. Fixed-nuclei approximation *R*-matrix calculations of the elastic collision cross sections are presented for a set of internuclear distances at three levels of correlation. The aim of this work is to study the role of electronic correlation on the properties of the $^2\Sigma_u$ resonance. The Feshbach-Fano *R*-matrix method of resonance-background separation is used to study the effect of inclusion of various levels of correlation on the energy and width of the $^2\Sigma_u$ resonance. Data required for construction of the nonlocal resonance model (construction of a discrete state and its coupling to the continuum) which allows the calculation of inelastic processes such as dissociative electron attachment and vibrational excitation [W. Domcke, Phys. Rep. **208**, 97 (1991)] including the correlation are presented. © *2007 American Institute of Physics*. [DOI: 10.1063/1.2789430]

I. INTRODUCTION

Understanding of the electron-molecule collisions is important for determining the energy balance and transport properties of electrons in low-temperature gases and plasmas under variety of conditions. Important applications of these processes include thermonuclear fusion, astrophysics, physics of upper atmosphere layers of planets as well as technological applications connected with laser physics or surface physics. In this context it is desirable to study electron scattering off the fluorine molecule. It plays an important role in the determination of properties of the electron-beam energized fluoride excimer lasers as well as in other applications.[1]

Significant progress has been made in development of quantum scattering theory methods for resonant electron-molecule collisions based on *ab initio* methods of quantum chemistry. Recently, particular attention was paid to application of the Feshbach-Fano projection formalism,[2] the complex absorbing potential (CAP) method,[3,4] complex rotation method[5] as well as to the *R*-matrix theory[6] and several others. All of them have been successfully applied to electron scattering off polyatomic molecules. In particular, method for combining the Feshbach-Fano formalism with the *R*-matrix method (called Feshbach-Fano *R*-matrix) has been developed and successfully applied to the separation of resonances in the potential scattering[7] as well as in the electron-molecule collisions.[8–10] This method enables the extraction of the discrete state and its coupling to the background continuum on the basis of the standard *R*-matrix calculations. From these quantities it is possible to construct the nonlocal resonance model (NRM) used to study the processes connected with the nuclear dynamics such as dissociative electron attachment (DEA), associative electron detachment, and vibrational excitation (VE).[11,12]

The electron scattering off fluorine molecule has been investigated theoretically several times. The first *ab initio* calculation of DEA and VE has been carried out by Hazi *et al.*[13] using the method developed by O' Malley.[14] In this calculation the correlation has been included on the level of configuration interaction (CI) expansion consisting of very restricted number of configurations. Moreover, this calculation did not give the relative position of the potential curve of the neutral target and negative ion. Subsequent *R*-matrix study of elastic electron collision with the F_2 molecule by Morgan and Noble[15] has included the correlation on the level of the static exchange with polarization (SEP). This study found that the ionic state is stable against autodetachment at the equilibrium internuclear separation of the neutral molecule. Another calculation of the potential energy curve of the $X^2\Sigma_u^+$ resonance by Ingr *et al.*[14] made use of the CAP/CI method. This calculation treats the correlation by the multireference CI (MRCI) method. The crossing point of the neutral target potential curve with the resonance state potential curve is determined by the extrapolation of the resonance width to zero. This calculation does not provide the energy-dependent width function as required for NRM. Brems *et al.*[11] studied the DEA and VE of the F_2 molecule using the *R*-matrix method with Feshbach-Fano *R*-matrix (FFR) separation of the discrete state. This discrete state and its coupling with the background continuum have been used to construct the NRM and to study the nuclear dynamics processes. The *R*-matrix calculation has been provided using the code of Nestmann *et al.*[6] at the SEP level of correlation. This calculation indicates that the position of the crossing point of the ionic and neutral potential curves, which is strongly influenced by the correlation included in the fixed-nuclei calculation, is of particular importance in the nuclear dynamics calculation.

The implementation of the *R*-matrix method by Nestmann *et al.* enables the static exchange (SE) and SEP ap-

[a)]Electronic mail: tarana@mbox.troja.mff.cuni.cz

proach to the correlation. Recently this code has been extended in order to allow single and double excitations multireference CI (Ref. 17) (SD-MRCI) treatment of the correlation. This enables us to compare the scattering calculations on different levels of correlation and to study correlation effects in the subsequent FFR separation. The main aim of this work is to test the SD-MRCI approach in the electron scattering off the fluorine molecule studied previously on the SEP level and to study the correlation effects in the FFR separation.

This paper is organized as follows: The R-matrix theory is briefly reviewed in Sec. II A and different models of correlation included are discussed in Sec. II B. The FFR formalism is briefly summarized in Sec. II C. Technical details of the calculations are explained in Sec. III, and results obtained on different levels of correlation are discussed in Sec. IV.

II. THEORY

A. *R*-matrix theory

The basic idea of the R-matrix method is the division of the coordinate space into two regions separated by a sphere Ω with center in the center of mass of the molecule. Its radius r_Ω is chosen so that for scattering problem it is possible to neglect the exchange interaction between the projectile and the target molecule electrons outside the sphere, where their interaction is treated as the movement of the scattered electron in an average single particle potential.

In the fixed-nuclei approximation H_{N+1} is the $(N+1)$-particle electronic Hamiltonian. The scattering process is described by the time-independent Schrödinger equation

$$H_{N+1}\Psi_E = E\Psi_E, \quad \Psi_E = \sum_k \Psi_k A_{Ek}, \tag{1}$$

where Ψ_k are basis functions, which can be written in the form of the close coupling expansion

$$\Psi_k(\mathbf{x}_1, \ldots, \mathbf{x}_{N+1}) = \mathcal{A}\sum_{ijlm} c_{ijlmk}\bar{\Phi}_{ilm}(\mathbf{x}_1, \ldots, \mathbf{x}_N, \hat{\mathbf{r}}_{N+1}\sigma_{N+1})\frac{u_{jlm}(r_{N+1})}{r_{N+1}}, \tag{2}$$

where $u_{jlm}(r_{N+1})$ represent set of molecular orbitals (MOs) of the target molecule and continuum orbitals (COs). The channel functions $\bar{\Phi}_{ilm}$ in Eq. (2) are formed by coupling the target wave functions Φ_i with the spin-angle functions of the scattered electron $Y_l^m(\vartheta_{N+1}, \varphi_{N+1})s(\sigma_{N+1})$, and $\mathbf{x}_n = (\mathbf{r}_n, \sigma_n)$ denote the space and spin electron coordinates. The multiindex $\chi = \{i, l, m\}$ defines the scattering channel. The antisymmetry of the functions Ψ_k with respect to changes of all the spatial electronic coordinates is ensured by the antisymmetrization operator $\mathcal{A}$. Finally, the expansion coefficients c_{ijlmk} in Eq. (2) are obtained by solving the equation

$$(H_{N+1} + L_{N+1})\Psi_k = E_k\Psi_k \tag{3}$$

in the inner region. The Bloch operator[18]

$$L_{N+1} = \sum_{i=1}^{N+1} \frac{1}{2}\delta(r_i - r_\Omega)\left(\frac{\mathrm{d}}{\mathrm{d}r_i} + \frac{1}{r_i}\right) \tag{4}$$

guarantees the hermicity of the modified Hamiltonian $H_{\Omega,N+1} = H_{N+1} + L_{N+1}$ in the inner region.

Equation (1) is solved formally in the inner region[6] using the basis [Eq. (2)] and its solutions are projected onto the channel functions $\bar{\Phi}_{ilm}$. This gives for the radial wave functions of the projectile $w_{ilm}(r)$ on the sphere

$$w_{ilm}(r_\Omega) = \sum_{i'l'm'} R_{ilmi'l'm'}(E) r_\Omega \left.\frac{\mathrm{d}w_{i'l'm'}(r)}{\mathrm{d}r}\right|_{r=r_\Omega}, \tag{5}$$

where the R-matrix is defined by

$$R_{ilmi'l'm'}(E) = \frac{1}{2r_\Omega}\sum_k \left.\frac{\langle\bar{\Phi}_{ilm}|\Psi_k\rangle'\langle\Psi_k|\bar{\Phi}_{i'l'm'}\rangle'}{E_k - E}\right|_{r_{N+1}=r_\Omega}. \tag{6}$$

The primes mean that the integration is carried over all the coordinates except the radial coordinate r_{N+1}.

The form of the solution in the outer region differs from Eq. (2) by the absence of the antisymmetrization operator $\mathcal{A}$ only (since the exchange interaction is negligible). Substitution of this solution into the Schrödinger equation (1) and projection onto the channel functions yield the system of coupled second-order differential equations

$$\left(\frac{\mathrm{d}^2}{\mathrm{d}r^2} - \frac{l(l+1)}{r^2} + 2(E - E_i^N)\right)w_{ilm}(r) = 2\sum_{jl'm'} V_{ilmjl'm'}(r) w_{jl'm'}(r), \tag{7}$$

where E_i^N is the target energy and $V_{ilmjl'm'}(r)$ is given by the interaction potential between the target and projectile.[6] The scattering wave function in the outer region is obtained by solving this system with boundary condition (5) providing the correct connection between the solutions in the inner and outer regions. All the scattering information can be obtained from the asymptotic form of the solutions $w_{ilm}(r)$ in the outer region by application of standard methods of scattering theory.

B. Different models of correlation

In the SE approximation no correlation is introduced in the scattering system. The R-matrix basis set is written in the form (2), where Φ_0 is the Hartree-Fock determinant $|\Phi_0\rangle$ consisting of lowest N spin orbitals $(a, b, \ldots)$. $u_{jlm}(r)/r$ are the virtual MOs $(k, l, \ldots)$ and COs $(u, v, \ldots)$ in the symmetry of the interest. Higher eigenstates Φ_i, $i > 0$ are not taken into account.

The SEP approximation introduces the correlation between the molecule as a whole and the projectile, but not inside the molecular target. The SE space of configurations is augmented by states with singly excited target and scattered electron in virtual MO. In this approximation the R-matrix basis states can be written in the following form:

$$|\Psi_a\rangle = \sum_k c_{ka}|\Phi_0 k\rangle + \sum_u c_{ua}|\Phi_0 u\rangle + \sum_{bkl} c_{bkla}|\Phi_b^k l\rangle. \quad (8)$$

The matrix elements (The subscript int denotes that the integration is carried over the inner region.) $\langle\Psi_a|H_{N+1}|\Psi_b\rangle_{\rm int}$ of the R-matrix Hamiltonian in this basis contain terms corresponding to the $(N+1)$-electron Hartree-Fock (HF) Hamiltonian, terms corresponding to the correlation between the projectile and the target electrons as well as terms of form $\langle\Phi_a^k m|H_{N+1}|\Phi_b^l m\rangle_{\rm int}=\langle kb||al\rangle_{\rm int}$ introducing the additional correlation into the target. These elements are also present in the calculation of the N-electron neutral target ground state wave function in the basis set containing the $|\Phi_0\rangle$ and all the monoexcitations $|\Phi_a^k\rangle$, but according to the Brillouin theorem they do not contribute to the $|\Phi_0\rangle$ energy due to the fact that off-diagonal elements of the Fock operator are zero. On the other hand, in the $(N+1)$-electron calculation these elements contribute to the R-matrix poles E_k. This difference in the correlation treatment of the neutral target and the scattering system causes incorrect relative positions of the R-matrix poles with respect to the HF ground state energy of the neutral-target molecule.

The CI level of the correlation treatment introduces the correlation into the target in addition to the correlation between the projectile and the target. The target wave functions Φ_i in expansion [Eq. (2)] take the form of the MRCI expansion consisting of the single and double excitations from selected references into the virtual MOs. Inclusion of the double excitations improves the behavior of the wave functions for internuclear distances, where the target is not described correctly by single-determinant wave function.

C. Feshbach-Fano *R*-matrix

In the following we give a brief survey of the FFR method extensively discussed by Nestmann[8] and Kolorenč *et al.*[7]

The projection formalism developed by Feshbach[2,19,20] provides separation of the Hilbert space of the scattering problem into the resonance scattering subspace $\mathcal{Q}$ and background scattering subspace $\mathcal{P}$ by introduction of the corresponding projection operators Q and P. Using the corresponding decomposition of the scattering Hamiltonian H it is possible to express the matrix elements $\langle\epsilon'|T|\epsilon\rangle=T(\epsilon',\epsilon)$ as sum of the background and resonance terms. We choose

$$Q=|\varphi_{\rm d}\rangle\langle\varphi_{\rm d}|, \quad P=\int {\rm d}\epsilon {\rm d}\hat{\epsilon}|\phi_\epsilon^+\rangle\langle\phi_\epsilon^+|, \quad (9)$$

where $\langle\mathbf{r}|\varphi_{\rm d}\rangle$ is the square-integrable function (discrete state function) and $|\phi_\epsilon^+\rangle$ is the scattering solution of the operator PHP. We define the discrete state-energy $\epsilon_{\rm d}$ and the discrete state-continuum coupling $V_{{\rm d}\epsilon}$ by

$$\epsilon_{\rm d}=\langle\varphi_{\rm d}|H|\varphi_{\rm d}\rangle, \quad V_{{\rm d}\epsilon}=\langle\varphi_{\rm d}|H|\phi_\epsilon^+\rangle. \quad (10)$$

Using these quantities and explicit form of the projection operators [Eq. (9)] it is possible to express energy-dependent complex level shift $F(\epsilon)=\Delta(\epsilon)-i\Gamma(\epsilon)/2$:

$$\Gamma(\epsilon)=2\pi\int {\rm d}\hat{\epsilon}|V_{{\rm d}\epsilon}|^2, \quad \Delta(\epsilon)=\frac{1}{2\pi}\mathcal{P}\int {\rm d}\epsilon'\frac{\Gamma(\epsilon')}{\epsilon-\epsilon'}. \quad (11)$$

The quantities $\epsilon_{\rm d}$ and $V_{{\rm d}\epsilon}$ fully describe resonant scattering.

The main assumption of the FFR method is the confinement of the discrete state wave function associated with the resonance inside the R-matrix sphere Ω. Then the discrete state can be expressed in terms of the R-matrix basis (2):

$$|\varphi_d\rangle=\sum_{E_k\in\Sigma_{\rm res}} c_k|\Psi_k\rangle. \quad (12)$$

The region $\Sigma_{\rm res}$ is chosen so that it covers all the spectral domain where the discrete state interacts with the background continuum. The requirement of vanishing of the discrete state wave function outside the R-matrix sphere gives the condition

$$r_{N+1}^{-1}\langle\bar{\Phi}_\chi|\varphi_d\rangle'_{r_{N+1}=r_\Omega}=\sum_{E_k\in\Sigma_{\rm res}} c_k w_{\chi k}(r_\Omega)=0. \quad (13)$$

The corresponding projection operators Q and P can be defined by

$$Q=\sum_{E_j,E_k\in\Sigma_{\rm res}}|\Psi_j\rangle c_j c_k\langle\Psi_k|, \quad P=1-Q. \quad (14)$$

With the background Hamiltonian $H_{{\rm bg},\Omega}=PH_\Omega P$ it is possible to solve the background R-matrix problem

$$H_{\Omega,{\rm bg}}|\Psi_j^{\rm bg}\rangle=E_j^{\rm bg}|\Psi_j^{\rm bg}\rangle, \quad |\phi_\epsilon\rangle=\sum_j A_{\epsilon j}^{\rm bg}|\Psi_j^{\rm bg}\rangle \quad (15)$$

corresponding to Eqs. (3) and (1). Then it is possible to calculate ϵ_d and $V_{{\rm d}\epsilon}$ using Eq. (10) and Eq. (11) gives energy-dependent width and level shift.

Since condition (13) does not define the discrete state unambiguously, another criterion of the resonance definition is needed. It can be found by comparison with a similar system possessing no resonance in the region $\Sigma_{\rm res}$ represented by the Hamiltonian H^0 (its restriction to the sphere Ω is denoted H_Ω^0, and corresponding eigenstates and eigenenergies are denoted by $|\phi_{\chi k}^0\rangle$ and $E_{\chi k}^0$). This model system is usually represented by the target molecule plus noninteracting free electron.

It is possible to show that under certain conditions[8] the expansion coefficients c_k in Eq. (12) are solutions of the system of linear equations

$$\sum_{E_k\in\Sigma_{\rm res}} c_k\langle\phi_{\chi j}^0|\Psi_k\rangle=0, \quad E_{\chi j}^0\in\Sigma_{\rm res}. \quad (16)$$

In realistic cases it is usually impossible to find H^0 such that solution of this system exists. However, it is possible to find an approximation of the overlaps $\langle\phi_{\chi j}^0|\Psi_k\rangle$ such that condition (13) is satisfied when Eq. (16) is solved:[8]

$$\langle\phi_{\chi j}^0|\Psi_k\rangle\sim\frac{1}{E_k-E_{\chi j}^0}. \quad (17)$$

TABLE I. Exponents of the continuum basis set.

s	*p*	*d*
0.130 137	0.104 354	0.111 252
0.101 981	0.082 488	0.089 412
0.080 524	0.065 610	0.072 361
0.063 367	0.052 121	0.058 496
0.049 648	0.041 110	0.047 005
0.038 298	0.032 122	0.037 397
0.029 151	0.024 635	0.029 225
0.021 901		

III. APPLICATION TO THE FLUORINE MOLECULE

In all the calculations performed the R-matrix sphere Ω of radius $r_\Omega = 10$ bohrs has been used. Since the dipole moment of F_2 is zero and its polarizability is small, it is sufficient to consider the scattered electron as free in the outer region and set $V_{ilmi'l'm'} \equiv 0$ in Eq. (7). The target is represented by the CC-pVTZ basis set,[21] and the continuum basis set used in all the calculations has been taken from the previously published R-matrix calculation[11] and is listed in Table I.

Since the continuum basis set has been optimized by fitting the set of spherical Bessel functions to the set of Gaussians[22,23] for the given angular momentum quantum number, this basis set might not be appropriate for representation of continuum wave functions for higher energies. It is difficult to fit higher Bessel functions with many nodes by the linearly independent Gaussians. Continuum states with considerable contribution of these higher Bessel functions are not represented well by the used continuum Gaussian basis set. The exact solution of the free particle R-matrix problem gives zero phase shift for every energy of the free particle. In order to estimate the energy interval of validity of the Gaussian continuum basis set we solved the free particle R-matrix problem in the Gaussian basis set listed in Table I. The corresponding phase shifts are very small for $E \lesssim 14$ eV (see Fig. 1). This graph shows that the Gaussian basis set listed in Table I is appropriate in the energy region of interest (0–12 eV).

TABLE II. R-matrix poles on the SE level for internuclear separation $R = 2.4$ bohrs and configurations strongly contributing to the R-matrix eigenstates with their weights. The energies are relative to the HF ground state. The configurations are represented by the orbital occupied by the scattered electron. Virtual MOs have numbers 1–13 and COs have numbers 14–18.

	E (eV)	Orbital (weight)
1	1.026	14(0.603) 15(0.273)
2	4.730	3(0.520) 15(0.225) 16(0.121)
3	7.880	3(0.446) 4(0.110) 12(0.173) 14(0.105) 15(0.136)
4	15.038	4(0.276) 15(0.120) 16(0.428) 17(0.103)
5	25.677	5(0.447) 17(0.406)
6	31.966	4(0.468) 14(0.104) 15(0.172) 17(0.150)
7	47.722	5(0.177) 17(0.112) 18(0.493)
8	64.700	6(1.0)
9	80.414	5(0.252) 7(0.348) 18(0.154)
10	101.750	7(0.568) 18(0.173)
11	170.494	8(0.959)
12	207.122	9(1.0)
13	239.546	10(0.869)
14	242.274	11(1.0)
15	242.274	12(0.618) 13(0.300)
16	404.273	12(0.120)

In the expansion (2) only the ground electronic state of the target has been included. Due to the $^2\Sigma_u$ symmetry the lowest partial wave contributing to the scattering in our basis set is the p wave, and the d wave does not contribute to the scattering. These two facts allow the single channel scattering calculation.

The R-matrix poles E_k as well as transition density matrix used to calculate the R-matrix amplitudes[16] in Eq. (6) have been calculated using the MRCI program package DIESEL.[17] The R-matrix amplitudes as well as elastic scattering eigenphases and cross sections have been calculated using R-matrix program package by Nestmann *et al.*[6] Calculations at the different levels of correlation have been carried out. Due to technical complications with implementation of the MRCI method it is usually possible to obtain only four lowest R-matrix poles and corresponding amplitudes at the SEP and CI levels in the case of the fluorine molecule. The calculated R-matrix states $|\Psi_k^{\mathrm{SEP}}\rangle$, respectively, $|\Psi_k^{\mathrm{CI}}\rangle$ are

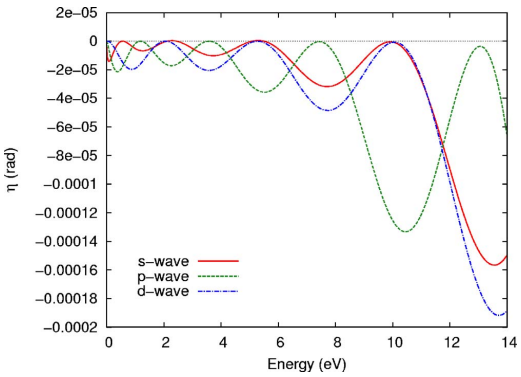

FIG. 1. (Color online) Phase shifts corresponding to potential-free R-matrix problem calculated in the Gaussian continuum basis set described above.

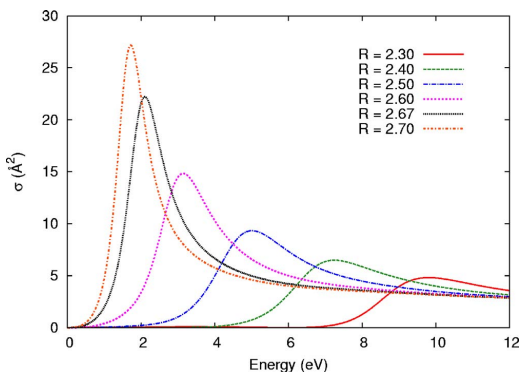

FIG. 2. (Color online) Elastic scattering cross section at the SE level as a function of E at several internuclear separations R (in bohrs).

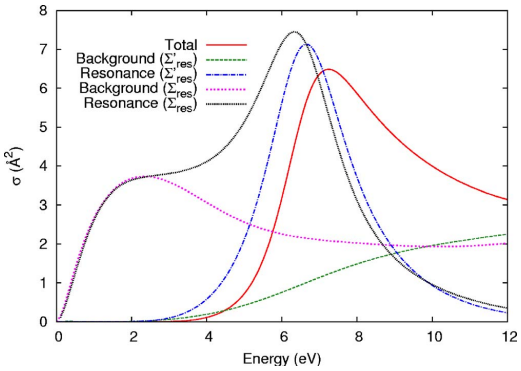

FIG. 3. (Color online) FFR separation of the cross section for internuclear distance $R=2.4$ bohrs in the SE approximation.

completed by the R-matrix states calculated on the SE level $|\Psi_k^{\mathrm{SE}}\rangle$ and orthogonalized on $|\Psi_k^{\mathrm{SEP}}\rangle$, respectively, $|\Psi_k^{\mathrm{CI}}\rangle$ (keeping the original space unchanged) forming a new basis set

$$\begin{pmatrix} \{|\Psi^{\mathrm{CI,SEP}}\rangle\} \\ \{|\Psi^{\mathrm{SE}'}\rangle\} \end{pmatrix} = \begin{pmatrix} 1 & 0 \\ \mathbb{A} & \mathbb{B} \end{pmatrix} \begin{pmatrix} \{|\Psi^{\mathrm{CI,SEP}}\rangle\} \\ \{|\Psi^{\mathrm{SE}}\rangle\} \end{pmatrix}. \tag{18}$$

The restricted Hamiltonian $H_{\Omega,N+1}$ is diagonalized in the basis set $\{|\Psi^{\mathrm{SE}'}\rangle\}$ and resulting R-matrix poles and amplitudes are added to those calculated on the SEP, respectively, CI level.

The FFR method has been used to calculate the discrete state. The Σ_{res} region has been taken such that it contains the four lowest R-matrix states. The separation of the cross sections and phase shifts to the resonance and background parts has been calculated as well as the discrete state-continuum coupling and the discrete state energies. The data obtained can be therefore used to construct the NRM in the future work. Discussion of nuclear dynamics is, however, beyond the scope of the present paper.

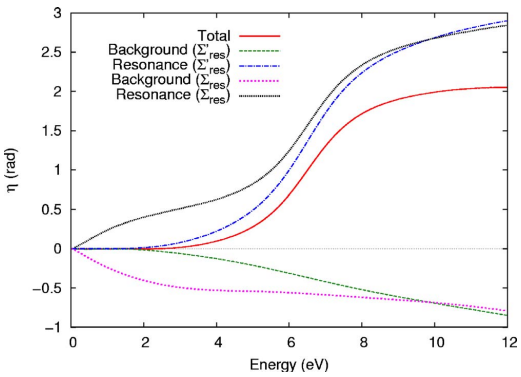

FIG. 4. (Color online) FFR separation of the eigenphase for internuclear distance $R=2.4$ bohrs in the SE approximation.

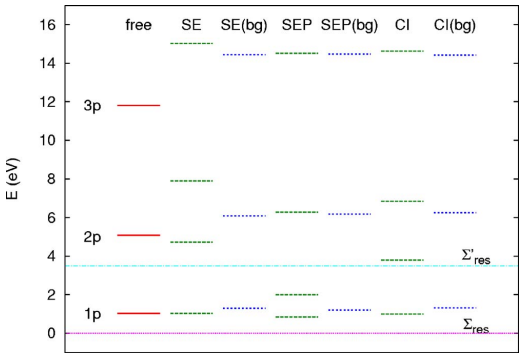

FIG. 5. (Color online) Lowest R-matrix poles of the free particle compared with poles calculated at different levels of correlation and with the corresponding background R-matrix poles. In the case of the SE and SEP poles the energy is relative to the HF energy of the neutral molecule, and in the case of CI poles the energy is relative to the SDCI energy of the neutral target. The regions Σ_{res} and Σ'_{res} are bounded by corresponding lines and the top of the picture.

IV. RESULTS

A. Static exchange (SE) and static exchange with polarization (SEP)

Before the discussion of the SEP calculation we briefly discuss results of the SE calculation. This is important for understanding of the effects of correlation included at the SEP and CI levels. At this level of correlation 16 R-matrix poles have been calculated for every considered internuclear separation R near the equilibrium internuclear distance $R_{\mathrm{eq}}=2.67$ bohrs. Configurations containing the scattered electron in the virtual MOs contribute to the eigenstates of the restricted Hamiltonian with coefficients comparable to configurations containing the scattered electron in the COs (see Table II as an example for $R=2.4$ bohrs). Several higher eigenstates of $H_{\Omega,N+1}$ consist of single configurations with the electron in the virtual MO. Corresponding amplitudes in Eq. (6) are zero, since the MOs vanish on the sphere. These eigenstates do not contribute to the R-matrix (6) at all.

The integral cross section of the electron-F_2 collision for

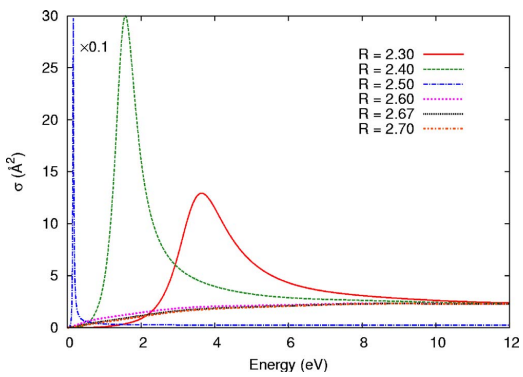

FIG. 6. (Color online) Elastic scattering cross section in the SEP model as a function of E in several internuclear separations R (in bohrs).

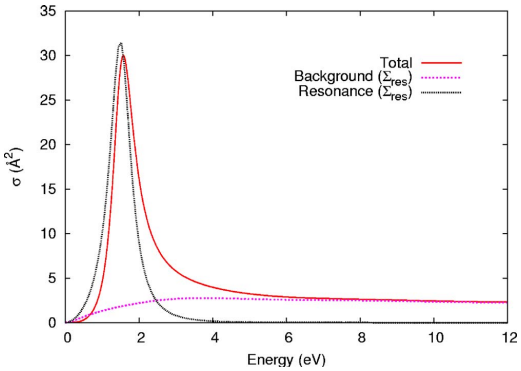

FIG. 7. (Color online) FFR separation of the cross section at the SEP level of correlation for internuclear separation $R=2.4$ bohrs calculated including four lowest R-matrix eigenstates into Σ_{res}.

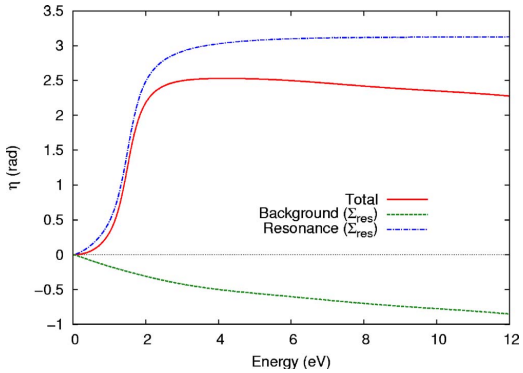

FIG. 8. (Color online) FFR separation of the eigenphases at the SEP level of correlation for internuclear separation $R=2.4$ bohrs calculated including four lowest R-matrix eigenstates into Σ_{res}.

several internuclear distances is presented in Fig. 2. This figure shows a well pronounced peak located at 2.1 eV with a value of 22.2 Å^2 for the equilibrium internuclear separation. The resonance structure becomes narrower as R approaches the crossing point of the potential curve of neutral molecule ground state with the negative ion.

The FFR method has been used to separate the discrete state in two variants. In one of them the Σ_{res} region includes the four lowest R-matrix poles in all considered geometries. For small internuclear separations ($R<R_{crit}$) the contribution of the lowest R-matrix eigenstate $|\Psi_1\rangle$ to the discrete state should be negligible. The approximation[17] of the overlaps, however, leads to unreasonably large value of coefficient c_1. The separation by projectors Q and P results therefore into an additional peak in the background cross section. The corresponding separations of the cross section and eigenphases are shown in Figs. 3 and 4 for $R=2.4$ bohrs. In order to avoid this behavior another calculation has been carried out with Σ'_{res} excluding the lowest R-matrix eigenstate (see Fig. 5). The corresponding cross section and eigenphase separation are also plotted in Figs. 3 and 4.

With increasing R ($R>R_{crit}$) it is necessary to include the lowest R-matrix state into Σ_{res} in order to avoid the poles with small imaginary part in the background T matrix and to obtain smooth transition to the bound state region of R.

Results of the R-matrix calculations at the SE level of correlation show the resonance structure in every considered geometry (the presence of the resonance in the equilibrium internuclear separation is in agreement with earlier results of Morgan and Noble[15]).

TABLE III. R-matrix poles on the SEP level for internuclear separation $R=2.4$ bohrs and configurations strongly contributing to the R-matrix eigenstates with their weights. The representation of the configurations is the same as in Table II.

	E (eV)	Orbital (weight)
1	0.848	3(0.222) 14(0.517) 15(0.185)
2	1.999	3(0.678) 15(0.145)
3	6.266	4(0.229) 14(0.217) 15(0.278) 16(0.209)
4	14.509	4(0.271) 16(0.443) 17(0.103)

At the SEP level of correlation 4 R-matrix poles have been calculated and additional 16 poles have been added on the SE level. Single excitations of the neutral molecule contribute to the SEP R-matrix poles. As at the SE level, configurations consisting of the molecule in the HF ground state and the scattered electron in the virtual MO or CO still represent the major contribution to the CI expansion of the $H_{\Omega,N+1}$ eigenstates. However, the presence of single excitations of the neutral molecule strongly affects the respective weights of these dominating configurations (compare Tables II and III). The calculated cross sections for several values of R are presented in Fig. 6. Contrary to the SE calculation, for three largest considered geometries, the ionic state is bound. This means that at the SEP level of correlation the crossing point of the neutral target ground state potential with the first R-matrix pole curve is shifted towards smaller values of R compared to the SE level. The presence of the bound ionic state in the equilibrium geometry is in agreement with results of Morgan and Noble.[15]

The results of the FFR separation are shown in Figs. 7 and 8. The discussion of the lowest R-matrix pole exclusion from Σ_{res} remains valid also in the SEP calculation, but the

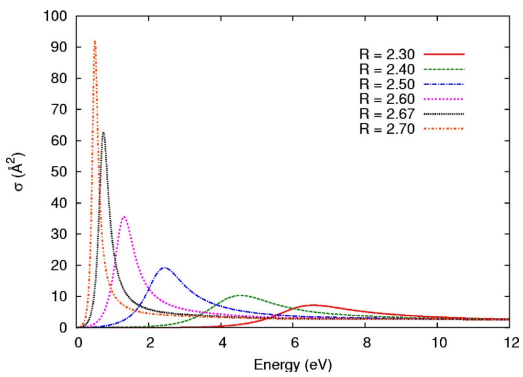

FIG. 9. (Color online) Elastic scattering cross sections for several internuclear separations R (in bohrs) calculated at the CI level.

TABLE IV. *R*-matrix poles at the CI level for internuclear separation $R=2.4$ bohrs and the configurations strongly contributing to the *R*-matrix eigenstates with their weights. The representation of the configurations is the same as in Table II. The energies are relative to the SDCI energy of the neutral target.

	E (eV)	Orbital (weight)
1	0.988	14(0.551) 15(0.236)
2	3.789	3(0.686) 15(0.138)
3	6.848	3(0.163) 4(0.181) 14(0.190) 15(0.182) 16(0.162)
4	14.640	4(0.255) 16(0.403)

critical geometry R_{crit}, where the lowest *R*-matrix pole becomes important, is smaller than in the SE calculation. Calculated *R*-matrix poles show good agreement with previously published SEP work enabling us to compare our calculations at the CI level with previous *R*-matrix results.[11] The small discrepancies are caused by different compact basis sets used.

B. Configuration interaction (CI)

At the CI level of the theory four *R*-matrix poles have been calculated for a range of geometries from 2.0 to 5.5 bohrs. These CI poles have been completed by 16 SE poles. For comparison with calculations at different levels of correlation the *R*-matrix poles and configurations dominating in corresponding eigenstates are listed in Table IV (compare with Tables II and III). These eigenstates consist of configurations with scattered electron in the continuum as well as of configurations with scattered electron in virtual MOs, both types with comparable weights. The comparison of numbers of configuration state functions (CSFs) in the SEP and CI calculations is presented in Table V.

The calculated cross sections are plotted in Fig. 9. This figure shows resonance structure at every considered internuclear distance with lower energies and smaller widths than in the SE calculation. The corresponding peak in the cross section is located at 0.75 eV for the equilibrium internuclear separation. With increasing internuclear distance the contribution of the excited configuration increases in the target eigenstates as well as in the eigenstates of $H_{\Omega,N+1}$ ($3\sigma_g \rightarrow 3\sigma_u$ since these orbitals become degenerated asymptotically). These excitations have not been allowed in the previous models of correlation. Double excitations allow the energy of the target state as well as the energies of the poles to be lower than in the previous models and more consistent with previous calculations of the neutral target ground state potential curves.[25] The electron affinity calculated at this level of correlation (2.2 eV) is much closer to the experimental value[26] (3.4 eV) than the value obtained at the SEP level[11] (13.5 eV). The discrepancy of our results with the experimental value is caused by the correlation imbalance in the calculation of the neutral target state and the negative ion state as well as not sufficiently large *R* used for calculation of the electron affinity. The incorrect value obtained at the SEP level is understandable, because the absence of double excited configurations in the wave functions leads to incorrect behavior of the potential curves for large values of *R*. In the SEP calculation the target ground state is represented by single closed-shell Slater determinant. In the asymptotic region of internuclear separations this gives ground state of system $F^+ + F^-$ and does not take into account the contribution of the open-shell configurations. Therefore the CI level of calculation improves the description of the target considerably for large internuclear distances.

TABLE V. Counts of CSFs generated in the SEP and CI calculations by allowed excitations from the given reference set for internuclear distance $R=2.4$ bohrs.

	SEP	CI
Target	0	64154
Ion	1430	612582

TABLE VI. Locations of the crossing points (bohr) where the resonance turns into the bound state.

Morgan and Noble (Ref. 15)	Ingr *et al.* (Ref. 4)	Brems *et al.* (Ref. 11)	This work
2.56	2.62	2.41	2.76

The *R*-matrix pole curves as functions of the internuclear distance are plotted in Fig. 10. These curves show the avoided crossing near the crossing point of the neutral target state with the lowest *R*-matrix pole. The crossing point where the resonance turns into the bound state is located at $R_{\text{thr}}=2.76$ bohrs at variance with previously calculated results[4,11,15] (see Table VI). The determination of the crossing point, which is of particular importance in the nuclear dynamics calculations, is complicated by the unbalanced correlation in independent calculations of the ionic and neutral target states.

The FFR method has been again used to determine the discrete state and corresponding separation of the cross sections and eigenphases for internuclear distance $R=2.4$ bohrs (see Figs. 11 and 12). Again two calculations

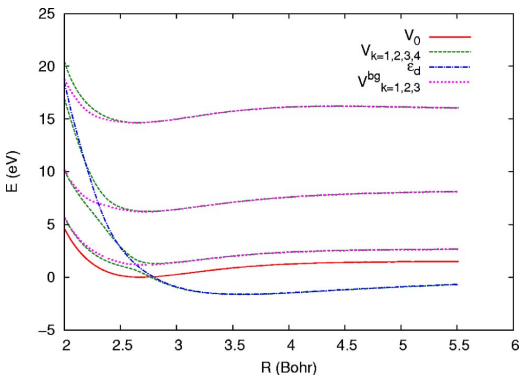

FIG. 10. (Color online) *R*-matrix poles calculated at the CI level as function of the internuclear distance. V_0 is the potential curve of the neutral target, $V_{k=1,\ldots,4}$ are the *R*-matrix pole curves, $V^{\text{bg}}_{k=1,\ldots,3}$ are the background *R*-matrix pole curves, and ϵ_{d} is the energy of the discrete state wave function. All energies are relative with respect to the neutral target energy in the equilibrium internuclear distance.

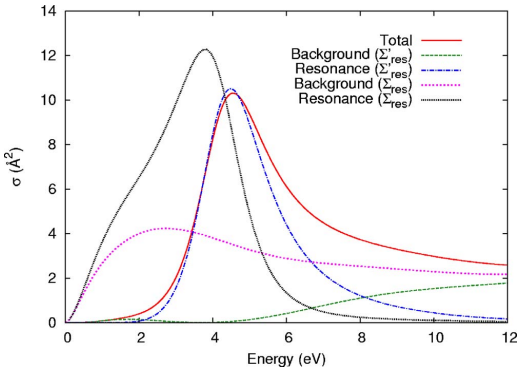

FIG. 11. (Color online) FFR separation of the cross section at the CI level of correlation for internuclear separation $R=2.4$ bohrs.

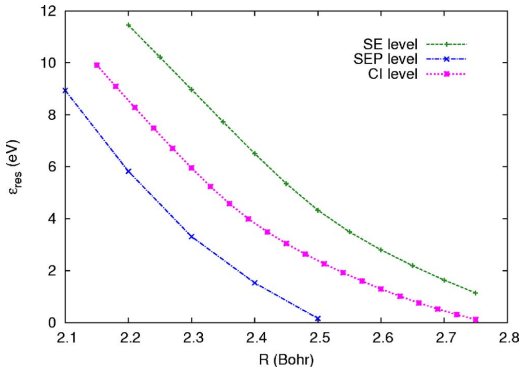

FIG. 13. (Color online) Approximate resonance position at different levels of correlation.

have been carried out in order to study the effect of inclusion of the lowest pole into the region Σ_{res} (see Fig. 5). The internuclear distance, where the lowest R-matrix pole becomes important, is near the avoided crossing point of the first and the second R-matrix state.

In order to compare the resonance positions in the considered correlation models the poles ϵ_{res} of the T matrix have been estimated assuming that the imaginary part is small enough to allow the solution in the form

$$\Re\epsilon_{res} - \epsilon_d - \Delta(\Re\epsilon_{res}) = 0, \quad \Im\epsilon_{res} = \tfrac{1}{2}\Gamma(\Re\epsilon_{res}). \tag{19}$$

Comparison of these estimated resonance positions is presented in Fig. 13. This figure shows that the resonance energies calculated at the CI level are larger than the values calculated at the SEP level and smaller than those calculated at the SE level.

V. CONCLUDING REMARKS

The Bonn implementation[16] of the R-matrix method has been used to study the $^2\Sigma_u$ resonance in electron scattering off the fluorine molecule using different levels of correlation including recently implemented SD-MRCI approach. The cross section calculated at the SE level of correlation shows well pronounced resonance for the equilibrium internuclear distance, while the SEP calculation yields a bound ionic state in this geometry. The obtained results are in agreement with previously published works of Morgan and Noble.[15] The resonance structure appears again at the CI level, but with different energy and width. The FFR method has been used to separate the resonance and to determine its coupling with the background continuum at three levels of correlation. The effect of the correlation on the resonance position and width has been studied. We have shown that inclusion of the doubly excited configurations in SD-MRCI expansions of the wave functions improves the results of the scattering calculations for larger internuclear distances, since the SD-MRCI approach correctly includes the neutral fragmentation channels of the target molecule. Our results show how the position of the crossing point of the neutral target potential curve with the ionic potential curve depends on the included correlation. Unlike previous results our calculation shows that the ion is unstable towards autodetachment even at the equilibrium internuclear separation of the neutral molecule. The results obtained here from the CI calculation present the first step in the construction of the nonlocal resonance model of the nuclear dynamics which will show the correlation effects in the DEA and VE of the fluorine molecule. This will be a subject of the forthcoming work.

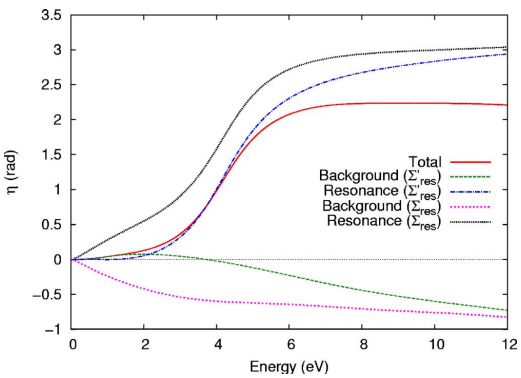

FIG. 12. (Color online) FFR separation of the eigenphases at the CI level of correlation for internuclear separation $R=2.4$ bohrs.

ACKNOWLEDGMENTS

The authors would like to acknowledge stimulating discussions with Dr. Karel Houfek, Dr. Přemysl Kolorenč, and Dr. Vincent Brems. This work was supported by the GAUK Grant No. 257718 of the Charles University in Prague and by the Center of Theoretical Astrophysics No. LC06014 of the Ministry of Education, Youth and Sports of the Czech Republic.

[1] *Current Status and Future Perspectives of Electron Interactions With Molecules, Clusters, Surfaces and Interfaces*, edited by K. Becker, C. McCurdy, T. Orlando, and T. Rescigno (Stevens Institute of Technology, Hoboken, NJ, 2000).
[2] W. Domcke, Phys. Rep. **208**, 97 (1991).
[3] T. Sommerfeld, U. Riss, and H. D. Meyer, and L. S. Cederbaum, Phys.

Rev. Lett. **79**, 1237 (1997).
[4] M. Ingr, H. Meyer, and L. Cederbaum, J. Phys. B **32**, L547 (1999).
[5] T. Rescigno, D. Horner, F. Yip, and C. McCurdy, Phys. Rev. A **72**, (2005).
[6] *Atomic and Molecular Processes: An R-matrix Approach*, edited by P. Burke and K. Berrington (IOP, Bristol, 1993).
[7] P. Kolorenč, V. Brems, and J. Horáček, Phys. Rev. A **72**, 012708 (2005).
[8] B. Nestmann, J. Phys. B **31**, 3929 (1998).
[9] T. Beyer, B. Nestmann, and S. Peyerimhoff, Chem. Phys. **255**, 1 (2000).
[10] T. Beyer, B. Nestmann, and S. Peyerimhoff, J. Phys. B **33**, 4657 (2000).
[11] V. Brems, T. Beyer, B. Nestmann, H. Meyer, and L. Cederbaum, J. Chem. Phys. **117**, 10635 (2002).
[12] P. Kolorenč and J. Horáček, Phys. Rev. A **74**, 062703 (2005).
[13] A. Hazi, A. Orel, and T. Rescigno, Phys. Rev. Lett. **46**, 918 (1981).
[14] T. O'Malley, Phys. Rev. **14**, 150 (1966).
[15] L. Morgan and C. Noble, J. Phys. B **17**, L369 (1984).
[16] B. Nestmann, R. Nesbet, and S. Peyerimhoff, J. Phys. B **24**, 5133 (1991).
[17] M. Hanrath and B. Engels, Chem. Phys. **225**, 197 (1997).
[18] C. Bloch, Nucl. Phys. **4**, 503 (1957).
[19] H. Feshbach, Ann. Phys. (N.Y.) **5**, 357 (1958).
[20] H. Feshbach, Ann. Phys. (N.Y.) **19**, 287 (1962).
[21] T. Dunning, J. Chem. Phys. **90**, 1007 (1989).
[22] B. Nestmann and S. Peyerimhoff, J. Phys. B **23**, L773 (1990).
[23] A. Faure, J. Gorfinkiel, L. Morgan, and J. Tennyson, Comput. Phys. Commun. **144**, 224 (2002).
[24] K. Pfingst, B. Nestmann, and S. Peyerimhoff, J. Phys. B **27**, 2283 (1994).
[25] M. Blomberg and P. Siegbahn, Chem. Phys. Lett. **81**, 4 (1981).
[26] C. Blondel, P. Cacciani, C. Delsart, and R. Trainham, Phys. Rev. A **40**, 3698 (1989).

2.2 Polarization treatment

The topic of polarization treatment in the R-matrix calculations is directly related to the problem of electron correlation discussed in the previous section. The reason is that the static dipole polarizability is a molecular property which reflects the quality of the target representation in the scattering calculation. In addition, the polarization effects have a large influence on the fixed-nuclei scattering cross sections close to the zero-energy threshold.

The static dipole polarizability α is the tensor quantity which specifies the linear response of the molecule to the weak homogeneous external electric field, i.e. the induced dipole moment of the molecule. Using the second-order perturbation theory, it is easy to show [26, p. 627] that the static dipole polarizability of the molecule in the electronic state Φ_i can be calculated using the sum-over-states (SOS) formula

$$\alpha_{ab} = 2 \sum_{n \neq i} \frac{\langle \Phi_i | r_a | \Phi_n \rangle \langle \Phi_n | r_b | \Phi_i \rangle}{E_n - E_i}, \tag{2.2}$$

where r_a and r_b are the corresponding coordinates, E_i and E_n are corresponding target eigenenergies and the summation is performed over all the electronic states, including continuum.

The separation of the configuration space into the inner region and outer region in the R-matrix theory enables us to separate the polarization treatment as well. In the inner region the polarizability is represented by coupling between different target states but the CI formulation of the problem automatically includes exchange and other effects which make the polarization impossible to represent as a single, energy-independent potential. Therefore, the reproduction of the neutral molecule polarizability by the CI model of the target states using the SOS formula (2.2) can be taken as one of the criteria to assess the quality of the target representation in the scattering calculation. It is well known that the CC expansions for systems with large polarizability converge slowly [27] due to large contribution of the highly excited target electronic states close to the ionization threshold and in the continuum above. In the first paper included in this section we are dealing with method that allows for improved representation of the target regarding the polarization effects (molecular R-matrix with pseudo-states - MRMPS) and for faster convergence of the CC expansion.

In the outer region the polarization potential is represented by the coupling of differ-

ent scattering channels represented by the multi-channel local potential described by the multipole moments between different target states calculated in the inner region [13]. In principle, this potential includes not only the polarization of the target ground state, but polarization effects of the excited states as well. This is the approach that we use in the first work presented in this section. On the other hand, in the second work we constructed the polarization potential corresponding to the target ground state and excited states polarizabilities and propagated the R-matrix in this model potential. The components of the polarizability tensor for corresponding states enter the calculation as a set of constants obtained from another independent quantum chemical calculations. Therefore, this approach allows us to study the influence of the polarization potential in the outer region on the electron scattering. We are able to distinguish the role of the polarization potential due to the excited states of the target. Comparison with the calculations mentioned above enables us to study the role of higher-order contributions to the potential in the outer region. The works presented here, are complementary in this sense. While in the first article we are dealing with the representation of the target in the inner region with respect to the polarizability reproduction, in the second article we study the effects of the polarization potential in the outer region in detail.

Both works mentioned above are dealing with electron scattering off Li_2. This molecule has a huge polarizability and provides a very stringent test of the ability of the methods used to treat the corresponding effects correctly. The ground-state and excited-state wave functions have quite large spatial extent what raises the issues with the R-matrix calculations since unusually large R-matrix spheres are necessary. This complicates the representation of the scattering continuum in the inner region and it restricts the interval of scattering energies for which the R-matrix calculations give reliable results. As this molecule represents a challenge for the *ab initio* scattering techniques, we decided to perform two independent calculations using two different codes (one using the Bonn codes and other using the UK R-matrix codes). The use of pseudo-states in the UK R-matrix calculation (described in the first article) allowed for smaller R-matrix sphere radius ($r_\Omega = 18\,a_0$) than in the Bonn calculation ($r_\Omega = 22\,a_0$, as discussed in the second article). We used the same CI model in both works for the CC expansion in the inner region. We kept four core electrons frozen in both calculations, therefore, we ended up with two-electron problem in calculation of Φ_i and with three-electron problem in calculation of Ψ_k. For these systems it is possible to construct the CAS-CI model using the SD-MRCI method by appropriate selection of the reference configurations. This we used in the Bonn calculations, therefore in both works the same (and balanced) electron correlation is included. The surprisingly good agreement of results obtained using the

UK R-matrix codes with results obtained using the Bonn codes proves that the features appearing in the fixed-nuclei scattering cross sections are not an artifact of the insufficient continuum or target representation, but real physical phenomena which lead to new considerations of the nuclear dynamics during DEA and VE.

In the second paper presented here we performed the R-matrix calculations for a set of internuclear separations with emphasis on the region where the anion becomes stable against autodetachment. Since the wave functions (describing scattering as well as anionic bound states) calculated using R-matrix method have correct asymptotic behavior, this technique is especially appropriate for calculation of weakly bound anionic states. This is what we demonstrate in the second paper presented here. In addition, the results obtained in this work can be used in calculation of VE in the diabatic nuclei approximation.

IOP PUBLISHING JOURNAL OF PHYSICS B: ATOMIC, MOLECULAR AND OPTICAL PHYSICS

J. Phys. B: At. Mol. Opt. Phys. **41** (2008) 205204 (8pp) doi:10.1088/0953-4075/41/20/205204

Polarization effects in electron collisions with Li_2: application of the molecular *R*-matrix method with pseudostates

M Tarana[1] **and J Tennyson**[2]

[1] Institute of Theoretical Physics, Charles University in Prague, V Holešovičkách 2, Prague, Czech Republic
[2] Department of Physics and Astronomy, University College London, Gower Street, London WC1E 6BT, UK

E-mail: tarana@mbox.troja.mff.cuni.cz

Received 17 June 2008, in final form 26 August 2008
Published 6 October 2008
Online at stacks.iop.org/JPhysB/41/205204

Abstract
Li_2 has a huge polarizability and a huge elastic cross section for collisions with low-energy electrons. The recently developed molecular *R*-matrix with pseudostates (MRMPS) method is applied to electron collisions with Li_2 at energies below 5 eV. The calculations, which are shown to be stable with respect to the choice of pseudostate basis, demonstrate the power of the MRMPS method for representing target polarizabilities and polarization effects in general. A previously identified low-lying $^2\Pi_u$ shape resonance is found at about 0.05 eV and several other low-lying resonances and resonance-like features are identified. Cross sections for elastic and electronically inelastic electron collisions are calculated and compared with previous studies.

(Some figures in this article are in colour only in the electronic version)

1. Introduction

Ab initio treatments of electron–molecule scattering have now become fairly routine for small and medium sized molecules at low energy, i.e. energies below the ionization threshold of the molecule. The hardest part of such calculations is to completely converge the polarization potential part of the calculation (Gil *et al* 1994), which is particularly important at low collision energies. The lithium dimer provides a benchmark system for this problem since it is the molecule with the largest known static polarizability. As a direct consequence of this it also has the largest low-energy, elastic, electron–molecule cross section so far observed for a neutral, nonpolar molecule (Miller *et al* 1982). The Li_2 molecule thus forms a theoretical benchmark against which the reliability of *ab initio* electron–molecule scattering procedures can be tested.

Recently, Gorfinkiel and Tennyson (2004, 2005) have developed a molecular *R*-matrix with pseudostates (MRMPS) method for treating electron collisions at intermediate energies. Although this was not their prime objective, Gorfinkiel and Tennyson found that their MRMPS calculations gave excellent values for the target polarizability and resulted in an improved representation of the polarization potential. Subsequent calculations on resonances in electron impact detachment from C_2^- (Halmová and Tennyson 2008, Halmová *et al* 2008) showed how polarization effects modelled using the MRMPS method could tackle problems not amenable to more standard treatments. The huge polarizability of Li_2 provides a very stringent test of the ability of the MRMPS to model such polarization effects and it is this that we test here.

Total cross sections for electron–Li_2 scattering have been measured by Miller *et al* (1982) and dissociative attachment measurements were performed by McGeoch and Schlier (1986). Theoretical treatments of the scattering problem have been performed by Padial (1985) and Gil *et al* (1993). These workers found a rich structure of Li_2^- resonances at low collision energies but found that their calculations were very sensitive to the precise treatment of polarization effects particularly at energies below 1 eV.

J. Phys. B: At. Mol. Opt. Phys. **41** (2008) 205204 M Tarana and J Tennyson

2. Method

The R-matrix method is based on dividing coordinate space into two regions using a spherical boundary centred on the centre-of-mass of the target molecule (Burke and Berrington 1993, Burke and Tennyson 2005). The radius of the boundary, a, is chosen so that the inner region contains all the electronic charge cloud of the target molecular states included in the calculation. The best value for a raises issues for Li_2 since the large internuclear separation (calculations here are presented for the equilibrium bondlength of 5.05 a_0) and the diffuse nature of the target wavefunction require the use of a larger than usual inner region. Hereafter for tests with a up to 22 a_0, a radius of 18 a_0 was chosen.

The accuracy of this method is strongly dependent on the representation of the problem in the inner region (Tennyson 1996) where it is necessary to consider all short-range interactions between the N target electrons and the scattering one. In standard, low-energy calculations, the wavefunction for an (N+1)-electron system in the inner region is given by the expansion

$$\psi_k^{N+1} = \mathcal{A}\sum_{ij} a_{ijk}\Phi_i(\mathbf{x}_1\cdots\mathbf{x}_N)u_{ij}(\mathbf{x}_{N+1}) + \sum_i b_{ik}\chi_i(\mathbf{x}_1\cdots\mathbf{x}_{N+1}), \quad (1)$$

where k represents the kth solution of the inner region Hamiltonian, $\mathcal{A}$ is the antisymmetrization operator, $\mathbf{x}_i$ are the spatial and spin coordinates of electron i, u_{ij} are continuum orbitals (COs) which represent the scattering electron (Tennyson and Morgan 1999), a_{ijk} and b_{ik} are variational coefficients, Φ_i is the wavefunction of the ith target state and χ_i are L^2 functions constructed from the target occupied and virtual molecular orbitals. These functions represent electron correlation and polarization effects. In the first sum, the configuration state functions are constrained to give the correct (target) space and spin symmetry for the first N electrons as well as the correct total, $(N+1)$-electron space–spin symmetry. The target wavefunctions are expanded as linear combinations of the configurations ϕ_k

$$\Phi_i(\mathbf{x}_1\cdots\mathbf{x}_N) = \sum_k c_{ik}\phi_k(\mathbf{x}_1\cdots\mathbf{x}_N), \quad (2)$$

where the c_{ik} coefficients are determined by diagonalizing the Hamiltonian of the molecular target.

The central idea of the MRMPS method is the augmentation of the close-coupling expansion (1) with extra pseudo-state 'target' wavefunctions Φ_i which are represented using an extra basis of pseudo-continuum orbitals (PCOs). Unlike the usual target wavefunctions, these pseudo-states are not approximations to true eigenstates of the target, but are used to represent a discretized version of both the electronic continuum and the high-lying target states not included in the expansion. These pseudo-states are obtained by diagonalizing the target electronic Hamiltonian expressed in an appropriate basis of configurations.

The addition of an extra basis means that care must be taken with orthogonalization of the final orbital set. This is done by first Schmidt orthogonalizing the PCO to the target molecular orbitals (MOs) and then deleting those transformed PCOs with the eigenvalues of the overlap matrix less than a deletion threshold $\delta_{\rm thr}^{\rm PC}$. This procedure is then repeated for the COs which are orthogonalized to the target MOs plus PCOs and those COs whose eigenvalues of the overlap matrix are less than $\delta_{\rm thr}^{\rm CO}$ are deleted. Further discussion on this can be found in the original references (Gorfinkiel and Tennyson 2004, 2005).

Calculations were performed using Gaussian type orbitals (GTOs) and the UK polyatomic R-matrix code (Morgan *et al* 1997). In the polyatomic suite target orbitals, COs and MRMPS PCOs are all represented by a linear combination of GTOs. The highest symmetry available in the polyatomic code is D_{2h} which is a subgroup of the true $D_{\infty h}$ symmetry of Li_2. All calculations presented here were performed in D_{2h} symmetry.

3. Calculations

3.1. Target representation

The Li_2 target was represented using Hartree–Fock molecular orbitals (MOs) using a cc-pVTZ GTO basis set from which we removed the most diffuse p-orbital in order to confine the molecule inside a sphere with $a = 18$ a_0. The removal of this GTO is compensated by the PCOs used in the MRMPS calculations (see below). As all the usual GTO bases of the lithium atom contain at least one diffuse Gaussian, use of smaller primary basis set would not lead to more compact MOs without loss of quality of the ground-state description. On the other hand, use of a larger primary target basis set raises issues for the optimization of the COs. Therefore, use of the cc-pVTZ GTO basis with the most diffuse orbital removed is a good compromise between the compactness of the MOs and quality of the target representation (see below). We note that as the majority of our target MOs were retained in the calculations and used to represent the target wavefunction, our calculation should therefore not be sensitive to the details of the choice of target orbitals, as has been found previously (Gil *et al* 1993).

Calculations using three different sets of N-particle states in the close-coupling expansion were carried out. In the first of them no PCOs were used, the COs were orthogonalized on the MOs only. Two other calculations were performed using different PCO bases. This allows us to understand the effect of polarization as well as to control the stability of our calculations with respect to small changes of the PCO basis.

For the PCOs we followed Gorfinkiel and Tennyson (2004, 2005) and used their even-tempered bases rescaled for $a = 18$ a_0. The first of them with $\alpha_0 = 0.0525$, $\beta = 1.3$ (denoted as PC-1 in the following) was obtained by multiplying $\alpha_0^{\rm orig} = 0.17$ by a factor of $\gamma = (10/18)^2$. The second basis with $\alpha_0 = 0.0463$, $\beta = 1.3$ (denoted as PC-2 in the following) was adopted in the same way from the original basis as $\gamma \times 0.15$. In all cases we restricted the PCO basis to $l \leqslant 3$ (10s, 10p, 6d, 5f) in order to keep the calculation tractable. To avoid problems with linear dependence of the COs, the two highest virtual MOs from the irreducible representation

Table 1. The number of molecular orbitals (MOs), pseudo-continuum orbitals (PCOs) and continuum orbitals (COs) in the irreducible representations of the D_{2h} point group. The numbers in the second and third lines without brackets correspond to the PC-1 basis ($\alpha_0 = 0.0525$), while the numbers in the brackets correspond to the PC-2 basis ($\alpha_0 = 0.0463$).

	A_g	B_{2u}	B_{3u}	B_{1g}	B_{1u}	B_{2g}	B_{3g}	A_u
MOs	10	6	6	3	8	6	6	2
PCOs	9	7	7	4 (3)	3	2	2	1
COs	16 (15)	15	15	5	15	5	5	5

A_g were removed as well as the four highest MOs from B_{1u} and the highest MO from A_u. The numbers of MOs used in the calculations are listed in table 1. To avoid the linear dependence with the PCOs a deletion threshold in the orthogonalization between the PCOs and target MOs was set to $\delta_{\rm thr}^{\rm PC} = 5 \times 10^{-4}$, as a result not all the orthogonalized PCOs were used in the scattering calculation. The numbers of used PCOs in all the irreducible representations are listed in table 1.

The Li_2 target states were represented using a complete active space (CAS) valence configuration interaction (CI) wavefunction. In these calculations we kept the two lowest MOs doubly occupied. Using the notation for the irreducible representations of D_{2h} this gives a CAS of the form

$$(1a_g, 1b_{1u})^4 \\ (2-10a_g, 1-6b_{2u}, 1-6b_{3u}, 1-3b_{1g}, \\ 2-8b_{1u}, 1-6b_{2g}, 1-6b_{3g}, 1-2a_u)^2. \quad (3)$$

For the MRMPS calculations a second, additional set of target configurations was generated using the following prescription and added to configurations (3):

$$(1a_g, 1b_{1u})^4 2a_g^1 \\ (11-19a_g, 7-13b_{2u}, 7-13b_{3u}, 4-7b_{1g}, \\ 9-11b_{1u}, 7-8b_{2g}, 7-8b_{3g}, 3a_u)^1 \quad (4)$$

for PC-1; for PC-2 the highest b_{1g} PCO is absent. Table 2 shows vertical excitation energies for the low electronic states of Li_2 calculated using these models. Our results both with and without PCOs are consistent with, but slightly higher than, accurate *ab initio* calculation of Hanrath (2005) which appears to be due to neglect of correlation effects associated with the core electrons. The corresponding distribution of calculated CI physical and pseudostates for different bases is plotted in figure 1. It shows that both calculations including PCOs produce some pseudostates with energy above the ionization threshold which is marked.

To check how well our target models represent the target ground-state polarizability of Li_2 we calculate the parallel ($\alpha_\parallel$) and perpendicular ($\alpha_\perp$) components of the polarizability tensor from the transition dipole moments using the following sum-over-states formulae,

$$\alpha_\parallel = \frac{1}{2}\sum_{i>1}\frac{|\langle\Phi_1|z|\Phi_i\rangle|^2}{\Delta E_i}, \\ \alpha_\perp = \frac{1}{2}\sum_{i>1}\frac{|\langle\Phi_1|x|\Phi_i\rangle|^2}{\Delta E_i}, \quad (5)$$

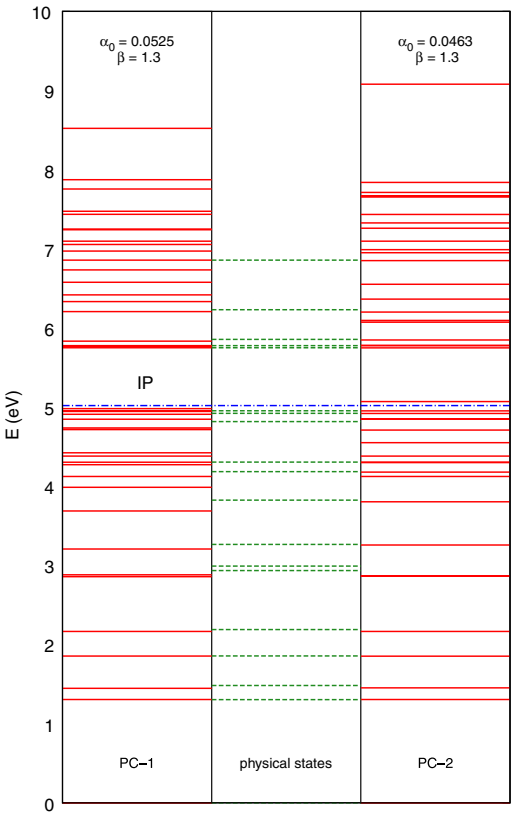

Figure 1. Calculated distribution of pseudostates for PC-1 and PC-2 bases (left and right columns) and physical target state distribution (middle column). All energies are relative to $X^1\Sigma_g^+$. The line with label IP indicates the ionization threshold taken from Boldyrev *et al* (1993).

where Φ_1 and Φ_i are wavefunctions of the target ground state and ith electronic state (2), ΔE_i is the corresponding ith excitation energy. By construction this sum runs only over states in the inner region; however the MRMPS method is designed to allow for the contribution of the continuum. Provided the state for which the polarizability is being computed is contained within the inner region, this method should recover all contributions to the polarizability.

Our tests are summarized in table 3. Target calculations without pseudostates show that only very few states are needed to reach convergence. While the parallel component ($\alpha_\parallel$) converges to within high accuracy using three lowest $^1\Sigma_u^+$ states, the perpendicular component ($\alpha_\perp$) converges to underestimated value as can be seen in table 3.

Calculation using the same set of states including the PC-1 basis shows improvement of $\alpha_\perp$. As table 3 shows, use of five pseudostates in the corresponding irreducible representations improves the results to better than 90% agreement with previously published *ab initio* calculations (Mérawa and Rérat

J. Phys. B: At. Mol. Opt. Phys. **41** (2008) 205204 M Tarana and J Tennyson

Table 2. Ground state (in hartree) and vertical excitation energies (in eV) for the basis without PCOs, for bases PC-1 ($\alpha_0 = 0.0525$, $\beta = 1.3$), PC-2 ($\alpha_0 = 0.0463$, $\beta = 1.3$) and Hanrath (Hanrath 2005).

Electronic state		Vertical excitation			
$D_{\infty h}$	D_{2h}	No PCOs	PC-1	PC-2	Hanrath
$X\,^1\Sigma_g^+$	^1A_g	−14.9027	−14.9027	−14.9027	−14.9134
$1\,^3\Sigma_u^+$	$^3B_{1u}$	1.305	1.305	1.305	1.231
$1\,^3\Pi_u$	$^3B_{2u} + {}^3B_{3u}$	1.483	1.447	1.454	1.370
$1\,^1\Sigma_u^+$	$^1B_{1u}$	1.856	1.854	1.854	1.778
$1\,^3\Sigma_g^+$	^3A_g	2.190	2.166	2.166	2.122
$1\,^1\Sigma_g^+$	^1A_g	2.936	2.882	2.868	2.783
$1\,^1\Pi_u$	$^1B_{2u} + {}^1B_{3u}$	2.992	2.858	2.864	2.798
$1\,^1\Pi_g$	$^1B_{2g} + {}^1B_{3g}$	3.266	3.208	3.259	2.998
$1\,^3\Pi_g$	$^3B_{2g} + {}^3B_{3g}$	3.825	3.689	3.806	3.130

Table 3. Static dipole polarizability (au) of the Li_2 ground state using PC-1, PC-2 and basis without PCOs. The second and third columns give number of states used in the sum-over-states formula contributing to the corresponding component.

	Number of states		Polarizability	
Basis set	$^1\Sigma_u^+$	$^1\Pi_u$	$\alpha_\parallel$	$\alpha_\perp$
Without PCOs	3	1	308	127
Without PCOs	141	126	309	132
PC-1	3	1	306	143
PC-1	4	5	307	146
PC-1	144	133	308	147
PC-2	4	5	306	145
Accurate *ab initio* value (Mérawa and Rérat 2001)			303	160

2001). For all the models tested the main contribution to the polarizability is due to the lowest state. These results show the advantage of pseudostates in our next calculations: with quite a small number of pseudostates we are able to represent the low target excited states correctly as well as the target ground-state polarizability better than with a larger number of target states without any PC basis. Tests showed that using all PCOs gives results close to the *ab initio* values of Mérawa and Rérat (2001). We decided not to use these additional PCOs in our scattering calculations to avoid problems with linear dependence of the COs.

Here it is worth making two points about the polarization potential in the scattering calculation. The first is that the polarizabilities, as shown in table 3, do not appear in this form in the actual calculation. They are represented in the outer region by coupling to (often closed) channels by the transition dipole moments which are included in the multipole expansion. In the inner region the polarizability is similarly represented by coupling between target states but the CI formulation of the problem automatically includes exchange and other effects which make the polarization impossible to represent as a single, energy-independent potential. Secondly, as shown to be important below, this formulation also allows for the polarization of excited states of the target. Given that these states are increasingly diffuse, their polarizabilities are even larger than the already very large polarizability of the ground state. Tests showed that our MRMPS values for these polarizabilities are in good agreement with previously calculated values (Mérawa and Rérat 2001). The effect of this is clearly seen in the difference between our MRMPS and non-MRMPS calculations reported below at energies above the lowest threshold for electronic excitation.

3.2. Scattering calculation

The larger R-matrix radius used in our calculations requires larger continuum basis sets than used in standard calculations with smaller R-matrix spheres. The corresponding single centre GTO exponents are listed in table 4. This basis set was optimized using the program GTOBAS (Faure *et al* 2002). Tests of the validity of this basis set using calculations in a potential-free R-matrix (Tarana and Horáček 2007) and static exchange calculations for the elastic electron collision with Li_2 in different symmetries showed that it represents the scattering continuum correctly for scattering energies $E \lesssim 5$ eV i.e. below the threshold to ionization (Boldyrev *et al* 1993). We restrict our study to energies below this threshold.

A continuum basis up to $l = 3$ (10s, 9p, 10d, 9f) is used in most of our calculations; g-orbitals were also optimized but their role showed to be negligible at energies below 1 eV. However, as discussed below, they become more important at higher energies but their use leads to a significant increase in the cost of the calculation. The deletion threshold in the orthogonalization procedure for the COs was set to $\delta_{\rm thr}^{\rm CO} = 2 \times 10^{-5}$ (Morgan *et al* 1997). Using this rather high value we optimized 81 (80) COs in the calculation without PC bases and in the calculation with PC-1 (PC-2), see table 1.

Scattering models using the PC-1 and PC-2 bases can be compared with calculations not using pseudostates. The MRMPS (non-RMPS) calculation included all states up to

J. Phys. B: At. Mol. Opt. Phys. **41** (2008) 205204 M Tarana and J Tennyson

Table 4. The exponents of the uncontracted continuum GTO basis set used in the calculations optimized for the *R*-matrix sphere with radius $a = 18\ a_0$.

$l = 0$	$l = 1$	$l = 2$	$l = 3$	$l = 4$
0.0 396 299	0.0 397 592	0.0 409 729	0.0 425 261	0.0 368 324
0.0 301 133	0.0 311 803	0.0 326 507	0.0 342 543	0.0 295 860
0.0 230 215	0.0 246 211	0.0 262 072	0.0 277 975	0.0 239 172
0.0 175 737	0.0 194 282	0.0 210 283	0.0 225 556	0.0 193 086
0.0 133 473	0.0 152 654	0.0 168 071	0.0 182 352	0.0 155 100
0.0 100 611	0.0 119 135	0.0 133 474	0.0 146 512	0.0 123 578
0.0 075 100	0.0 092 122	0.0 105 059	0.0 116 696	0.0 097 304
0.0 055 326	0.0 070 341	0.0 081 677	0.0 091 824	0.0 075 149
0.0 039 930	0.0 052 652	0.0 062 261	0.0 070 855	
0.0 023 000		0.0 031 000		

Table 5. Positions and widths of resonances (eV) using the PC-1, PC-2 and basis without PCOs.

Symmetry		Without PCOs		PC-1		PC-2	
$D_{\infty h}$	D_{2h}	Position	Width	Position	Width	Position	Width
$^2\Pi_u$	$^2B_{2u} + {}^2B_{3u}$	0.072	0.054	0.055	0.038	0.055	0.040
$^2\Delta_g$	^2A_g	1.582	0.239	1.514	0.174	1.522	0.176
	$^2B_{1g}$	1.568	0.158	1.506	0.141	1.514	0.142
$^2\Pi_g$	$^2B_{2g} + {}^2B_{3g}$	1.120	0.372	1.036	0.583	1.094	0.704
				2.310	0.329		
				2.944	0.190		
$^2\Delta_u$	$^2B_{1u}$			2.170		2.170	
	^2A_u	2.244	0.613	2.105	0.449		
$^2\Sigma_u^-$	^2A_u			1.576	0.597	1.710	0.514

5.8 eV above the ground state; selected states above this energy were included to ensure (a) minimum of 5 (3) states in each of A_g, B_{1u} (B_{2u}, B_{2g}) symmetries and (b) that in all cases both members of a degenerate pair were included. As a result, our close-coupling expansions corresponding to the PC-1 and PC-2 models include 68 pseudostates and expansion not using PCOs includes 28 target states.

4. Results

4.1. Resonances

Our calculated eigenphase sums show resonance features in several symmetries for all models. Their parameters were determined by fitting to a Breit–Wigner formula (Tennyson and Noble 1984). It should be noted that the large number of electronic excited states in the 2–4 eV range led to a number of resonance-like features whose eigenphases show a sharp rise of less than π which stops upon the opening of a new target state. This sort of behaviour has been observed in previous detailed calculations (Branchett *et al* 1990). Those resonances whose parameters could be successfully characterized in this fashion are summarized in table 5; features lying above 3 eV are not included as our characterization of excited states is less complete at these energies.

In general all resonances are shifted down slightly with the introduction of the pseudostates as would be expected from the improved treatment of polarization effects and, indeed, from the variational nature of the calculations. Sufficient PCOs were included in the calculations so that the positions and widths of the low-lying resonances are stable as indeed they are to changes of PCO basis. None of our calculations showed any pseudoresonance below 2 eV. The lowest lying resonance is a $^2\Pi_u$ shape resonance. Our parameters calculated can be compared with those of Padial (1985) who found a position of 0.00 645 eV and a width of 0.0017 eV. Gil *et al*'s (1993) calculations show this resonance in the elastic cross section near 0.06 eV, although the authors do not give any parameters.

A $^2\Delta_g$ Feshbach resonance was found independently in the ^2A_g and $^2B_{1g}$ irreducible representations of the D_{2h} point group. Fits in both symmetries give similar position and width. Analysis of the ^2A_g and $^2B_{1g}$ eigenphases assigned to particular eigenchannels (not given) showed several clear resonance-like changes of the eigenphases in the energy interval 2–3 eV. These structures are not strongly pronounced in the eigenphase sum and their fitting to a Breit–Wigner formula was unstable, especially for the resonance width.

The richest resonance structure appears in $^2\Pi_g$ symmetry. The lowest resonance in this symmetry is of a Feshbach nature showing a well-pronounced peak in the elastic scattering cross section. Padial (1985) found a 'very broad' $^2\Pi_g$ shape resonance about 1 eV. Our position agrees with this and, somewhat unusually, this resonance gets broader as the polarization potential is improved.

There are two further $^2\Pi_g$ resonances below 3 eV, each appears in the eigenphases assigned to particular eigenchannels. However, they do not lead to rapid change of the eigenphase sum and we were only able to determine the corresponding resonance parameters in the PC-1 basis calculation. In the remaining calculations the corresponding structures in the eigenphases disappear or are too close to

J. Phys. B: At. Mol. Opt. Phys. **41** (2008) 205204 M Tarana and J Tennyson

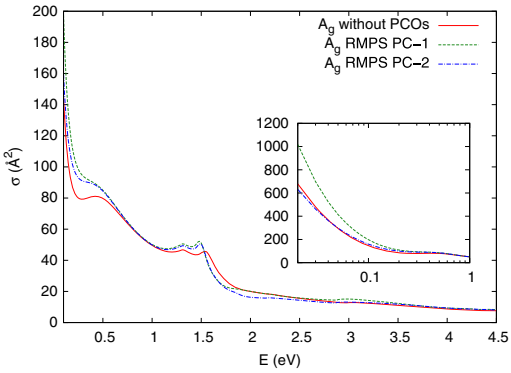

Figure 2. Elastic electron scattering cross section in the ^2A_g symmetry.

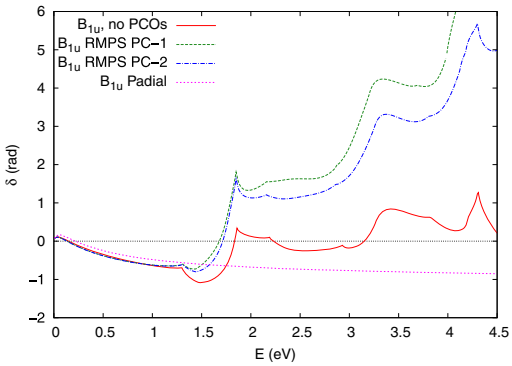

Figure 3. $^2B_{1u}$ symmetry eigenphase sums as a function of model; note that the π has been subtracted from the published values of Padial (1985) to aid comparison.

electronic thresholds to be fitted. It is possible that these resonances are artefacts of the PCO basis.

The presence of the low-lying target states and pseudostates also complicates fitting of resonances in $^2B_{1u}$ symmetry. The corresponding eigenphase sum (figure 3) as well as the elastic scattering cross section (not shown) show a resonance near 1.8 eV. There is no similar structure in ^2A_u eigenphases, indicating that this resonance has $^2\Sigma_u^+$ symmetry in $D_{\infty h}$. The discontinuity in the eigenphases at the $^1\Sigma_u^+$ excitation threshold prevents stable fits of this resonance. In calculations using PCOs we determined the position of another resonance at 2.17 eV, but were unable to find its width due to instability of the fits. The corresponding structure appears in the ^2A_u symmetry calculated, therefore this resonance has $^2\Delta_u$ symmetry. An additional resonance appears in the ^2A_u symmetry at energy 1.576 eV (1.710 eV) using the PC-1 (PC-2) basis set. It is assigned to $^2\Sigma_u^-$ symmetry of the $D_{\infty h}$ point group and does not appear in calculations without pseudostates.

4.2. Cross sections and eigenphases

Our elastic scattering cross sections calculated with pseudostates are, in general, in good agreement with calculations not using PCOs; nevertheless there are points where the polarization plays its role. The ^2A_g symmetry cross section, shown in figure 2, calculated without pseudostates shows a peak around 0.5 eV. This is not a resonance and the corresponding eigenphases are dominated by the s-wave (Tarana *et al* 2008) without any resonance-like features. We did not find any pseudoresonances in the energy region below 2 eV. This peak, which is present at similar energies in previous studies (Tarana *et al* 2008), disappears in the calculations with the PC-1 and PC-2 bases. Its presence is therefore just an artefact of an incomplete treatment of polarization. The exceptionally large ^2A_g cross section at ultra-low energies is due to a virtual state which is present at the Li_2 equilibrium geometry (Gil *et al* 1993, Tarana *et al* 2008). As can be seen in figure 2, the calculation using PC-2 is in good agreement with calculation not using PCOs. The cross section with PC-1 differs almost by a factor of 2 in this energy region. The reason is in the sharp change of the eigenphases close to the zero-energy threshold. At these energies even a very small change in the target basis, leading to a small change in the eigenphases, causes a large change of the cross sections. All our calculated elastic cross sections are in good agreement at energies above 1 eV.

A sharp change in the $^2B_{1u}$ symmetry cross section is also found at very low energies. The presence of a sharp peak in the cross section at zero energy is connected with the large spatial extent of the negative ionic wavefunction which leads to rapid changes of the eigenphases at very low energies. The $^2B_{1u}$ cross sections show a minimum near 0.1 eV due to the eigenphase sum passing through zero, see figure 3.

In general the cross sections and eigenphase sums show very good agreement between all our models below 1 eV. At higher energies cross sections using different PC bases correspond to each other but show pronounced structures corresponding to resonances absent in cross sections computed without PCOs. However above this the eigenphase sums and hence also the cross sections are very sensitive to inclusion of electronically excited states in the calculation. This is illustrated in figure 3 which shows that our results differ radically from the single-state calculations of Padial (1985) at these energies. Figure 3 shows that the eigenphases corresponding to different MRMPS calculations differ more with increasing energy while the elastic cross sections remain very close to each other. This sensitivity is largely due to the behaviour of eigenphases associated with channels coupling to electronically excited states of Li_2. Presumably, this is a reflection of the treatment of polarization in these channels. This behaviour is displayed by all symmetries.

Our total elastic scattering cross sections are given in figure 4 which shows excellent agreement between our calculations. The low-energy behaviour is determined by the large cross section in $^2\Sigma_g^+$ symmetry and by the presence of the resonance in $^2\Pi_u$ symmetry (see table 5). As the figure shows, the slight change of the resonance position and the threshold

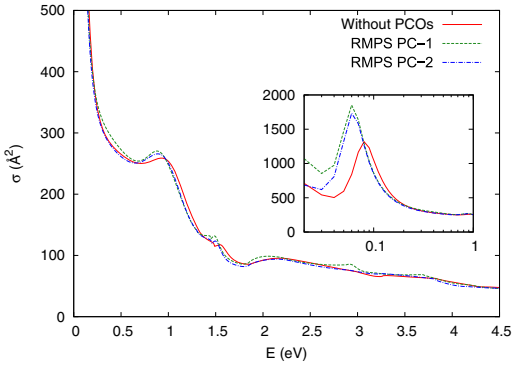

Figure 4. Total elastic electron scattering cross sections.

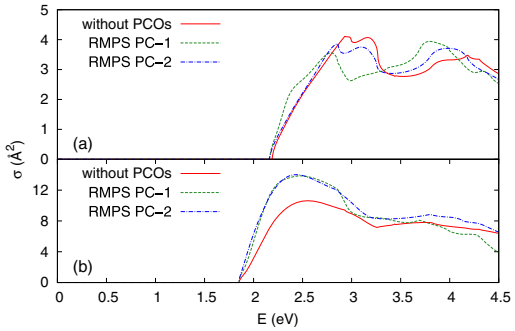

Figure 5. Electron impact electronic excitation cross sections for excitation into the $1^3\Sigma_g^+$ excited state (a) and $1^1\Sigma_u^+$ excited state (b).

behaviour with change of the PCO basis is the dominant factor in the differences between compared results.

Figure 5 shows the integral cross sections for electronic excitation from the ground state to the $1^3\Sigma_g^+$ and $1^1\Sigma_u^+$ states. Although the cross sections calculated using different basis sets differ in detail, the general character of the corresponding cross sections is very similar. Both cross sections are fairly small compared to the corresponding elastic cross section, although the dipole-allowed excitation to the $1^1\Sigma_u^+$ state is larger.

Figure 6 compares our elastic cross sections with previous calculations. Our results, which are for the PC-1 model, are in particularly good agreement with the best model of Gil *et al* (1993) in the 0.1–1 eV energy interval. Gil *et al* (1993) did not consider higher energies while at lower energies their results depend strongly on the target basis set used. While the calculation with averaged natural orbitals shows very good correspondence near the peak assigned to the $^2\Pi_u$ resonance, the cross-section calculated using the ground-state natural orbitals increases rapidly with energy approaching the zero threshold. The difference between our results and Gil *et al*'s (1993) at the low-energy limit might also be caused by the different treatment of the long-range polarization potential.

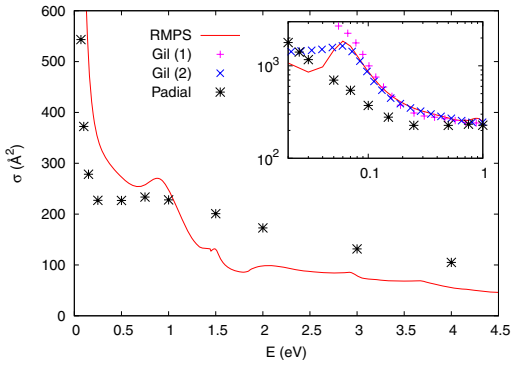

Figure 6. Elastic scattering cross section calculated using the PC-1 basis given by the solid line. Cross sections due to Padial (1985) are given by stars; *Ab initio* elastic cross section due to Gil *et al* (1993) using ground-state (1) and averaged (2) natural orbitals are indicated in the figure.

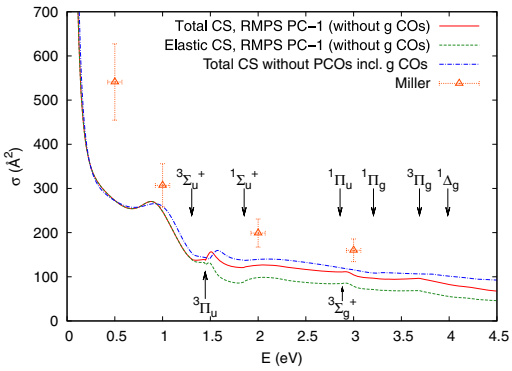

Figure 7. Total (elastic plus electronic excitation) cross section calculated using the PC-1 basis. Experimental data due to Miller *et al* (1982) are given by triangles with errorbars.

Padial (1985) also reported strong dependence of the elastic cross sections on the asymptotic polarization treatment for energies below 1 eV. Figure 6 contains its total cross-section calculated using a model without the cutoff polarization potential. These values are systematically below our results for energies below 1 eV. Padial's (1985) model with a cutoff potential shows a peak close to the $^2\Pi_u$ resonance in better agreement with our calculations, but its position and width were found to change rapidly with the cutoff parameter.

Miller *et al* (1982) measured total rather than just elastic cross sections. Figure 7 compares these measurements with the sum of our MRMPS elastic and electronically inelastic cross sections. The measurements are systematically higher than our results; at higher energies this could be in part due to the truncated set of partial waves used for our COs. However these are very difficult experiments which were performed using a beam of Li_2 at about 1000 K; it is therefore hard to be sure if figure 7 really presents a like-for-like comparison.

5. Conclusions

We report a study of low-energy electron collisions with the Li_2 molecule using the molecular *R*-matrix with pseudostates (MRMPS) method. Using only a few pseudostates we are able to treat the polarizability of this system in more consistent way than previous studies (Padial 1985, Gil *et al* 1993) and represent low-lying target states correctly. We show that our results are stable with respect to small changes of the pseudostate basis. We confirm the presence of a low-energy $^2\Pi_u$ shape resonance found in previous studies (Padial 1985, Gil *et al* 1993) and found several new Feshbach resonances at energies below 3 eV. However it proved difficult to fully characterize these resonances due to the density of low-lying target states.

We present elastic and electronically inelastic scattering cross sections for energies below the Li_2 ionization threshold. This appears to be the first *ab initio* calculation of electron collisions with the Li_2 molecule at energies above 1 eV which includes excited target states and thus allows for electronically inelastic processes.

Acknowledgments

This work is partially supported by the ESF EIPAM—exchange grant 1789, by the grant GAUK 116-10/257718 of the Charles University Prague and by the Center of Theoretical Astrophysics no. LC06014 of the Ministry of Education, Youth and Sports of the Czech Republic.

References

Boldyrev A I, Simons J, von R and Schleyer P 1993 *J. Chem. Phys.* **99** 8793–804
Branchett S E, Tennyson J and Morgan L A 1990 *J. Phys. B: At. Mol. Opt. Phys.* **23** 4625–39
Burke P G and Berrington K A (ed) 1993 *Atomic and Molecular Processes, an R-matrix Approach* (Bristol: Institute of Physics Publishing)
Burke P G and Tennyson J 2005 *Mol. Phys.* **103** 2537–48
Faure A, Gorfinkiel J D, Morgan L A and Tennyson J 2002 *Comput. Phys. Commun.* **144** 224–41
Gil T J, Lengsfield B H, McCurdy C W and Rescigno T N 1994 *Phys. Rev.* A **49** 2551–60
Gil T J, McCurdy C W, Rescigno T N and Lengsfield B H 1993 *Phys. Rev.* A **47** 255–263
Gorfinkiel J D and Tennyson J 2004 *J. Phys. B: At. Mol. Opt. Phys.* **37** L343–50
Gorfinkiel J D and Tennyson J 2005 *J. Phys. B: At. Mol. Opt. Phys.* **38** 1607–22
Halmová G, Gorfinkiel J D and Tennyson J 2008 *J. Phys. B: At. Mol. Opt. Phys.* **41** 155201
Halmová G and Tennyson J 2008 *Phys. Rev. Lett.* **100** 213202
Hanrath M 2005 *J. Chem. Phys.* **123** 084102
McGeoch M W and Schlier R E 1986 *Phys. Rev.* A **33** 1708–17
Mérawa M and Rérat M 2001 *Euro. Phys. J.* D **17** 329
Miller T M, Kasdan A and Bederson B 1982 *Phys. Rev.* A **25** 1777–78
Morgan L A, Gillan C J, Tennyson J and Chen X 1997 *J. Phys. B: At. Mol. Opt. Phys.* **30** 4087–96
Padial N T 1985 *Phys. Rev.* A **32** 1379–1383
Tarana M and Horáček J 2007 *J. Chem. Phys.* **127** 154319
Tarana M, Nestmann B M and Horáček J 2008 at press
Tennyson J 1996 *J. Phys. B: At. Mol. Opt. Phys.* **29** 6185–201
Tennyson J and Morgan L A 1999 *Phil. Trans.* A **357** 1161–73
Tennyson J and Noble C J 1984 *Comput. Phys. Commun.* **33** 421–4

PHYSICAL REVIEW A **79**, 012716 (2009)

R-matrix calculations of the ^2A_g elastic electron scattering off the Li_2 molecule

Michal Tarana,[1,*] Bernd M. Nestmann,[2] and Jiří Horáček[1]
[1]*Institute of Theoretical Physics, Faculty of Mathematics and Physics, Charles University in Prague, V Holešovičkách 2, Prague, Czech Republic*
[2]*Institute for Physical and Theoretical Chemistry, University of Bonn, Wegelestrasse 12, Bonn, Germany*
(Received 16 September 2008; published 29 January 2009)

Elastic electron scattering off the lithium dimer in the ^2A_g symmetry is studied. *R*-matrix calculations in the fixed-nuclei approximation are presented for a set of internuclear separations as well as energies of the stable negative ion. The aim of this work is to study effects of the polarization taken into account in the outer region on the elastic scattering cross sections. This work is the first part of a larger project dealing with Li_2 leading to calculations of nonelastic processes like vibrational excitation and dissociative electron attachment.

DOI: 10.1103/PhysRevA.79.012716 PACS number(s): 34.80.Bm

I. INTRODUCTION

The electron scattering off the lithium dimer represents a challenge for quantum scattering theory methods. Li_2 is a weakly bound molecule with an equilibrium internuclear separation of $5.05a_0$ and a dissociation energy of about 1 eV. The very large bond length leads to large static dipole polarizability [1] which is assumed to be the largest known for molecules. Quite extensive theoretical and experimental attention has been paid to the structure of the Li_2 molecule [2,3] as well as to the structure of its negative ion [4–6]. In contrast, only very few presentations concerning the electron scattering off Li_2 are available.

Miller *et al.* [7] measured the total cross sections for electron scattering by Li_2 for energies above 0.5 eV. They found out that the total cross section for low energies is the largest observed for neutral diatomic molecule with zero permanent dipole moment. McGeoch and Schlier [8] studied the dissociative electron attachment (DEA) to Li_2 experimentally and confirmed many features common with H_2. Padial [9] calculated the elastic scattering cross sections in the fixed-nuclei approximation using a cutoff potential model of the polarization and *ab initio* representation of the target ground state at the Hartree-Fock level. These results are uncertain for energies below 1 eV due to the cutoff parameter in the polarization potential. Gil *et al.* [10] used the complex Kohn variational principle to study the polarization and correlation effects in the fixed-nuclei approximation. They compare various models using natural orbitals with the static-exchange approach. For energies below 1 eV the resulting cross sections confirm predicted strong dependence on the basis set used. The theoretical work concerning the DEA is due to Wadehra [11]. He used the potential model based on the argument of Michels *et al.* [4] that the $^2\Sigma_g^+$ state of Li_2^- is a Feshbach resonance turning into the bound state with increasing internuclear separation.

It is the aim of this work to investigate the low-energy ^2A_g elastic electron scattering off Li_2 in the fixed-nuclei approximation using the *R*-matrix theory. We present cross sections in the ^2A_g symmetry for internuclear separations between $3a_0$ and $7.5a_0$. It is well known that large polarizability of the target complicates the convergence in calculations based on the close-coupling expansion of the $N+1$ particle wave function [12]. The *R*-matrix theory separates the collision region into a short-range electron-molecule-interaction region and a long-range region. The short-range polarization effects in electron collisions with Li_2 were studied extensively by Tarana and Tennyson [13]. They deal with such representation of the target, which gives correct ground-state polarizability and discuss its impact on the scattering cross sections. While the work due to Tarana and Tennyson [13] presents several models of the target, in the present work we focus our attention to the long-range effects of the polarization potential outside the *R*-matrix sphere using the *R*-matrix propagation recently introduced into the *R*-matrix codes [14]. We also discuss the long-range effects of the closed electronically excited channels. In addition, we discuss the existence of a stable negative ionic state as a function of the internuclear distance. Results of our present work provide data necessary to calculate cross sections of the vibrational excitation (VE) within Born-Oppenheimer approximation [15].

We restricted our study to the ^2A_g symmetry for the following reasons. Wadehra [11] considered the $^2\Sigma_g^+$ metastable state predicted by Michels *et al.* [4] to be the essential channel for DEA to Li_2. A virtual state [9,10] was found in this symmetry and it is expected that the low-energy elastic cross section in this symmetry represents important component to the total elastic electron scattering. The ^2A_g cross section is dominant in the limit of zero scattering energy and we investigate its threshold behavior. We also wanted to reconsider prediction of the low-lying $^2\Sigma_g^+$ Feshbach resonance due to Michels *et al.* [4] and investigate the energies of the anion for internuclear separations where it is bound. Especially we focus our attention to the position of the crossing point of the neutral target ground-state potential curve with the $^2\Sigma_g^+$ anionic curve since it plays an important role in the study of the nonelastic electron scattering.

II. THEORY

The basic idea of the *R*-matrix method is the division of the scattering-coordinate space into two regions. The inner

*tarana@mbox.troja.mff.cuni.cz

region is bounded by a sphere Ω, center of which coincides with the center of nuclear charges of the molecule. Its radius a is chosen large enough that the electronic wave function of the target is completely confined inside the sphere. Therefore, it is possible to neglect the exchange interaction between the projectile and the target molecule electrons outside the sphere.

In standard R-matrix calculations, the eigenfunctions Ψ_k of the $(N+1)$-electron Hamiltonian restricted to the inner region H_Ω [14] are given by the following expansion [14,16]:

$$\Psi_k(\boldsymbol{x}_1,\ldots,\boldsymbol{x}_{N+1}) = \sum_i c_{ik} A[\Phi_i(\boldsymbol{x}_1,\ldots,\boldsymbol{x}_N) f_{ik}(\boldsymbol{x}_{N+1})] + \sum_i b_{ik}\chi_i(\boldsymbol{x}_1,\ldots,\boldsymbol{x}_{N+1}). \quad (1)$$

The index k specifies the eigenstate of the inner Hamiltonian. Φ_i is the wave function of the ith target state given as a linear combination of configuration state functions. $\boldsymbol{x}_n$ are the spatial and spin coordinates of nth electron, $f_{ik}(r_{N+1})$ describe the wave function of the scattered electron, A is the antisymmetrization operator. c_{ijk} and b_{ik} are the variational coefficients and χ_i are L^2 functions constructed from the molecular orbitals (MOs). Correct description of the target states and reproduction of the polarizability is controlled by the configuration interaction (CI) model and primary Gaussian basis set.

As the correlation and exchange interaction between the scattered and target electrons can be neglected in the outer region, the projectile is considered to move in a local potential $V_{ilmjl'm'}(r)$ obtained from the transition multipole moments of the target outside the sphere. The radial wave functions $w_{E;ilm}(r)$ of the scattered electron satisfy the following set of coupled second-order differential equations:

$$\left(\frac{d^2}{dr^2} - \frac{l(l+1)}{r^2} + 2(E - E_i^N)\right) w_{E;ilm}(r) = 2\sum_{jl'm'} V_{ilmjl'm'}(r) w_{E;jl'm'}(r), \quad (2)$$

where l, m denote corresponding partial waves of the scattered electron, E is the total energy, E_i^N is energy of the ith target state and $V_{ilmjl'm'}(r)$ is given by the interaction potential between the target and projectile [16]. In addition, the solutions of Eq. (2) which correspond to the (regular) scattering wave function obey the following boundary condition:

$$w_{E;ilm}(a) = \sum_{i'l'm'} R^a_{ilm,i'l'm'}(E) \left.\frac{d}{dr}\right|_a w_{E;i'l'm'}(r). \quad (3)$$

The elements $R^a_{ilm,i'l'm'}(E)$ of the R-matrix $R^a(E)$ are determined by eigenvalues of H_Ω and by projections of the corresponding eigenfunctions on the scattering channels (ilm) at $r=a$. The boundary value problem given by Eq. (2) and Eq. (3) can be solved by propagating $R^a(E)$ to $R^{a_p}(E)$ along Eq. (2) [17]. The distance $r=a_p$ should be large enough that $V_{ilmjl'm'}(a_p)$ can be considered to be zero.

In Sec. IV we will discuss effects of the polarization potential outside the R-matrix sphere. It is given by the mean polarizability (α_{0i}) and polarizability anizotropy $(\Delta\alpha_i)$ of the ith target state in the Σ symmetry:

$$V_i^p(\boldsymbol{r}) = -\frac{\alpha_{0i} + \frac{2}{3}\Delta\alpha_i P_2(\cos\vartheta)}{r^4}, \quad (4)$$

where P_2 is the Legendre polynomial and ϑ is the angle between the molecular axis and the vector from the center of the molecule pointing to the approaching electron.

It is easy to show [16] that if the projectile outside the sphere is affected by a single-center potential $V_{ij}^e(\boldsymbol{r})$, then matrix $V_{ilmjl'm'}(\boldsymbol{r})$ in Eq. (2) can be written in the following form:

$$V_{ilmjl'm'}(r) = \int_{\mathcal{S}^2} Y_l^{m*}(\hat{r}) V_{ij}^e(\boldsymbol{r}) Y_l^m(\hat{r}) d^2\hat{r}. \quad (5)$$

Indices i, j denote different target states contributing to the potential outside the sphere. In our calculations this potential is approximated by the polarization of the target eigenstates, i.e.,

$$V_{ij}^e(\boldsymbol{r}) = V_i^p(\boldsymbol{r})\delta_{ij}. \quad (6)$$

Therefore, we take into account polarization potential of the lowest target states and neglect any coupling terms. Boardman *et al.* [18] show that if a nonspherical potential can be written as the expansion

$$V(\boldsymbol{r}) = \sum_l v_l(r) P_l(\hat{\Omega}_l \cdot \hat{r}), \quad (7)$$

where $\hat{\Omega}_l$ is the unit vector denoting the direction of the $2l$-pole axis, and if this potential is axially symmetric, then the projection of the Schrödinger equation onto the spherical harmonics yields the system of coupled radial differential equations similar to Eq. (2) with real symmetric potential matrix. Consider the form of the total scattering wave function outside the R-matrix sphere different from Eq. (1) in absence of the antisymmetrization operator [16] and the interaction potential between the target and projectile in the form $V_{ij}^e(\boldsymbol{r})$ [Eq. (6)]. Following the argumentation of Boardman *et al.* [18], one yields the system of radial differential equations (2) with the potential matrix

$$V_{ilmjl'm'}(r) = 2\sum_L (-1)^m [(2l+1)(2l'+1)]^{1/2} \begin{pmatrix} l & l' & L \\ 0 & 0 & 0 \end{pmatrix} \times \begin{pmatrix} l & l' & L \\ m & -m & 0 \end{pmatrix} v_{ijL}(r)\delta_{mm'}. \quad (8)$$

Comparison of Eq. (4) with Eq. (7) shows that the only nonzero elements $v_{ijL}(r)$ in Eq. (8) are

$$v_{ij0}(r) = -\frac{\alpha_{0i}}{r^4}\delta_{ij}, \quad v_{ij2}(r) = -\frac{2\Delta\alpha_i}{3r^4}. \quad (9)$$

Parameters $\alpha_{0i}=(\alpha_{\|i}+2\alpha_{\perp i})/3$ and $\Delta\alpha_i=\alpha_{\|i}-\alpha_{\perp i}$ can be obtained from the polarizability tensor calculated using the sum-over-states formulas (SOSF)

TABLE I. The number of molecular orbitals (MOs) and continuum orbitals (COs) in the irreducible representations of the D_{2h} point group for different intervals of internuclear distance R (in a_0).

	A_g	B_{2u}	B_{3u}	B_{1g}	B_{1u}	B_{2g}	B_{3g}	A_u
MOs	13	7	7	3	13	7	7	3
COs ($R \leqslant 3.8$)	15	5	5	5	5	5	5	0
COs ($3.8 \leqslant R \leqslant 6.5$)	16	5	5	5	5	5	5	0
COs ($R \geqslant 6.5$)	17	5	5	5	6	5	5	0

$$\alpha_{\parallel i} = \frac{1}{2}\sum_{j\neq i} \frac{|\langle \Phi_i|z|\Phi_j\rangle|^2}{E_j^N - E_i^N}, \quad \alpha_{\perp i} = \frac{1}{2}\sum_{j\neq i} \frac{|\langle \Phi_i|x|\Phi_j\rangle|^2}{E_j^N - E_i^N}, \quad (10)$$

where E_i^N is the energy of the ith target state Φ_i.

This treatment of the polarization potential in the outer region is different from [13], where the polarizabilities do not directly appear in the actual calculation. They are represented in the outer region by coupling to different channels by transition dipole moments which are included in the multipole expansion. The approach used in the present work enables us to construct different models of long-range polarization without change of the target representation and to study the role of closed electronically excited channels in the outer region.

III. CALCULATIONS

We performed R-matrix scattering calculations of the electron collision with Li_2 using Gaussian type orbitals (GTOs) and code due to Nestmann [14]. The continuum orbitals are represented by linear combinations of GTOs. All the calculations were performed using the D_{2h} point group which is the highest Abelian subgroup of the true $D_{\infty h}$ symmetry available in the codes used.

A. Target representation

The neutral target was represented by the restricted active space self-consistent field (RASSCF) MOs using a correlation consistent polarized valence triple zeta (cc-pVTZ) basis set [19]. These orbitals were optimized to minimize the energy of the $^1\Sigma_g^+$ ground state and are more appropriate for representation of the target at larger internuclear separations than the Hartree-Fock MOs as they respect the open-shell character of the lithium atom. The GTO basis set used is optimized for representation of the ground-state polarizability and therefore the polarization effects should be treated correctly in the inner region. Numbers of MOs used in the calculations are listed in the first row of Table I.

The neutral target states were represented by the singe-double multireference CI (SD-MRCI) wave function [20,21], all the CI calculations were performed using the package DIESEL [22]. The lowest two MOs were kept doubly occupied in all the calculations. Since Li_2 has six electrons, the SD-MRCI with the Hartree-Fock ground state as the only reference is in this case equivalent to complete active space (CAS) CI. Using the notation of the D_{2h} point group this configuration space can be expressed as follows:

$$(1a_g, 1b_{1u})^4(2-13a_g, 1-7b_{2u}, 1-7b_{3u}, 1-3b_{1g}, 2-13b_{1u}, 1-7b_{2g}, 1-7b_{3g}, 1-3a_u)^2. \quad (11)$$

Table II shows energies of the ground state and vertical excitation energies of the lowest electronic states for several internuclear separations. These results are consistent with accurate full CI calculations presented previously [23], although our excitation energies are slightly higher.

Target states appearing in Table II were used to calculate the components of the ground-state polarizability tensor along the SOSF. Calculated polarizabilities are plotted in Fig. 1 as a function of the internuclear distance. For comparison we performed the second-order particle propagator

TABLE II. Ground state (in Hartree) and vertical excitation energies (in eV) for several internuclear separations compared with Hanrath [23].

Electronic state		Vertical excitation					
		$R=3a_0$		$R=5a_0$		$R=7a_0$	
$D_{\infty h}$	D_{2h}	This work	Hanrath	This work	Hanrath	This work	Hanrath
$X\ ^1\Sigma_g^+$	^1A_g	−14.82850	−14.83975	−14.90304	−14.91342	−14.88886	−14.90105
$1\ ^3\Sigma_u^+$	$^3B_{1u}$	1.895	1.861	1.323	1.231	0.611	0.544
$1\ ^3\Pi_u$	$^3B_{2u}+^3B_{3u}$	0.893	0.994	1.383	1.370	1.461	1.441
$1\ ^1\Sigma_u^+$	$^1B_{1u}$	2.685	2.650	1.859	1.778	1.426	1.371
$1\ ^3\Sigma_g^+$	^3A_g	3.216	3.301	2.150	2.122	1.729	1.688
$1\ ^1\Pi_u$	$^1B_{2u}+^3B_{3u}$	2.834	3.318	2.609	2.797	2.304	2.397

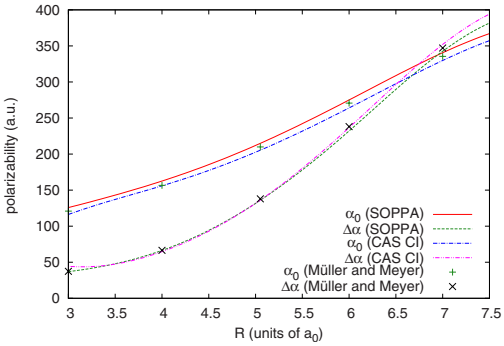

FIG. 1. (Color online) The spherical polarizability α_0 and the polarizability anisotropy $\Delta\alpha$ of the neutral target ground state as a function of the internuclear separation calculated using our CAS CI model (sum-over-states formulas) and using the SOPPA method and their comparison with previously presented results [24].

approximation (SOPPA) calculation of polarizability implemented in the Dalton program [25]. In this calculation the augmented correlation consistent polarized valence triple zeta (aug-cc-pVTZ) GTO basis was used and the ground state was calculated using the CAS CI method with all but valence electrons frozen. These results are stable with respect to extension of the primary GTO basis and are plotted in Fig. 1 as well. The figure shows that both the calculations (SOPPA in larger basis and SOSF using our CAS-CI model) give very similar results, although the polarizabilities using the SOSF are slightly underestimated for all the geometries. This might be an artefact of missing higher target states, especially the Rydberg states, in our model. However, all the calculated polarizabilities are in very good agreement with previous results presented by Müller and Meyer [24], as can be seen in Fig. 1. The comparison shows that target states listed in Table II represent the polarizability correctly and it justifies us to use the polarization potential with parameters from Fig. 1 in the outer region. In order to study the effect of the excited target states polarizabilities in the outer region, the corresponding polarizabilities were calculated using the same program for the equilibrium geometry of the Li_2 ground state. The calculated results are summarized in Table III. The scattering calculations (see below) showed that the polarizabilities of the excited states do not affect the results considerably for the equilibrium internuclear distance. Therefore, the ground-state polarizability only was included in calculations for other geometries.

TABLE III. Static dipole polarizabilities of the singlet and triplet states ${}^{1,3}\Sigma_{g,u}^{+}$ of Li_2 at the internuclear separation $R_e=5.05a_0$.

States	$\bar{\alpha}$	$\Delta\alpha$
$X\ {}^1\Sigma_g^+$	214	135
$1\ {}^3\Sigma_g^+$	−123	−812
$1\ {}^1\Sigma_u^+$	486	393
$1\ {}^3\Sigma_u^+$	843	949

TABLE IV. The exponents of the uncontracted continuum GTO basis set used in the calculations rescaled for the R-matrix sphere with radius $a=22a_0$.

s	p	d
0.026887	0.021560	0.022985
0.021070	0.017042	0.018473
0.016637	0.013555	0.014950
0.013092	0.010768	0.012085
0.010257	0.008493	0.009711
0.007912	0.006636	0.007726
0.006022	0.005089	0.006038
0.004525		

B. Scattering calculation

The Φ_i and χ_i appearing in Eq. (1) are constructed in the same basis of MOs. From our polarizability calculations as discussed in Sec. III A we conclude that the target basis set used is suitable to describe the polarization effects in the inner region sufficiently. Due to the requirement that the target states be completely inside the sphere, the R-matrix sphere must be rather large. All our scattering calculations were performed in the sphere of radius $a=22a_0$ since the large bond lengths lead to diffuse MOs. For the representation of functions f_{ik} a set of diffuse GTOs was added, all centered at the origin of the sphere. This basis (originally used for a sphere with radius $a'=10a_0$) was rescaled for our sphere by multiplying every exponent by a factor $\beta=(a'/a)^2$. The rescaled GTO exponents $(8s,7p,7d)$ are listed in Table IV. In our previous work [26] it is estimated that the original basis [27] is suitable for energies of the scattered electron $E\lesssim 14$ eV. The rescaling of the basis reduced the upper energy limit, for which this basis set is appropriate, by factor β, i.e., we carried our calculations for energies $E\lesssim 2.9$ eV. The continuum orbitals (COs) were obtained by orthogonalization of the additional continuum GTOs to the target MOs and subsequent diagonalization of the corresponding overlap matrix. In order to avoid linear dependence, the COs with norm smaller than $\delta_{\rm thr}=10^{-7}$ were removed. The remaining COs are normalized with respect to the R-matrix sphere. Numbers of COs generated by this procedure are listed in Table I for three intervals of internuclear distance R, where different number of COs was deleted.

In all our R-matrix calculations the expansion (1) in the inner region included all the target states listed in Table II (both members of every π-degenerate pair were included correctly). This set was selected to include all the target states at the equilibrium geometry up to 2.89 eV above the ground state. As the energies of these states decrease with increasing R, the results for energies above the highest target state included (see Table II) should be considered as less reliable for larger geometries.

The R-matrix eigenstates were also calculated using the SD-MRCI method. In the $N+1$ particle calculation, the two lowest orbitals were kept doubly occupied. We selected such set of references that single and double excitations of re-

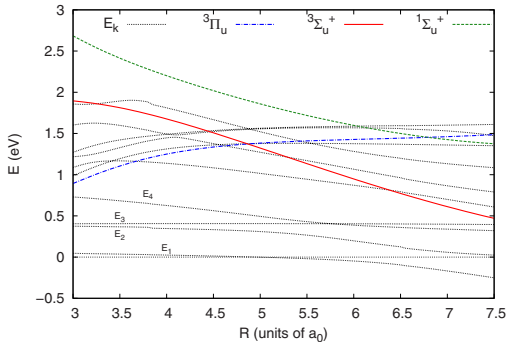

FIG. 2. (Color online) Lowest poles (E_k) of $R^a(E)$ as a function of the internuclear distance R and neutral target potential curves in $^1\Sigma_u^+$, $^3\Sigma_u^+$, and $^3\Pi_u$ symmetries. All the curves are relative to the neutral target ground eigenstate $^1\Sigma_g^+$.

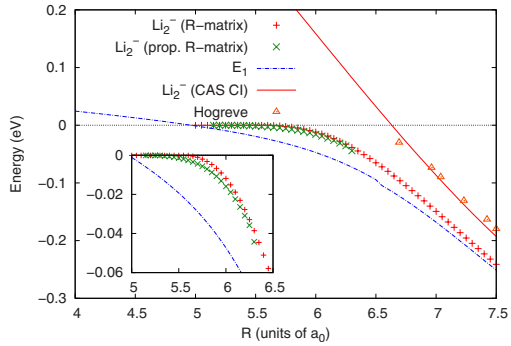

FIG. 3. (Color online) Energy of the $^2\Sigma_g^+$ negative ionic state as a function of the internuclear distance. Calculation using polarization potential (propagated R-matrix) in the outer region is compared with calculation neglecting the electron-molecule interaction outside the box (R-matrix). For comparison the lowest R-matrix pole (E_1) calculated on the inner region boundary is plotted. CAS-CI calculations of the $^2\Sigma_g^+$ negative ionic state in the cc-pVTZ GTO basis are compared with previous calculations by Hogreve [6]. All curves are plotted relatively to the $^1\Sigma_g^+$ ground-state curve.

maining three active electrons from these references cover all the space of triple excitations. In the second step, all the configurations with more than one electron in the continuum, were deleted. This approach is consistent with calculation of the target states as described above. In our calculation of the R-matrix we included 50 lowest $N+1$ particle states. Inclusion of additional states did not show considerable influence on the cross sections and eigenphases.

IV. RESULTS

We performed the R-matrix calculations of the elastic electron scattering off the Li_2 molecule for internuclear separations from $R=3a_0$ to $R=7.5a_0$ in the ^2A_g irreducible representation. The lowest R-matrix poles as functions of R are shown in Fig. 2 together with the lowest target potential curves. All the curves are plotted relatively with respect to the ground-state energy of the target. Since the calculations were performed in the subgroup of the true symmetry point group of Li_2, our poles include symmetries $^2\Sigma_g^+$ and $^2\Delta_g$. The lowest two R-matrix poles (E_1,E_2) in Fig. 2 correspond to $^2\Sigma_g^+$ symmetry, while the eigenstate corresponding to E_3 has $^2\Delta_g$ symmetry and crosses another $^2\Sigma_g^+$ pole (E_4). The lowest $^2\Sigma_g^+$ lines show two blurred avoided crossings suggesting a pole in the S-matrix which turns into a bound state with increasing R. This pole is discussed in Sec. IV B. The lowest $^2\Delta_g$ curve is almost parallel with the target ground-state curve. Its energy 0.406 eV above the target ground-state energy at $R=3a_0$ slowly changes with increasing R to 0.395 eV at $R=7.5a_0$. These values are close to the lowest pole (0.421 eV) of the potential-free R-matrix in the same box calculated for $l=2$. This suggests that the contribution of the $^2\Delta_g$ component to the ^2A_g scattering will be very small for energies below 0.4 eV.

A. Negative ionic bound state

The R-matrix method allows for the determination of negative ionic bound states as far as they exist. Corresponding equations can be found in [28] and more recently in [29]. Since the method ensures the correct asymptotic behavior of the wave function, it is suitable for description of bound states with very small electron detachment energies. Our calculation shows existence of a stable negative ion for internuclear separations larger than a certain value R_b. The $^2\Sigma_g^+$ bound state energy as a function of the internuclear distance is plotted in Fig. 3. This figure shows that inclusion of the polarization potential outside the sphere decreases the energy by very small values (less than 10 meV) when compared with results obtained under neglecting of the electron-molecule interaction outside the sphere. The conspicuously flat character of both potential curves close to R_b is a consequence of the correct asymptotic behavior of the corresponding wave functions. To emphasize its effect we performed a CAS-CI calculation of this anionic state in the cc-pVTZ GTO basis set (Fig. 3). In this calculation two lowest MOs were kept doubly occupied and all the excitations of the remaining three electrons giving the required symmetry of the total wave function were allowed. The results are in good agreement with previously presented potential curves [6]. Calculated energies are systematically higher than the R-matrix results and in particular, the slope of the CI potential does not display any feature similar to the R-matrix results in the neighborhood of the autodetachment limit. This difference can be explained by lack of diffuse basis functions in the CI calculation.

Typically, in R-matrix calculations an anionic bound state is accompanied by a negative R-matrix pole lying below the bound state energy. Figure 3 shows the lowest pole in the present R-matrix calculation as a function of the internuclear separation. As this pole provides a low boundary of the anionic bound state energy, its crossing point with target ground-state potential curve R_x can be taken from a left-hand boundary of R_b. The small slope of the anionic bound state

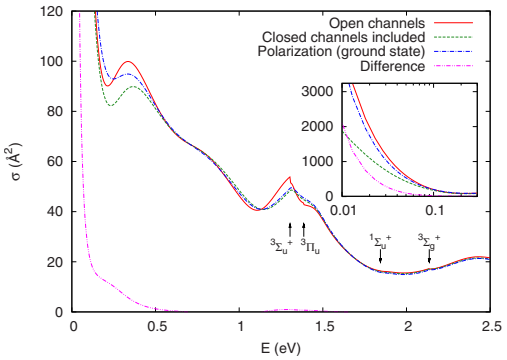

FIG. 4. (Color online) Elastic scattering cross sections in the ^2A_g symmetry at the equilibrium internuclear separation $R=5.05a_0$. Calculation in the open channels, results including coupling with the closed channels and long-range polarization outside the box using polarizability of the target ground state. The lowest curve is the difference between the cross section including the polarization potential and cross section including the closed channels. The arrows with labels denote thresholds of the corresponding channels.

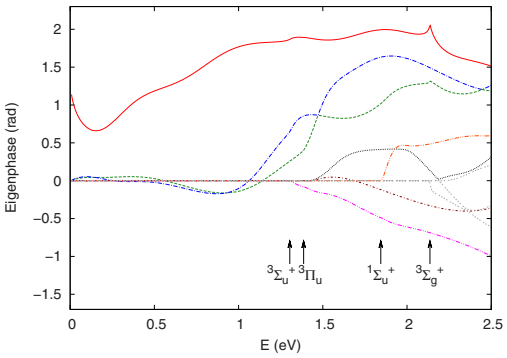

FIG. 5. (Color online) The eigenphases for the equilibrium internuclear separation $R=5.05a_0$ calculated including the long-range polarization potential using the target ground-state polarizability. The arrows with labels denote thresholds of the corresponding channels. The eigenchannel corresponding to the solid line is predominated by the s-wave component at energies below 0.3 eV.

potential curve in our calculations complicates the precise determination of R_b. In our calculation, the value R_b cannot be distinguished from R_x, even when the electron-molecule interaction outside the sphere is neglected. Therefore, R_x appears to be a good approximation of R_b, at least in the present calculations. We determined $R_b \sim 5.0a_0$ in the case when the electron-molecule interaction was neglected in the outer region and $R_b \sim 5.15a_0$ when the polarization potential outside the R-matrix sphere was included.

B. Cross sections and phase shifts

The elastic scattering cross sections for the equilibrium internuclear separation $R_e=5.05a_0$ are plotted in Fig. 4. Three different treatments of the projectile outside the R-matrix sphere are compared in this graph. The R-matrix for any given energy includes all considered scattering channels, regardless whether they are open or closed. In the calculation represented by the solid line the external potential was set to zero and the coupling between open and closed channels [29] was not taken into account. The dashed line in Fig. 4 was again calculated using zero potential outside the sphere but including the coupling with closed channels and by projection onto open channels [29]. The remaining dotted-dashed line in Fig. 4 was calculated using the R-matrix propagation in the polarization potential to distance $a_p=100a_0$, where the polarization potential can be neglected. The coupling of the open channels with closed channels is negligible at this distance as well, therefore it was not necessary to combine the R-matrix propagation with treatment of the closed channels [29]. This cross section was obtained using the target ground-state polarizability only. Inclusion of the excited target states polarizabilities (Table III) did not show any visible influence.

For energies above 1.5 eV all the cross sections are in very good agreement. The propagation takes into account not only the long-range polarization effects but also the closed channels. Therefore, the influence of the polarization to the cross sections can be estimated by the difference between the curve obtained after propagating the R-matrix and the curve including closed channels. This difference is plotted in Fig. 4 as well. It clearly shows that the polarization becomes important for energies below 0.5 eV. In addition, an enhancement can be observed in the region around two lowest electronic excitation thresholds. However, the major effect of the propagation at this threshold is due to the inclusion of closed channels.

The structure around 0.3 eV which appears in all three curves is provided by the dominating eigenphase which shows a pronounced minimum at these energies in all the treatments of the projectile considered (see Fig. 5 for propagated R-matrix results). This minimum may be a consequence of a change in the angular dependence of the wave function corresponding to this eigenchannel. While this wave function has almost pure s-wave character at lower energies, the d_0 and d_2 contributions merge into the wave function at higher energies. This s-d interaction is obviously enhanced by the R-matrix propagation leading to a flatter minimum and a weakening of the corresponding structure in the cross section.

A question with respect to the threshold behavior of the curves discussed remains open. While the large effect of the polarizability at the threshold is expected, the strong influence of the closed channels and the unexpected good agreement between the open-channel approach and propagation cannot be explained yet.

The corresponding eigenphases for calculation including the ground-state polarizability are plotted in Fig. 5. It shows a resonance very close to energy 1.5 eV as a well pronounced increase in the corresponding eigenphase. The detailed analysis of the eigenphases as well as of the R-matrix

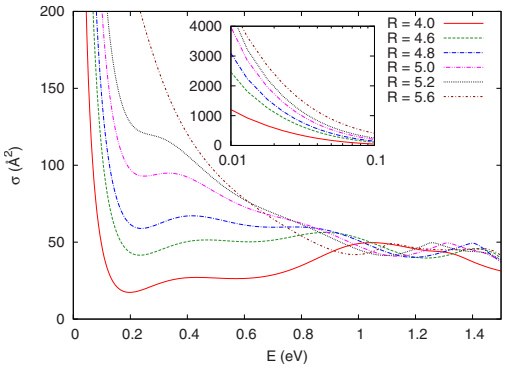

FIG. 6. (Color online) The ^2A_g elastic scattering cross section calculated for several internuclear distances (in units of a_0) around the equilibrium geometry. For low energies the lower curves correspond to smaller internuclear distances.

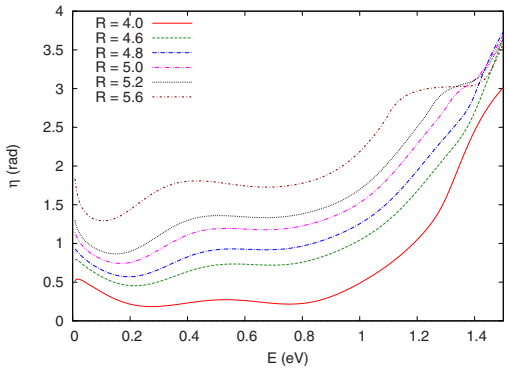

FIG. 7. (Color online) The ^2A_g eigenphase sum at several internuclear distances (in units of a_0) around the equilibrium geometry including the long-range polarization potential using the target ground-state polarizability. For low energies the lower curves correspond to shorter internuclear separations.

poles shows that this resonance has $^2\Delta_g$ symmetry and is of the Feshbach nature. The eigenphases plotted in Fig. 5 do not show any indication of a Feshbach resonance at the energy 0.34 eV for equilibrium geometry predicted by Michels *et al.* [4].

For energies below the $1\,^3\Sigma_u^+$ channel threshold the scattered-electron wave function is a linear combination of the s, d_0, and d_2 waves. The d_2 wave contributes to the $^2\Delta_g$ scattering only, while the remaining waves contribute to the $^2\Sigma_g^+$ scattering. Detailed analysis of the K-matrices for energies below 0.3 eV shows that the eigenchannel corresponding to the largest eigenphase in Fig. 5 is predominated by the s-wave component in this energy interval and contribution of the d_0 wave to the $^2\Sigma_g^+$ elastic cross section is negligible.

The CI expansions of few lowest R-matrix eigenstates (1) for the equilibrium geometry consist of configurations where the projectile occupies one of the COs or virtual MOs. Both types of configurations contribute to the wave function with comparable weights. The leading configuration including MOs only is $1\sigma_g^2, 1\sigma_u^2, 2\sigma_g^2, 3\sigma_g^1$. It is the same configuration which provides the major contribution to the negative ionic ground-state wave function in the CI calculations performed in the target basis set only (see Sec. IV A). The lowest R-matrix eigenstates for other internuclear separations show this character as well.

The elastic scattering cross sections calculated for different geometries using the R-matrix propagation in the polarization potential are showed in Fig. 6. Corresponding eigenphase sums are plotted in Fig. 7. None of these graphs show formation of any structures with change of the geometry that could be interpreted as the resonance turning into the bound state. In order to emphasize the large elastic scattering cross sections at very low energies, the eigenphase sums calculated below 5 meV at several internuclear separations are plotted in Fig. 8. As the graph shows, for geometries R smaller than R_b, the eigenphases raise more rapidly with increasing internuclear distance to some maximum. This maximum moves towards lower energies and its value approaches $\pi/2$ as $R \to R_b$. The phases in Fig. 8 are plotted in such way that they approach zero at threshold energy for $R < R_b$ and π for $R > R_b$. The rapid changes plotted in Fig. 8 at geometries close to R_x and R_b lead to large elastic scattering cross sections plotted in Fig. 6.

Figure 9 shows comparison of our elastic cross sections for the equilibrium geometry using the ground-state polarizability only with previously presented calculations. Another calculation using the molecular R-matrix with pseudostates (MRMPS) method was carried [13] parallel with the present work. Figure 9 shows that our present results are in quite good agreement with the MRMPS calculations [13] for energies above 0.1 eV although there are some small differences in structures at higher energies. These discrepancies might be caused by missing higher partial waves in our present continuum basis set which are present in the MRMPS calculations [13]. The differences at energies below 0.1 eV might be due to different treatment of the long-range

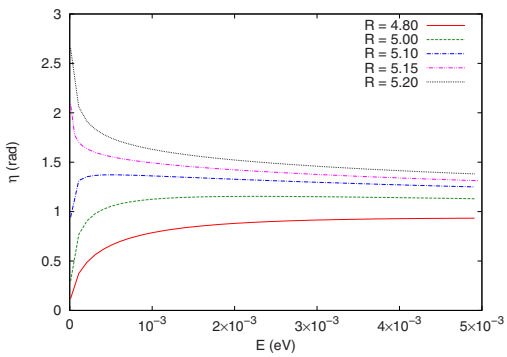

FIG. 8. (Color online) The eigenphase sums for very low energies at several geometries calculated using the R-matrix propagation. The lower curves correspond to shorter internuclear separations.

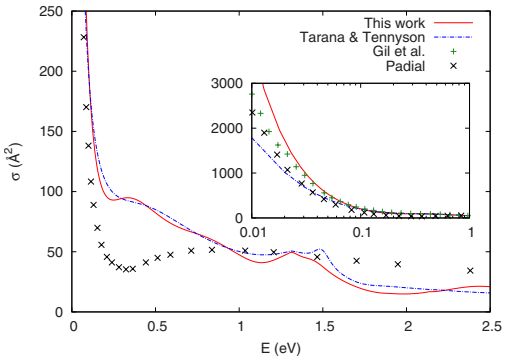

FIG. 9. (Color online) The ^2A_g elastic cross section at the equilibrium internuclear separation calculated using the target ground-state polarizability. MRMPS calculations due to Tarana and Tennyson [13]. Previously presented calculations of Gil *et al.* [10] ($^2\Sigma_g^+$ symmetry) and Padial [9] ($^2\Sigma_g^+$ was added to $^2\Delta_g$ symmetry).

polarization effects and due to different target representation. However, the correspondence of our present calculations to [13] suggests that the most important long-range effects in the electron scattering at low energies are represented by the ground-state target polarizability and coupling of open and closed channels as discussed above. A negligible contribution of the $^2\Delta_g$ scattering for small energies enables the comparison of our ^2A_g cross sections with $^2\Sigma_g^+$ cross sections taken from [10]. The differences between our results and [10] (also plotted in Fig. 9) is also mainly due to different target representation and polarizability treatment. Gil *et al.* [10] found that their results strongly depend on the MOs basis used for energies below 0.1 eV. Figure 9 shows results of Padial [9] as well. Contrary to our calculations, Padial [9] does not take into account effects of any electronically excited channels. This might explain the differences from our results above 1.5 eV. In addition, Padial [9] uses a cutoff polarization potential and her results are strongly dependent on the cutoff parameter for energies below 1 eV. This might be the reason for differences from our results at low energies. Miller *et al.* [7] measured total rather than just elastic cross sections. This experiment was performed using a beam of Li_2 at about 1000 K. Since we restricted our calculation to fixed-nuclei elastic scattering in ^2A_g symmetry, the cross sections obtained cannot be compared directly with results of Miller *et al.* [7]. However, the pronounced threshold peak present in our calculations was also observed in experiment. The measured cross sections exceed values obtained in our calculations.

V. CONCLUSIONS

We performed *R*-matrix calculations of ^2A_g elastic electron collision with Li_2 in the fixed-nuclei approximation for a set of different internuclear separations using the *R*-matrix codes due to Nestmann [14]. Several different approaches to the treatment of the polarization potential in the outer region were compared and we studied effects of the closed electronically excited channels. This study of the effects in the outer region is complementary to the previous work [13]. Our results show that the *R*-matrix propagation in the polarization potential represented by the target ground-state polarizability provides a good treatment of the polarization effects in the outer region.

We also confirm the presence of a Feshbach resonance at 1.5 eV found in another work [13] performed parallel with the present calculations. In general results of the MRMPS calculations [13] using different treatment of polarization and using different *R*-matrix sphere are in good agreement with the present work. On the other hand, the internuclear separation R_b where the $^2\Sigma_g^+$ negative ionic state becomes bound found in this work is different from previous results [6]. Presence of the low-lying $^2\Sigma_g^+$ Feshbach resonance also does not correspond to our results. On the other hand, a low-lying shape resonance was found in previous works [9,10,13] at the equilibrium geometry. Regarding these facts, previous calculations due to Wedehra [11] should be reconsidered and the nuclear dynamics of the nonelastic processes like DEA and VE should be studied using results presented in this work and in [13]. This is the prospect of our forthcoming work.

ACKNOWLEDGMENTS

The authors would like to acknowledge Professor Roland Lindh for his contribution to the Molcas package which enables its use in *R*-matrix calculations and Dr. Vincent Brems for his contribution to the *R*-matrix codes. M.T. would like to acknowledge Dr. Michael Hanrath and Dr. Ivana Paidarová for stimulating discussions of the DIESEL program use and of the methods for calculations of the polarizabilities. This work is partially supported by the ESF EIPAM exchange Grant No. 1296, by the Grant No. GAUK 116-10/257718, and by the Center of Theoretical Astrophysics LC06014 of the Ministry of Education, Youth and Sports of the Czech Republic.

[1] M. Mérawa and M. Rérat, Eur. Phys. J. D **17**, 329 (2001).
[2] D. Konowalow and J. Fish, Chem. Phys. **84**, 463 (1984).
[3] R. Molof, T. M. Miller, H. Schwartz, B. Bederson, and J. Park, J. Chem. Phys. **61**, 1816 (1974).
[4] H. H. Michels, R. H. Hobbs, and L. A. Wright, Chem. Phys. Lett. **118**, 67 (1985).
[5] H. Sarkas, S. Arnold, J. Hendricks, V. Slager, and K. Bowen, Z. Phys. D: At., Mol. Clusters **29**, 209 (1994).
[6] H. Hogreve, Eur. Phys. J. D **8**, 85 (2000).
[7] T. M. Miller, A. Kasdan, and B. Bederson, Phys. Rev. A **25**, 1777 (1982).
[8] M. W. McGeoch and R. E. Schlier, Phys. Rev. A **33**, 1708

(1986).
[9] N. T. Padial, Phys. Rev. A **32**, 1379 (1985).
[10] T. J. Gil, C. W. McCurdy, T. N. Rescigno, and B. H. Lengsfield, Phys. Rev. A **47**, 255 (1993).
[11] J. M. Wadehra, Phys. Rev. A **41**, 3607 (1990).
[12] T. J. Gil, B. H. Lengsfield, C. W. McCurdy, and T. N. Rescigno, Phys. Rev. A **49**, 2551 (1994).
[13] M. Tarana and J. Tennyson, J. Phys. B **41**, 205204 (2008).
[14] K. Pfingst, B. Nestmann, and S. Peyerimhoff, J. Phys. B **27**, 2283 (1994).
[15] M. LeDourneuf, B. I. Schneider, and P. G. Burke, J. Phys. B **12**, L365 (1979).
[16] P. Burke and J. Tennyson, Mol. Phys. **103**, 2537 (2005).
[17] K. Baluja and P. Burke, Comput. Phys. Commun. **27**, 299 (1982).
[18] A. Boardman, A. Hill, and S. Sampanthar, Phys. Rev. **160**, 472 (1967).
[19] T. Dunning, J. Chem. Phys. **90**, 1007 (1989).
[20] R. Buenker and S. Peyerimhoff, Theor. Chim. Acta **35**, 33 (1974).
[21] R. Buenker and S. Peyerimhoff, Theor. Chim. Acta **39**, 217 (1975).
[22] M. Hanrath and B. Engels, Chem. Phys. **225**, 197 (1997).
[23] M. Hanrath, J. Chem. Phys. **123**, 084102 (2005).
[24] W. Müller and W. Meyer, J. Chem. Phys. **85**, 953 (1986).
[25] Dalton, a molecular electronic structure program, release 2.0, 2005, http://www.kjemi.uio.no/software/dalton/dalton.html
[26] M. Tarana and J. Horáček, J. Chem. Phys. **127**, 154319 (2007).
[27] V. Brems, T. Beyer, B. Nestmann, H. Meyer, and L. Cederbaum, J. Chem. Phys. **117**, 10635 (2002).
[28] P. G. Burke and W. D. Robb, in *Advances in Atomic and Molecular Physics*, edited by D. R. Bates (Academic, New York, 1975), Vol. 11, pp. 144–211.
[29] B. M. Nestmann and T. Beyer, Chem. Phys. **343**, 281 (2008).

Chapter 3

Effects of multiple vibrational modes in the DEA and VE

In previous chapters we discussed the calculations of the electron collisions with small molecules in the fixed nuclei approximation. We showed several interesting applications for diatomic molecules. In this chapter we will concentrate our attention on the theoretical treatment of the nuclear dynamics of the DEA and VE using the LCP approximation. The methods discussed in previous chapter are used to provide the resonance widths and positions used in the LCP calculations, although in the work presented here, these data were obtained in different way.

3.1 Dissociative electron attachment

Almost all of the DEA calculations published so far include only one vibrational mode representing the reaction coordinate. To the best of our knowledge, there are only few exceptions including model calculations of the DEA to CO_2 [28], *ab initio* calculations for water [29], ClCN and BrCN [30], and recent study of the DEA to the C_2H_2 molecule [31]. All these calculations were carried out within the framework of the LCP theory. Many DEA calculations for polyatomic molecules have been performed using an approximation of "frozen" fragments. However, the role of other vibrational modes than the reaction one has not been investigated so far. The mode coupling effects are well known in molecular spectroscopy and photodissociation dynamics, but they are relatively less studied in DEA processes. In particular, it is not clear if all the other coordinates should be fixed

in these calculations or optimized in terms of the least energy value. According to the Franck-Condon principle, the nuclear geometry should not change during the electron capture, therefore from this point of view other coordinates should not be optimized, but rather fixed at the values corresponding to the nuclear configuration of the neutral molecule. However, after the initial capture, when two fragments (anion and neutral radical) separate, all nuclear coordinates evolve. The paper presented in this chapter addressed this problem for polyatomic molecules. We have chosen CF_3Cl to study the resonance process

$$e + CF_3Cl(\nu_2, \nu_3) \rightarrow CF_3Cl^- \rightarrow CF_3(\nu_2') + Cl^-. \tag{3.1}$$

Here ν_2 and ν_3 stand for the symmetric deformation vibrations (so-called "umbrella" mode) and the symmetric stretch vibrations, ν_2' represents the umbrella mode of the free CF_3 radical. At this point we restrict our considerations to one mode only, in addition to the reaction mode ν_3. Inclusion of additional vibrational modes in description of the DEA to CF_3Cl is of interest due to two reasons:

- First, it allows us to study the distribution of the internal energy of the fragment, in our case the energy of the umbrella mode in the CF_3 radical. This energy can be significant due to a large Franck-Condon factor of the transition from the initial vibrational state of CF_3Cl to the excited umbrella vibrational mode of the intermediate anion CF_3Cl^- or due to the final-state interaction between Cl^- and CF_3 redistributing the internal energy of CF_3.
- The second motivation for study of the DEA with inclusion of the vibrational umbrella mode is the strong sensitivity of the DEA cross section to the initial vibrational state of the target, or to the initial vibrational temperature. The one-mode approximation fails [32, 33] to give the correct quantitative description of the observed temperature dependence [34] of the low-energy peak in the DEA to CF_3Cl. There are experimental indications that the umbrella mode in perfluoromethyl halides can be important in the mechanism responsible for the high sensitivity of the DEA cross sections to the initial vibrational state of the target.

In the Introduction we mentioned that it is possible to obtain the diabatic complex potential energy surfaces necessary for calculation of the nuclear dynamics from the fixed-nuclei scattering calculations performed for a set of nuclear geometries. However, due to technical issues with the electron correlation treatment in the R-matrix fixed-

nuclei calculations we decided for different approach. For construction of the real part of the LCP, potential energy surface of the negative ion calculated by Roszak et al. [35] was used. In their work, Roszak et al. [35] used the methods of quantum chemistry for bound states to obtain the positions of the resonance. The imaginary part of the LCP (resonance width) was taken from the previous one-dimensional calculations [32] and arbitrarily, athough reasonably, extended to two dimensions. In the fixed-nuclei scattering calculations, the resonance position and width are both usually determined from the eigenphase sum or scattering cross section. However, in the work included below we take these quantities from different sources. Because of this model approach, we did not expect the present calculations to improve the quantitative agreement with experimental data. Rather, we aimed to investigate the effect of the additional vibrational mode on the final-state energy distribution and the magnitude of the total cross section.

PHYSICAL REVIEW A **79**, 052712 (2009)

Effects of two vibrational modes in the dissociative electron attachment to CF_3Cl

Michal Tarana,[1,2,*] Pawel Wielgus,[3] Szczepan Roszak,[3] and Ilya I. Fabrikant[2,†]
[1]*Institute of Theoretical Physics, Faculty of Mathematics and Physics, Charles University in Prague, V Holešovičkách 2, 18000 Prague, Czech Republic*
[2]*Department of Physics and Astronomy, University of Nebraska, 510 Stadium Drive, Lincoln, Nebraska 68588, USA*
[3]*Institute of Physical and Theoretical Chemistry, Wroclaw University of Technology, Wyb. Wyspianskiego 27, 50-370 Wroclaw, Poland*
(Received 23 March 2009; published 28 May 2009)

We present a study of multimode effects in dissociative electron attachment to CF_3Cl molecules using a time-independent version of the local complex potential theory. Symmetric stretch C-Cl vibrations ν_3 and symmetric deformation (or so-called umbrella) vibrations ν_2 are included. The neutral and anion potential energy surfaces are calculated using the second-order Møller-Plesset perturbation theory with an empirical adjustment of the vertical attachment energy. The final-state vibrational distribution in the $CF_3(\nu_2)$ fragment is dominated by the $\nu_2=2$ state. We also find an increase in the total cross section as compared with the one-dimensional calculations. This is explained by an increase in the anion survival probability.

DOI: 10.1103/PhysRevA.79.052712 PACS number(s): 34.80.Ht, 34.80.Lx

I. INTRODUCTION

Almost all of the dissociative electron attachment (DEA) calculations performed so far include only one vibrational mode representing the reaction coordinate. To the best of our knowledge, the only three exceptions are model calculations of the DEA to CO_2 [1], *ab initio* calculations for water [2], and recent study of the DEA to the C_2H_2 molecule [3]. All these calculations were carried out within the framework of the local complex potential (LCP) theory. In view of the tremendous amount of computational work necessary to obtain multidimensional complex potential energy surfaces and the solution of the multidimensional Schrödinger equation for the nuclear motion, it is apparent that the way to solve the DEA problems for molecules with more than three atoms is to make further (in addition to local) approximations. The one most common is to "freeze" all modes other than one corresponding to the reaction coordinate. Many calculations for polyatomic molecules have been performed in this way. However, the role of other modes in these calculations has not been investigated so far. The mode coupling effects are well known in molecular spectroscopy and photodissociation dynamics, but they are relatively less studied in DEA processes. In particular, it is not clear if all the other coordinates should be fixed in these calculations or optimized (in terms of the least energy value). According to the Franck-Condon principle, the nuclear geometry should not change during the electron capture, therefore from this point of view other coordinates should not be optimized, but rather fixed at the values corresponding to the nuclear configuration of the neutral molecule. However, after the initial capture, when two fragments (anion and neutral radical) separate, all nuclear coordinates evolve.

This paper presents an attempt to solve this problem for polyatomic molecules. We have chosen CF_3Cl to study the resonance process

$$e + CF_3Cl(\nu_2,\nu_3) \rightarrow CF_3Cl^- \rightarrow CF_3(\nu_2') + Cl^-. \qquad (1)$$

Here ν_2 and ν_3 stand for the symmetric deformation vibrations (so-called "umbrella" mode) and the symmetric stretch vibrations, ν_2', represent the umbrella mode of the free CF_3 radical. At this point we restrict our considerations to one mode only, in addition to the reaction mode ν_3. This restriction can be justified by the same reasoning as that given by Shapiro and Bershon [4] in their studies of photodissociation of CH_3I. First, the intermediate anionic state responsible for the DEA at low energies has A_1 symmetry, therefore degenerate vibrations ν_4, ν_5, and ν_6 of the e type can be excited resonantly only in pairs. (They can also be excited directly due to the transition dipole moment, but this should not significantly affect the pure resonant DEA process.) Second, the C-F bond length $R_{FC}=1.34$ Å [5] is very close to that for the anion, 1.37 Å [5] and free CF_3 radical, 1.32 Å [6]. Therefore, we can assume that the C-F symmetric stretching mode ν_1 is unlikely to be excited as well. These assumptions are confirmed by measurements of Mann and Linder [7] who observed strong electron-impact vibrational excitation of the ν_3 and ν_2 modes in the A_1 resonance region, whereas other modes were not significantly excited.

Inclusion of additional vibrational modes in description of the DEA to CF_3Cl is of interest due to two reasons. First, it allows us to study the distribution of the internal energy of the fragment, in our case the energy of the umbrella mode in the CF_3 radical. This energy can be significant due to a large Franck-Condon factor of the transition from the initial vibrational state of CF_3Cl to the excited umbrella vibrational mode of the intermediate anion CF_3Cl^- or due to the final-state interaction between Cl^- and CF_3 redistributing the internal energy of CF_3. Studies of the Rydberg electron attachment to CH_3I, CF_3I, and CF_3Br molecules [8] showed that at high principal quantum number n (or at low electron energies) the major portion of the energy released by electron capture appears in translation, indicating insignificance of the internal energy redistribution in the final state. However, at lower n (or higher electron energies) the final-state interaction becomes important [9–11], although there are no

*tarana@mbox.troja.mff.cuni.cz
†iif@unlserve.unl.edu

quantitative theoretical or experimental results of the radical fragment internal energy redistribution.

The second motivation for study of the DEA with inclusion of the vibrational umbrella mode is the strong sensitivity of the DEA cross section to the initial vibrational state of the target or to the initial vibrational temperature. The one-mode approximation explains quite well the observed temperature dependence of the DEA in electron collisions with methyl halides [12,13]. However, it fails [14,15] to give the correct quantitative description of the observed temperature dependence [16] of the low-energy peak in the DEA to CF_3Cl. Recent joint experimental and theoretical work on the DEA to CF_3Br [17] demonstrates that the DEA rate calculated in the one-mode approximation gives a slower growth at high temperatures than that observed. This indicates that the umbrella mode in perfluoromethyl halides is more important than in methyl halides. This is consistent with the fact that corresponding vibrational quanta are lower in perfluoromethyl halides (e.g., compare 168 meV in CH_3Cl with 97 meV in CF_3Cl). Therefore, the excited umbrella mode is more populated there than in methyl halides.

The aim of this work is to study the effects of additional vibrational mode in the DEA to the CF_3Cl molecule and to compare the results with the one-dimensional treatment. In all our calculations we are using a model resonance width from the previous one-dimensional calculations [14] which is arbitrarily, although reasonably, extended to two dimensions. Because of this model approach, we do not expect the present calculations to improve the quantitative agreement with experimental data. Rather, we aim to investigate the effect of the additional vibrational mode on the final-state energy distribution and the magnitude of the total cross section.

This paper is organized as follows: In Sec. II we describe our theoretical model and methods used to solve the corresponding equations, in Sec. III we describe the potentials used in our calculations, and in Sec. IV we discuss the results of the two-dimensional and one-dimensional calculations. Atomic units are used throughout the paper.

II. THEORETICAL APPROACH

In the present work we employ the LCP theory [18–20] of the DEA. Since the nonlocal calculations are rather complicated even in the one-dimensional case, it is desirable to get the results using a simpler approach as a first step. In addition, the A_1 shape resonance in CF_3Cl appears at a relatively high energy 1.83 eV [21] and it is rather narrow (the width about 0.6 eV). This justifies the use of the local theory for CF_3Cl. Another justification is given by the comparison of our local calculations with previously published nonlocal results [14,15] as discussed below in Sec. IV A.

A. Coordinates and Hamiltonian

In our calculations the potential energy surfaces V and U for the neutral molecule CF_3Cl and the anion CF_3Cl^- are represented using two coordinates: C-Cl internuclear separation R and the distance between the C atom and the plane formed by the fluorine atoms $r=-R_{CF}\cos\theta$, where θ is the F-C-Cl angle and R_{FC} is the F-C bond length. Since we do not include the C-F stretching mode into our considerations, R_{CF} is fixed and set to the value 1.342 Å corresponding to the equilibrium geometry of the neutral CF_3Cl. We take all the potentials relatively to the equilibrium potential energy of the neutral molecule. Asymptotically ($R\to\infty$) both surfaces are represented by the harmonic approximation $D_e+k(r-r_m)^2/2$ for the neutral molecule and $D_e+k(r-r_m)^2/2-E_A$ for the anion, where k and r_m are the force constant of the umbrella mode and equilibrium value of r for the free CF_3 radical, D_e is the dissociation energy of the C-Cl bond, and E_A is the electron affinity of the Cl atom.

The classical kinetic energy for the nuclear motion taking into account the degrees of freedom described above can be derived from the general Hamiltonian for XY_3Z molecules [22] by fixing of all variables except R and r. In addition, we assume in the present work that the approximation of harmonic oscillations with small amplitude is suitable for the CF_3 umbrella motion. In principle, the angle θ_0 corresponding to the equilibrium geometry of the CF_3 radical at given R changes with the C-Cl distance. However, the potential surfaces show that this dependence is rather weak and enables us to assume that θ_0 is constant and take its value at the equilibrium geometry of the neutral CF_3Cl. Then we can write the classical kinetic energy in the following form:

$$T=\frac{1}{2}\mu_\rho\dot{R}^2+\frac{3}{2}m_F\left(\cot^2\theta_0+\frac{m_C+m_{Cl}}{M}\right)\dot{r}^2+\frac{3m_{Cl}m_F}{M}\dot{R}\dot{r}, \tag{2}$$

where m_C, m_{Cl}, and m_F are the masses of corresponding atoms, $M=m_C+m_{Cl}+3m_F$ is the total mass of the molecule, and $\mu_\rho=m_{Cl}(m_C+3m_F)/M$ is the reduced mass for the relative motion of the Cl atom and the CF_3 radical. All our calculations were performed in the following reaction coordinates [4] ρ and r which decouple kinetic energy (2),

$$\rho=R+\eta r,\quad \eta=\frac{3m_F}{m_C+3m_F}, \tag{3}$$

and r remains unchanged. The reaction coordinate ρ is simply the distance between the center of mass of the CF_3 radical and the Cl atom. Corresponding linear operator of the kinetic energy can be written in the reaction coordinates as follows:

$$T_\rho+T_r=-\frac{1}{2\mu_\rho}\frac{\partial^2}{\partial\rho^2}-\frac{1}{2\mu_r}\frac{\partial^2}{\partial r^2}, \tag{4}$$

where

$$\mu_r=3m_F\left(\cot^2\theta_0+\frac{m_C}{m_C+3m_F}\right). \tag{5}$$

As long as we are not dealing with the DEA to CF_3Cl in vibrationally highly excited states, we can use the harmonic approximation for $V(\rho,r)$ and diagonalize the Hamiltonian $H=T_\rho+T_r+V$. This gives us the normal frequencies and

normal-mode coordinates expressed as linear combinations of $\rho-(R_0+\eta r_0)$ and $r-r_0$, where R_0 and r_0 are the equilibrium coordinates of the neutral molecule.

B. Local theory of the dissociative electron attachment

We start the derivation of the formula for the DEA cross sections using the basic equation for the nuclear wave function $\chi_E(\rho,r)$ in the LCP approximation [18,19]:

$$[T_\rho + T_r + U(\rho,r) - i\Gamma(\rho,r)/2 - E]\chi_E(\rho,r) = V_{dk}(\rho,r)\zeta_i(\rho,r), \tag{6}$$

where $V_{dk}(\rho,r)=\sqrt{\Gamma(\rho,r)/2\pi}$ is the amplitude for electron capture into the resonance state, $\zeta_i(\rho,r)$ is the vibrational wave function of the neutral molecule in the initial state, and $U(\rho,r)$ represents the anionic potential surface.

To solve Eq. (6), we expand $\chi_E(\rho,r)$ in a basis depending on r only [4]. Specifically, we select the eigenfunctions of the vibrational Hamiltonian for the CF_3 fragment [note that $\Gamma(\infty,r)=0$]:

$$[T_r + V^{\mathrm{h}}(\infty,r) - \epsilon_\nu]\phi_\nu(r) = 0, \tag{7}$$

where ϵ_ν are the corresponding eigenenergies $\epsilon_\nu=D_e+\omega_2^f(\nu+1/2)$, ω_2^f is the harmonic frequency of the CF_3 radical umbrella mode, and $V^{\mathrm{h}}(\infty,r)$ is the corresponding free CF_3 radical potential curve in the harmonic approximation with the minimum corresponding to the C-Cl bond dissociation energy. Thus, the expansion has the form

$$\chi_E(\rho,r) = \sum_\nu \psi_\nu(\rho)\phi_\nu(r). \tag{8}$$

Projection of Eq. (6) on the functions $\phi_\nu(r)$ yields the following system of coupled differential equations for functions $\psi_\nu(\rho)$:

$$[T_\rho + \epsilon_\nu - E]\psi_\nu(\rho) + \sum_{\nu'} U_{\nu\nu'}(\rho)\psi_{\nu'}(\rho) = \lambda_{i\nu}(\rho), \tag{9}$$

where

$$U_{\nu\nu'}(\rho) = \int \phi_\nu(r)[U(\rho,r) - i\Gamma(\rho,r)/2 - V^{\mathrm{h}}(\infty,r)]\phi_{\nu'}(r)dr, \tag{10}$$

$$\lambda_{i\nu}(\rho) = \int V_{dk}(\rho,r)\zeta_i(\rho,r)\phi_s(r)dr. \tag{11}$$

Expansion (8) defines the channels corresponding to the vibrational states of the free CF_3 radical. We solve system of equations (9) with the outgoing-wave boundary condition at $\rho\to\infty$,

$$\frac{d\psi_\nu(\rho)}{d\rho} \sim iK_\nu\psi_\nu(\rho), \tag{12}$$

where $K_\nu^2=2\mu_\rho(E-\epsilon_\nu)$. In case of the energetically closed channels we take the asymptotically decaying condition. The DEA cross section corresponding to the CF_3 fragment in the vibrational state with the quantum number ν can be written as follows [18–20]:

$$\sigma_\nu = \frac{2\pi^2}{k^2}\frac{K_\nu}{\mu_\rho}\lim_{\rho\to\infty}|\psi_\nu(\rho)|^2, \tag{13}$$

where $k^2/2$ is the initial electron energy. As it is well known, Eq. (13) is not consistent with the Wigner threshold law at small electron energies. To repair this deficiency of the local theory, we introduce an additional correction factor [20,23] into the capture amplitude $V_{dk}(\rho,r)$:

$$c(\rho,r) = \begin{cases} \left(\dfrac{k^2}{2E_r(\rho,r)}\right)^\tau & k^2 < 2E_r(\rho,r) \\ 1 & \text{otherwise}, \end{cases} \tag{14}$$

where τ is the threshold exponent and $E_r(\rho,r)$ is the resonance energy discussed below. For s-wave capture in the absence of the dipole moment, $\tau=1/4$. It should be slightly modified for CF_3Cl. However, this correction becomes important only in the energy region close to the threshold. Our calculations showed that it does not play any significant role in the energy interval of our interest.

System of equations (9) can be solved efficiently using the Green's function for the homogeneous equations. Taking into account asymptotic condition (12), the column vector $\boldsymbol{\psi}(\rho)$ of the solutions $\psi_\nu(\rho)$ can be written in the following matrix form:

$$\boldsymbol{\psi}(\rho) = \frac{1}{2i\mu_\rho}\left\{\boldsymbol{\psi}^{(\mathbf{r})}(\rho)\int_\rho^\infty \boldsymbol{\psi}^{(+)T}(\rho')\boldsymbol{\lambda}(\rho')d\rho' + \boldsymbol{\psi}^{(+)}(\rho) \times \int_0^\rho \boldsymbol{\psi}^{(\mathbf{r})T}(\rho')\boldsymbol{\lambda}(\rho')d\rho'\right\}, \tag{15}$$

where $\boldsymbol{\lambda}(\rho)$ is the column vector of the source terms (11), the symbol T means transposition of the corresponding matrix, and $\boldsymbol{\psi}^{(\mathbf{r})}(\rho)$, $\boldsymbol{\psi}^{(+)}(\rho)$ are matrix solutions of the homogeneous coupled equations [Eq. (9) without the source term] satisfying the following asymptotic conditions at $\rho\to\infty$:

$$\boldsymbol{\psi}^{(\mathbf{r})}(\rho) \sim \boldsymbol{\psi}^{(-)}(\rho) - \boldsymbol{\psi}^{(+)}(\rho)\mathbf{S}, \tag{16a}$$

$$\psi_{\nu\nu'}^{(\pm)}(\rho) \sim \sqrt{\frac{\mu_\rho}{K_\nu}}\exp(\pm iK_\nu\rho)\delta_{\nu\nu'}. \tag{16b}$$

Here $\mathbf{S}$ is the scattering matrix. According to the standard definition of the scattering matrix, the solutions $\boldsymbol{\psi}^{(\pm)}(\rho)$ are normalized to the unit flux in each channel. According to Eqs. (16a) and (16b), the required asymptotic factor in Eq. (13) is

$$\lim_{\rho\to\infty}|\psi_\nu(\rho)|^2 = \frac{|B_\nu|^2}{4\mu_\rho K_\nu}, \tag{17}$$

where coefficients B_ν are given by the following matrix equation:

$$\mathbf{B} = \int_0^\infty \boldsymbol{\psi}^{(\mathbf{r})T}(\rho')\boldsymbol{\lambda}(\rho')d\rho'. \tag{18}$$

To find the matrix $\boldsymbol{\psi}^{(\mathbf{r})}(\rho)$, we first integrate outward the homogeneous system of coupled equations corresponding to Eq. (9) with the regular boundary conditions at the origin.

TABLE I. The harmonic frequencies (in cm^{-1}) of the CF_3Cl calculated using our two-dimensional Hamiltonian, the frequency of the umbrella mode of the CF_3 radical, and their comparison with experimental data.

	Our Hamiltonian	Experiment
ω_2	775.12	862.18 [29]
ω_3	463.33	483.07 [29]
CF_3 fragment (ω_2)	747.38	701 ± 3 [30]

We form the square matrix of the solutions $\boldsymbol{\psi}^{(\mathbf{a})}(\rho_0)$ at some intermediate distance $\rho=\rho_0$. Similarly, we obtain the solutions $\boldsymbol{\psi}^{(\pm)}(\rho)$ by the inward integration of the homogeneous coupled system of equations corresponding to Eq. (9) from the asymptotic region to $\rho=\rho_0$, where we again form the matrix of solutions satisfying the asymptotic conditions (16a) and (16b). We match this matrix with the matrix $\boldsymbol{\psi}^{(\mathbf{a})}(\rho_0)$ to find the solution of the homogeneous system satisfying both boundary conditions using the equation

$$\boldsymbol{\psi}^{(\mathbf{a})}(\rho_0)\mathbf{C} = \boldsymbol{\psi}^{(-)}(\rho_0) - \boldsymbol{\psi}^{(+)}(\rho_0)\mathbf{S} \tag{19}$$

and similar for the derivatives of the solutions. Here $\mathbf{C}$ is a matrix of coefficients which should be determined together with the $\mathbf{S}$ matrix from the matching conditions. Since the exponentially growing solutions in the closed channels are unphysical, matrices $\mathbf{C}$, $\boldsymbol{\psi}^{(-)}(\rho_0)$, and $\mathbf{S}$ are rectangular with N rows and N_0 columns, where N is the total number of the vibrational channels and N_0 is the number of the open channels. After $\mathbf{S}$ and $\mathbf{C}$ are found, the column $\mathbf{B}$ is calculated as

$$\mathbf{B} = \int_0^{\rho_0} \mathbf{C}^T \boldsymbol{\psi}^{(\mathbf{a})T}(\rho)\boldsymbol{\lambda}(\rho)d\rho + \int_{\rho_0}^{\infty} [\boldsymbol{\psi}^{(-)T}(\rho) - \mathbf{S}\boldsymbol{\psi}^{(+)T}(\rho)]\boldsymbol{\lambda}(\rho)d\rho. \tag{20}$$

III. CALCULATIONS

In our multimode calculations we used the two-dimensional surfaces of CF_3Cl and the corresponding anion calculated by the second-order Møller-Plesset perturbation theory [24]. All calculations were performed with GAUSSIAN 03 suite of codes [25] employing the Dunning's augmented correlation-consistent polarized valence-triple-zeta (cc-pVTZ) basis set [26–28]. More details are given in Ref. [5].

Since we use the two-mode approximation for the vibrational wave functions in all our calculations, it is useful to check how well our two-dimensional Hamiltonian with the potential surface of the neutral molecule reproduces the corresponding normal-mode frequencies. Comparison of our results with experimental data due to Scanlon *et al.* [29] is given in Table I. As can be seen, our two-dimensional Hamiltonian gives slightly underestimated values for the normal-modes frequencies but they are still in good agreement with experiment and justify the use of our two-dimensional treatment of the neutral CF_3Cl.

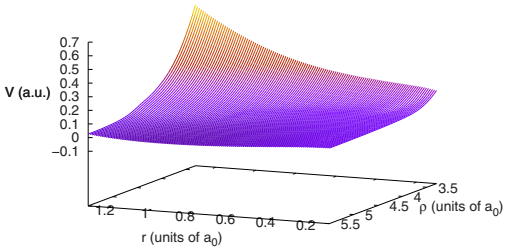

FIG. 1. (Color online) The two-dimensional anionic potential surface used in the multimode calculations. The zero potential corresponds to the minimum of the neutral target potential surface.

For the anion at $R<1.9$ Å the present calculation exhibits a kinklike behavior similar to that observed in the previously published one-dimensional calculation [14], where it was explained by variational collapse: an attempt to introduce a more diffuse basis set leads to larger contribution of the continuum states and the "collapse" of the anion energy to the neutral energy (with the zero-energy electron in the continuum). In order to remove this deficiency, we employed a semiempirical method used in several previously published calculations [13,14]: we extrapolated the calculated anionic potential surface toward smaller R so that it represents the correct vertical attachment energy, 1.83 eV, in the case of CF_3Cl [21]. The adjusted surface is plotted in Fig. 1.

In our multimode calculations the CF_3 fragment was represented by the potential curve $V(\infty,r)$ plotted in Fig. 2. The potential could be symmetrically continued toward negative values of r due to possible flip-flop of the CF_3 radical. However, in the present work we restrict our considerations to geometries of CF_3 which do not exceed the planar configuration. As can be seen in Table I, the fixation of the C-F bond in our treatment gives slightly higher vibrational frequency than previous experimental study [30].

In order to find the asymptotic solution of system of equations (9) we need to evaluate potential matrix (10) also for values of R and r exceeding the region in which the quantum

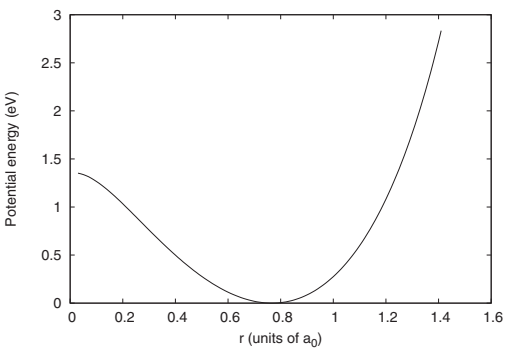

FIG. 2. The potential energy of the CF_3 radical as a function of the distance between the carbon atom and the plane of the fluorine atoms.

TABLE II. Parameters of the Morse potentials (in a.u.) used in our one-dimensional calculations taken from Ref. [14].

	β (units of a_0^{-1})	B (a.u.)	C (a.u.)	D (a.u.)
Neutral molecule	0.8507	0.1382	0.2764	0.1382
Negative ion	0.820	0.0928	0.009	−0.011

chemical calculation of the potential surfaces is available. Since the imaginary part of the potential matrix $U_{\nu\nu'}(\rho)$ vanishes outside this region, it is necessary to continue the anionic surface only. To this end we introduced the following parametrization of the surface:

$$U(R,r) = b(r)\exp[-2\beta(r)(R-R_0)] - c(r)\exp[-\beta(r)(R-R_0)] + V(\infty,r) - V(\infty,r_m) + D_e - E_a, \quad (21)$$

where r_m=0.77 a_0 is the position of the minimum of the CF_3 radical potential energy $V(\infty,r)$, D_e=4.014 eV is the C-Cl bond dissociation energy [5], and E_a=3.613 eV is the electron affinity of the Cl atom [31]. This parametrization reproduces correct asymptotic behavior in R of the anionic potential. For every fixed r it represents the Morse potential, the parameters $\beta(r)$, $b(r)$, and $c(r)$ are determined by the condition of the smooth connection between the region where the potential is given by quantum chemical calculation and the region where we use the parametrization.

In order to justify the use of the local theory of the DEA and to see the effect of the vibrational modes of the CF_3 radical we performed two local one-dimensional calculations [18–20] with fixed CF_3 radical. In the first calculation we used the Morse potentials

$$U_M(R) = B\exp[-2\beta(R-R_0)] - C\exp[-\beta(R-R_0)] + D \quad (22)$$

for the neutral and anionic curves as functions of the C-Cl distance. In both cases R_0=3.307 a_0 was taken and it corresponds to the position of the neutral potential surface minimum. These potentials were used previously by Wilde *et al.* [14] in the nonlocal semiempirical R-matrix calculation and corresponding parameters are given in Table II.

The parameters of the neutral potential were chosen to reproduce the experimental value of the vibrational frequency [29] and the anionic potential curve was obtained by fitting to the *ab initio* calculations [14]. Another one-dimensional calculation was performed using the potential curves extracted from our two-dimensional surfaces. We took the potential curves along R in the neutral and anionic surfaces with fixed r=0.877 a_0 corresponding to the value at the minimum of the neutral potential surface. These curves are compared with the Morse potentials in Fig. 3.

This graph shows that the different behavior in the vicinity of the crossing points of the neutral potential curve with the corresponding anionic potential leads to slightly different position of these crossing points. While in the case of the Morse potentials R_C=3.87 a_0, the potential curves extracted from the two-dimensional surface give the value R_C=3.80 a_0. We do not expect that the different behavior at larger C-Cl internuclear separation will have considerable influence on the DEA cross sections.

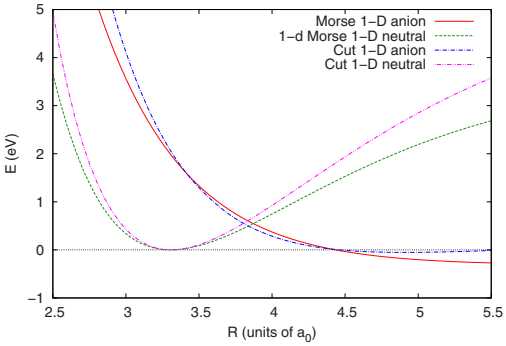

FIG. 3. (Color online) Potentials used in the one-dimensional calculations. The Morse potentials taken from [14] are compared with curves extracted from the two-dimensional surfaces.

All our calculations discussed in the present work employed the width function obtained from the semiempirical R-matrix theory as described in [14]. In this study, the surface amplitude of the semiempirical one-pole R matrix was fitted to the experimental vibrational excitation cross section of Mann and Linder [7]. As a result, the energy-dependent fixed-nuclei resonance width can be calculated using the general relation between the surface amplitude and the resonance width [32]. In the one-dimensional local calculations the local (adiabatic) width is represented as $\Gamma(E_r(R),R)$, where $E_r(R)=U(R)-V(R)$ is the resonance energy for a given C-Cl internuclear separation R. Its extension to the two-dimensional case requires an additional information on the dependence of the width on the second coordinate r. As a first step, we present here the two-dimensional width $\Gamma(E_r(R,r),R,r)$ as a function of $E_r(R,r)$ only. This function is plotted in Fig. 4.

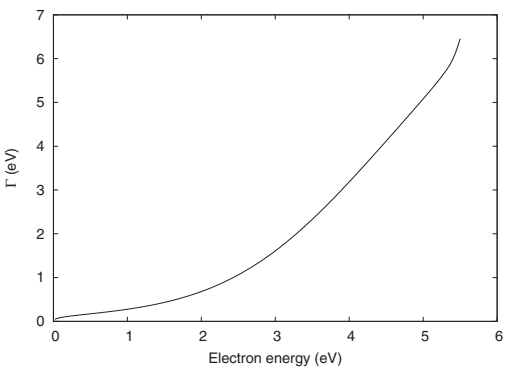

FIG. 4. The width function Γ used in our calculations taken from the nonlocal semiempirical R-matrix calculation [14].

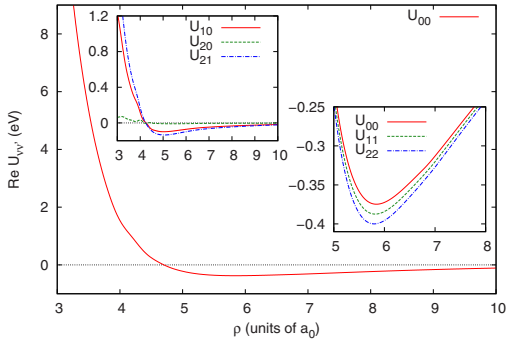

FIG. 5. (Color online) The lowest diagonal and off-diagonal elements of the real part of the potential matrix $U_{\nu\nu'}(\rho)$.

Near the threshold $\Gamma(E_r)$ exhibits the s-wave behavior slightly modified by a small permanent dipole moment (0.5 D). For larger E_r the behavior is more consistent with the $E^{3/2}$ dependence typical for σ^* resonances [21].

Using the potential surfaces and widths discussed above we calculated potential matrix (10). Few lowest elements (as functions of ρ) are plotted in Figs. 5 and 6.

The lowest diagonal elements are very similar to each other and the most pronounced differences between them appear in the region around their minima. However, due to the oscillatory character of the vibrational wave functions $\phi_s(r)$, $\phi_{s'}(r)$, the off-diagonal elements become smaller with increasing difference between the indices s and s'.

The system of differential equations (9) was integrated as discussed in Sec. II B using Milne's predictor-corrector method [33]. We employed this technique since it does not require the calculation of the first derivatives of the solution. To use this method it is necessary to have the solution corresponding to first four steps in the integration region. To this end we calculated the semiclassical wave functions [34] corresponding to the real part of potential matrix (10) deep enough in the classically forbidden region. This solution evaluated at four lowest steps of the outward integration was

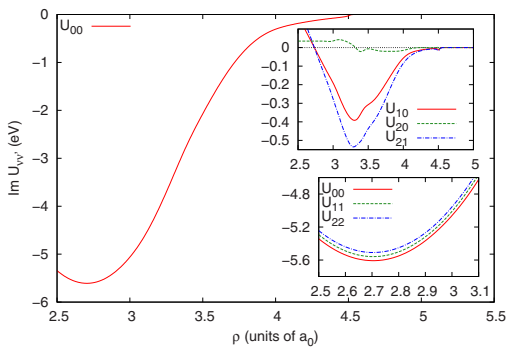

FIG. 6. (Color online) The lowest diagonal and off-diagonal elements of the imaginary part of the potential matrix $U_{\nu\nu'}(\rho)$.

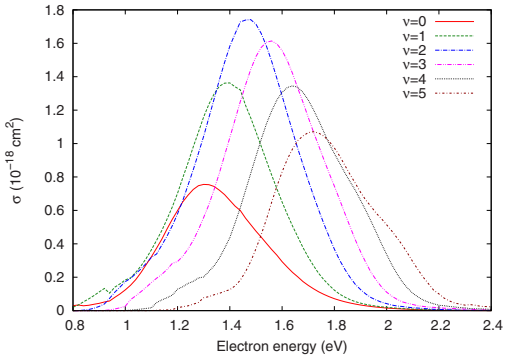

FIG. 7. (Color online) DEA cross sections obtained from the two-dimensional calculation for different final vibrational states of the fragment CF_3. The curves with peaks at higher energies correspond to higher vibrational states of the CF_3 fragment.

used to integrate the full system of equations (9). The small values of the semiclassical wave functions in the classically forbidden region enabled us to neglect the imaginary part of potential matrix (10). This method showed to be stable with respect to change of the starting point of the outward integration as far as it was far enough from the corresponding classical turning point. The inward integration was started in the region where potential matrix (10) can be neglected and where solutions satisfying conditions (16a) and (16b) can be used to start the predictor-corrector integration.

Since we start the outward integration in the classically forbidden region, the solutions of the homogeneous system of equations corresponding to Eq. (9) raise rather rapidly with increasing ρ in this region, especially in the case of energetically closed channels. In this case the exponentially increasing component of the solution becomes dominant and the linear dependence with the exponentially decreasing component raises the issues with the matching procedure described above. In order to keep the calculations numerically tractable, we did not include more than one closed channel into our calculations for every particular energy of the interest. However, the large masses of the nuclei suggest that the inclusion of the closed channels will not influence the results significantly.

IV. RESULTS

A. Local complex potential calculations

We performed the multimode calculation of the cross sections for the DEA to CF_3Cl in the ground vibrational state for initial electron energies from 0.8 to 3 eV. Using the basis set of 13 lowest vibrational wave functions of CF_3 to solve Eq. (9) we obtained converged results for final states of the fragment with vibrational quantum numbers $\nu \leq 6$ as well as converged total cross section. Due to the restriction to one closed channel only discussed above, the cross sections at energies with less than 12 open channels ($E < 1.48$ eV) were calculated using the smaller basis sets. The distribution of

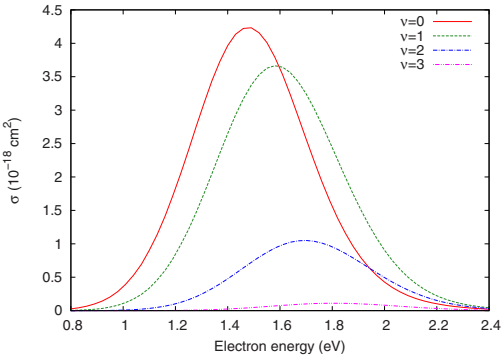

FIG. 8. (Color online) DEA cross sections obtained from the two-dimensional model for different final vibrational states calculated using the diagonal elements of potential matrix (10) only.

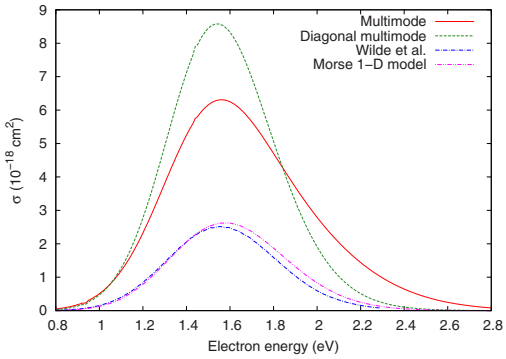

FIG. 9. (Color online) Comparison of the total DEA cross section corresponding to the multimode calculation (multimode) with calculation neglecting the off-diagonal elements of potential matrix (10) (diagonal multimode), with one-dimensional model using the Morse potentials [14] (Morse 1D model) and with previously published calculations [14].

final vibrational states of the CF_3 fragment is plotted in Fig. 7.

This graph shows that the cross section with the highest peak corresponds to the final vibrational state of the fragment with $\nu=2$. For every energy in the range of our interest the cross section corresponding to $\nu=0$ is below the cross section for $\nu=1$. This suggests that the DEA to CF_3Cl is an efficient way of vibrational excitation of CF_3. These results can be understood by analyzing two mechanisms taking place in the DEA: the vertical Franck-Condon transition and final-state interaction. The vertical transition leaves the CF_3 radical in a particular vibrational state. Then the CF_3 umbrella motion is influenced by the Cl^- ion in the temporal anionic complex, and as a consequence of this final-state interaction, the vibrational state of the fragment can be changed. In order to analyze the relative importance of these two mechanisms in production of the excited fragments, we performed another calculation where we neglected all the off-diagonal elements in potential matrix (10). Therefore, the coupling between different vibrational states of the radical due to the interaction with the Cl^- ion in Eq. (9) was not taken into account. Results of this calculation are plotted in Fig. 8.

As can be seen in this graph, the dominant cross sections correspond to the vibrational ground state ($\nu=0$) and first excited state of the fragment ($\nu=1$). All the peaks corresponding to higher excited states are successively decreasing with raising ν. Comparison of Fig. 7 with Fig. 8 shows that dominance of the cross section corresponding to $\nu=2$ around its peak is mainly due to interaction of the umbrella motion with the Cl^- ion in the anionic complex. As can be seen in Fig. 9, the reduction in the excited fragments due to the neglect of the coupling leads to a narrower peak in the total cross section when compared with calculation including the off-diagonal elements of potential matrix (10). This figure shows that our two-dimensional calculations give rather high total DEA cross sections when compared with previous studies [14].

In order to understand these results, we performed two one-dimensional LCP calculations using the Morse potentials described above and using the potential curves taken from the two-dimensional potential surfaces as discussed in Sec. III. Corresponding cross sections are plotted in Fig. 10.

It shows that the model using the potentials extracted from the two-dimensional surfaces gives cross section larger approximately by a factor of 2 than the cross section calculated using the Morse potentials. The peaks, however, appear at very close energy of about 1.65 or 1.7 eV. As can be seen in Fig. 10, our one-dimensional calculation using the Morse potentials is in very good agreement with previously published results of the nonlocal semiempirical *R*-matrix calculations [14]. This agreement justifies the use of the local theory. The same figure shows the comparison with previous nonlocal calculation due to Beyer *et al.* [15]. The fixed nuclei quantities used to construct the nonlocal model in Ref. [15]

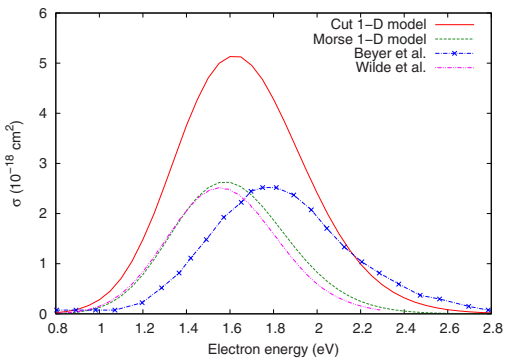

FIG. 10. (Color online) Comparison of the DEA cross section corresponding to the one-dimensional model using the potential extracted from the two-dimensional surface (cut 1D model) with model using the Morse potentials [16] (Morse 1D model) and with previously published one-dimensional nonlocal calculations by Wilde *et al.* [14] and Beyer *et al.* [15].

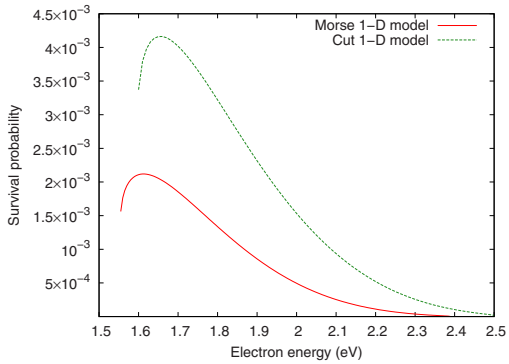

FIG. 11. (Color online) Survival probability calculated for the one-dimensional model using the Morse potential (Morse 1D model) is compared with the one-dimensional model using the potential extracted from the two-dimensional surface (cut 1D model).

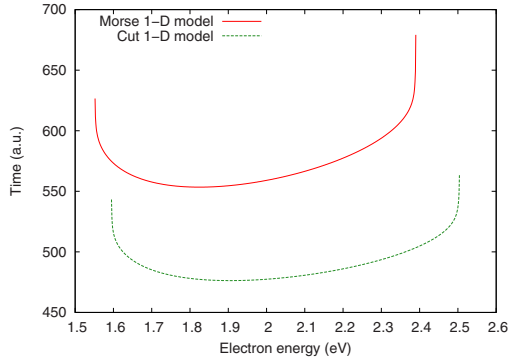

FIG. 12. (Color online) Stabilization time calculated for the one-dimensional model using the Morse potential (Morse 1D model) is compared with the one-dimensional model using the potential extracted from the two-dimensional surface (cut 1D model).

were obtained from the *ab initio* R-matrix calculations [35]. It can be seen that these results are in good correspondence to our calculations using the Morse potentials. However, the peak in our results appears at energy which is 0.15 eV below the peak position in Ref. [15] and its value is 0.004 Å^2 lower. This difference also can be attributed to different treatments of the resonant anionic state.

B. Classical calculations

To emphasize how the differences in potentials used in our one-dimensional calculations change the cross sections, we calculated the survival probability $\mathcal{P}$ of the negative ionic complex [36] for both models using the formula

$$\mathcal{P}(E) = \exp\left[-\sqrt{\frac{\mu_\rho}{2}}\int_{R_F(E)}^{R_C}\frac{\Gamma(R)dR}{\sqrt{E-U(R)}}\right], \tag{23}$$

where R_C is the crossing point of the anionic potential curve with the neutral potential. $R_F(E)$ is the Franck-Condon point given by the condition [37]

$$U(R_F(E)) - V(R_F(E)) = E - E_{\text{vib}}, \tag{24}$$

where E_{vib} is the corresponding vibrational energy of the neutral molecule. Calculated survival probabilities are plotted in Fig. 11.

This graph shows that the curve corresponding to the model using Morse potentials is smaller by a factor of 2 than the curve using the potentials extracted from the two-dimensional surfaces. This result corresponds to the DEA cross sections plotted in Fig. 10. Since we use the same resonance width $\Gamma(R)$ in both models, the difference arises from the different time needed to pass from $R_F(E)$ to R_C on the anionic curve for given electron energy. This time, given by the formula

$$T(E) = \sqrt{\frac{\mu_\rho}{2}}\int_{R_F(E)}^{R_C}\frac{dR}{\sqrt{E-U(R)}}, \tag{25}$$

is plotted in Fig. 12 for both one-dimensional models.

It shows that this time for Morse model is higher than for the model using the potentials extracted from the two-dimensional surface for every energy. These results suggest that the small differences in the potentials used in our models lead to rather large changes in the corresponding DEA cross sections. The more extensive discussion of the character of the stabilization time $T(E)$ and its relation with the maximum of the survival probability is presented in the Appendix.

It is an interesting feature of the results obtained from our two-dimensional LCP calculation that it exhibits a substantial increase in the total cross section when compared with the one-dimensional case. This is partly because of more favorable potential surfaces intersection in the multimode calculation. As has been shown, the one-dimensional potential curve extracted from the two-dimensional surface produces a higher survival probability. In the case of the two-dimensional potential surface, the negative ion motion can be even more favorable (in terms of the survival probability). To understand this better, we have performed classical simulations of the DEA process along the lines developed in Ref. [38] (see also Ref. [39]).

The classical DEA cross section can be written as

$$\sigma = \frac{2\pi^2}{k_i^2}\int d\mathbf{P}d\mathbf{Q}\Gamma(\mathbf{Q})W[\mathbf{q}(\mathbf{Q},\mathbf{P}),\mathbf{p}(\mathbf{Q},\mathbf{P})] \times \delta[H(\mathbf{Q},\mathbf{P}) - E]\mathcal{P}(\mathbf{Q},\mathbf{P}), \tag{26}$$

where $\mathbf{Q},\mathbf{P}$ are the sets of initial reaction coordinates and conjugated momenta, $\Gamma(\mathbf{Q})$ is the adiabatic width function, $W(\mathbf{q},\mathbf{p})$ is the Wigner distribution function expressed in terms of the set of normal coordinates $\mathbf{q}$ and conjugated momenta $\mathbf{p}$, $H(\mathbf{Q},\mathbf{P})$ is the classical Hamiltonian of the system, and $\mathcal{P}(\mathbf{Q},\mathbf{P})$ is the survival factor given by $\mathcal{P}=\exp[-\int\Gamma(t)dt]$ along the classical trajectory corresponding to the initial coordinates $\mathbf{Q}$ and momentum $\mathbf{P}$.

For interpretation of our two-dimensional LCP results we analyzed several classical trajectories which give the most

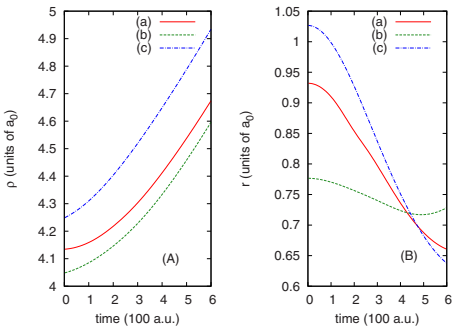

FIG. 13. (Color online) (a) The reaction coordinate ρ and (b) the reaction coordinate r as functions of time obtained from the classical two-dimensional calculation corresponding to the initial conditions listed in Table III.

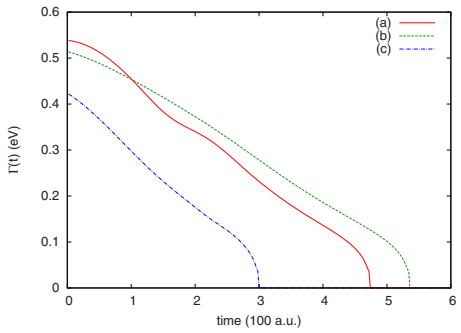

FIG. 14. (Color online) Resonance width as a function of time for the trajectories presented in Fig. 13 calculated using the initial conditions listed in Table III.

significant contribution to integral (26). They correspond to the maximum of the function

$$F(\mathbf{Q},\mathbf{P}) = W[\mathbf{q}(\mathbf{Q},\mathbf{P}),\mathbf{p}(\mathbf{Q},\mathbf{P})]\mathcal{P}(\mathbf{Q},\mathbf{P}) \tag{27}$$

with the constraint imposed by the conservation of energy

$$H(\mathbf{Q},\mathbf{P}) = E. \tag{28}$$

In our case of 2 degrees of freedom, we have three independent parameters corresponding to the initial conditions. We have chosen ρ, r, p_r, with p_ρ defined by Eq. (28).

In Figs. 13 and 14 we present the time dependence of ρ, r, and Γ for three classical trajectories with relatively high values of the function $F(\mathbf{Q},\mathbf{P})$. The incident electron energy is 1.7 eV and the corresponding initial positions and momenta are presented in Table III. Note that the case (a) corresponds to the maximum value of the function F, whereas case (c) to the maximum value of the survival probability. However, in case (c) the value of the Wigner distribution function is very low.

From the analysis of Figs. 13 and 14 we see that the optimal classical trajectory does not correspond to a constant value of r, therefore by going from one-dimensional to two-dimensional case we have more possibilities to increase the survival factor by expanding the class of possible trajectories. Typically optimal trajectories lead to substantially higher survival probabilities than we obtain in the one-dimensional case. Note, however, that, although this conclusion is qualitatively general, the quantitative results depend on the width function $\Gamma(\mathbf{Q})$, and in the present case the width is rather arbitrarily (although reasonably) extended from one-dimensional case to two-dimensional case.

V. CONCLUSIONS

We performed a two-dimensional LCP calculation of the DEA to CF_3Cl in the ground vibrational state at energies from 0.8 to 3 eV. The corresponding total cross section exhibits a substantial increase when compared with our one-dimensional models and previously published studies. Our classical two-dimensional calculation showed that this is due to the more optimal, with respect to the survival probability, paths performed by the final products in the two-dimensional case compared to those in the one-dimensional case. The classical trajectories with largest contribution to the DEA cross section do not correspond either to a fixed value of the coordinate r or optimal (in the sense of the minimal energy) path in the (ρ,r) plane. This suggests that the additional degree of freedom enables the increase in the DEA cross section. With the increasing number of vibrational degrees of freedom quantum-mechanical calculations become computationally very demanding, therefore a further development of classical and semiclassical methods [38–41] is necessary.

The results obtained for the distribution of the final vibrational states of the CF_3 radical show that the cross section with the highest peak corresponds to the vibrational state of the CF_3 fragment with $\nu=2$. We showed that this excitation is mainly due to the final-state interaction, leading to the energy exchange between the umbrella motion and the C-Cl

TABLE III. Parameters of classical trajectories presented in Figs. 13 and 14, together with corresponding value of the function F and the survival factor S. Initial coordinates and momenta are given in a.u., and function F in arbitrary units.

	ρ	r	P_ρ	P_r	F	S
(a)	4.134	0.932	2.611	0.103	1.000	0.0050
(b)	4.048	0.777	10.275	−0.100	0.0605	0.0026
(c)	4.248	1.027	18.777	−0.100	0.00095	0.0727

motion in the temporal anionic complex. Therefore, our results support the findings indicating the importance of the CF_3 vibrational energy redistribution during the DEA at higher energies [9–11].

Our new cross sections for attachment to the ground state of CF_3Cl are about a factor of 3 higher than those calculated within the framework of one-dimensional model. This also leads to worse agreement with experiment at room temperature [16,21,42,43] when only ground vibrational state of CF_3Cl is mostly populated. However, our width has been extrapolated from an empirical width obtained from one-dimensional calculations. For a proper comparison with experiment the two-dimensional adiabatic width should be calculated *ab initio*, or readjusted with the account of the second vibrational coordinate. As a next step, we plan calculations of vibrational excitation cross sections which would allow us to obtain a semiempirical two-dimensional width by its adjustment to experimental data [7] on vibrational excitation.

The next step will be the extension of our calculations of DEA to vibrationally excited states. This will allow us to study the temperature dependence of DEA cross sections and hopefully will explain the low-energy peak at 800 K [16] which cannot be explained by existing one-dimensional calculations [14,15].

ACKNOWLEDGMENTS

This work was partially supported by the National Science Foundation under Grant No. PHY-0652866, by Grant No. GAUK 116-10/257718 of the Charles University Prague and by the Center of Theoretical Astrophysics Grant No. LC06014 of the Ministry of Education, Youth, and Sports of the Czech Republic.

APPENDIX: DISCUSSION OF THE MAXIMUM OF THE SURVIVAL PROBABILITY

Here we will discuss the origin of the unexpected maximum of the survival probabilities shown in Fig. 11. The decreasing part of each curve corresponds to the raising parts of $T(E)$ plotted in Fig. 12. Since the temporal anionic system (treated classically) needs longer time to reach the stabilization point R_C, the survival probability decreases with raising energy. The increasing part at the smaller energies corresponds to the rapidly decreasing parts of the curves $T(E)$ plotted in Fig. 12. As a consequence of Eqs. (24) and (25), the larger energy leads to shift of the Franck-Condon point toward smaller values and prolongs the classical path of the anionic system to the stabilization point R_C (see Fig. 15). However, this time increase competes with increase in the classical velocity. Let us investigate the behavior of $T(E)$ in the limit of energies sufficiently close to $E_2 = U(R_2) - V(R_2) + E_{\mathrm{vib}}$, where R_2 is the right boundary of the Franck-Condon region of the ground vibrational state (see Fig. 15).

E_2 provides the left boundary of energies for which it is possible to define the survival probability. Consider E close to E_2, so that anionic turning point R_t, determined by the

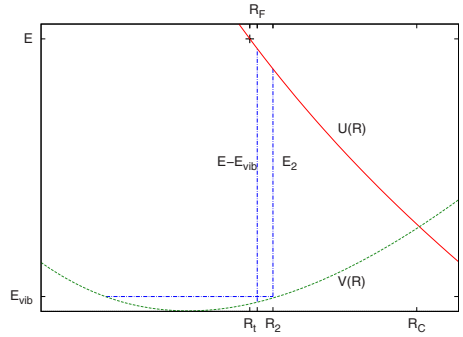

FIG. 15. (Color online) The relative positions of the turning point R_t, Franck-Condon point R_F and the crossing point R_C, and corresponding energies used in the calculations of the survival probabilities $\mathcal{P}(E)$ and times $T(E)$.

condition $U(R_t) = E$, can be approximated by a linear function of E,

$$R_t = R_2 + d(E_2 - E), \tag{A1}$$

where $d > 0$ is the constant dependent on the potentials in the vicinity of R_2. As the energy E decreases toward E_2, the corresponding Franck-Condon point R_F shifts toward R_2 as well as R_t (see Fig. 15) and can be approximated as

$$R_F = R_2 + b(E_2 - E), \tag{A2}$$

where $0 < b < d$, since $R_t < R_F$. These approximations are equivalent to the assumption that the kinetic energy for the motion in the anion potential between $R_t(E)$ and R_2 can be approximated by a linear function. Then we can write

$$E - U(R) \approx c(R - R_t), \tag{A3}$$

where $c > 0$ is another constant dependent on the behavior of the anionic potential between R_t and R_2. Using these assumptions we can express integral (25) for energies sufficiently close to E_2 as follows:

$$T(E) = \sqrt{\frac{\mu_\rho}{2c}} \int_{R_F(E)}^{R_2+\varepsilon} \frac{dR}{\sqrt{R - R_t}} + \sqrt{\frac{\mu_\rho}{2}} \int_{R_2+\varepsilon}^{R_C} \frac{dR}{\sqrt{E - U(R)}}, \tag{A4}$$

where $\varepsilon > 0$ is a constant small enough to make approximation (A3) valid at the interval $\langle R_t, R_2 + \varepsilon \rangle$. Then we can calculate the first integral in Eq. (A4) and obtain

$$T(E) = 2\sqrt{\frac{\mu_\rho}{2c}} \{ \sqrt{d(E - E_2) + \varepsilon} - \sqrt{(d - b)(E - E_2)} \} + \sqrt{\frac{\mu_\rho}{2}} \int_{R_2+\varepsilon}^{R_C} \frac{dR}{\sqrt{E - U(R)}}. \tag{A5}$$

This equation shows that T as a function of E exhibits a square-root singularity of the type const$-p\sqrt{E-E_2}$ where p is a positive constant. Therefore, when E starts to increase from E_2, $T(E)$ is always decreasing and reaches a minimum at higher E. Therefore the survival probability increases first and then reaches a maximum as can be seen in Fig. 11. Note that this result is not valid if $R_C=R_2$.

[1] A. Kazansky, J. Phys. B **28**, 3987 (1995).
[2] D. J. Haxton, Z. Zhang, H.-D. Meyer, T. N. Rescigno, and C. W. McCurdy, Phys. Rev. A **69**, 062714 (2004).
[3] S. T. Chourou and A. E. Orel, Phys. Rev. A **77**, 042709 (2008).
[4] M. Shapiro and R. Bersohn, J. Chem. Phys. **73**, 3810 (1980).
[5] S. Roszak, W. S. Koski, J. J. Kaufman, and K. Balasubramanian, J. Chem. Phys. **106**, 7709 (1997).
[6] A. Gedanken and M. D. Rowe, Chem. Phys. Lett. **34**, 39 (1975).
[7] A. Mann and F. Linder, J. Phys. B **25**, 1621 (1992).
[8] C. W. Walter, B. G. Lindsay, K. A. Smith, and F. B. Dunning, Chem. Phys. Lett. **154**, 409 (1989).
[9] A. Kalamarides, C. W. Walter, B. G. Lindsay, K. A. Smith, and F. B. Dunning, J. Chem. Phys. **91**, 4411 (1989).
[10] A. Kalamarides, R. W. Marawar, X. Ling, C. W. Walter, B. G. Lindsay, K. A. Smith, and F. B. Dunning, J. Chem. Phys. **92**, 1672 (1990).
[11] R. Parthasarathy, C. D. Finch, J. Wolfgang, P. Nordlander, and F. B. Dunning, J. Chem. Phys. **109**, 8829 (1998).
[12] D. M. Pearl, P. D. Burrow, I. I. Fabrikant, and G. A. Gallup, J. Chem. Phys. **102**, 2737 (1995).
[13] R. S. Wilde, G. A. Gallup, and I. I. Fabrikant, J. Phys. B **33**, 5479 (2000).
[14] R. S. Wilde, G. A. Gallup, and I. I. Fabrikant, J. Phys. B **32**, 663 (1999).
[15] T. Beyer, B. M. Nestmann, and S. D. Peyerimhoff, J. Phys. B **34**, 3703 (2001).
[16] I. Hahndorf, E. Illenberger, L. Lehr, and J. Manz, Chem. Phys. Lett. **231**, 460 (1994).
[17] S. Marienfeld, T. Sunagawa, I. I. Fabrikant, M. Braun, M.-W. Ruf, and H. Hotop, J. Chem. Phys. **124**, 154316 (2006).
[18] J. N. Bardsley, A. Herzenberg, and F. Mandl, Proc. Phys. Soc. **89**, 305 (1966).
[19] J. N. Bardsley, A. Herzenberg, and F. Mandl, Proc. Phys. Soc. **89**, 321 (1966).
[20] W. Domcke, Phys. Rep. **208**, 97 (1991).
[21] K. Aflatooni and P. D. Burrow, Int. J. Mass Spectrom. **205**, 149 (2001).
[22] W. H. Shaffer, J. Chem. Phys. **10**, 1 (1942).
[23] J. N. Bardsley, in *Electron-Molecule and Photon-Molecule Collisions*, edited by T. Rescigno, V. McKoy, and B. Schneider (Plenum, New York, 1979).
[24] C. Møller and M. S. Plesset, Phys. Rev. **46**, 618 (1934).
[25] M. J. Frisch, G. W. Trucks, H. B. Schlegel, G. E. Scuseria, M. A. Robb, J. R. Cheeseman, J. A. Montgomery, Jr., T. Vreven, K. N. Kudin, J. C. Burant *et al.*, *Gaussian 03, Revision C.02* (Gaussian, Inc., Wallingford, CT, 2004).
[26] J. Thom H. Dunning, J. Chem. Phys. **90**, 1007 (1989).
[27] D. E. Woon and J. Thom H. Dunning, J. Chem. Phys. **98**, 1358 (1993).
[28] A. K. Wilson, D. E. Woon, K. A. Peterson, and J. Thom H. Dunning, J. Chem. Phys. **110**, 7667 (1999).
[29] K. Scanlon, I. Suzuki, and J. Overend, J. Chem. Phys. **74**, 3735 (1981).
[30] M. Suto and N. Washida, J. Chem. Phys. **78**, 1012 (1983).
[31] R. Trainham, G. D. Fletcher, and D. J. Larson, J. Phys. B: At. Mol. Phys. **20**, L777 (1987).
[32] A. M. Lane and R. G. Thomas, Rev. Mod. Phys. **30**, 257 (1958).
[33] A. Bennett, W. E. Milne, and H. Bateman, *Numerical Integration of Differential Equations* (Dover Publications, New York, 1956).
[34] B. C. Eu, *Semiclassical Theories of Molecular Scattering* (Springer-Verlag, Berlin, 1984).
[35] B. M. Nestmann, J. Phys. B **31**, 3929 (1998).
[36] T. F. O'Malley, Phys. Rev. **150**, 14 (1966).
[37] S. A. Kalin and A. K. Kazansky, J. Phys. B **23**, 4377 (1990).
[38] S. Goursaud, M. Sizun, and F. Fiquet-Fayard, J. Chem. Phys. **65**, 5453 (1976).
[39] R. Schinke, *Photodissociation Dynamics of Small Polyatomic Molecules* (Cambridge University Press, Cambridge, 1993).
[40] L. Lehr and W. H. Miller, Chem. Phys. Lett. **250**, 515 (1996).
[41] L. Lehr, J. Manz, and W. H. Miller, Chem. Phys. **214**, 301 (1997).
[42] S. M. Spyrou and L. G. Christophorou, J. Chem. Phys. **82**, 2620 (1985).
[43] T. Underwood-Lemons, T. J. Gergel, and J. H. Moore, J. Chem. Phys. **102**, 119 (1995).

3.2 Vibrational excitation

The notation introduced in the article included above is used throughout this section. In addition, the equation numbers not including the chapter number, refer to the corresponding equations in the same paper.

The topic of DEA is closely related to the topic of VE. Having the nuclear scattering wave function $\chi_E(\rho, r)$ (solution of equation (6) in the paper included above) it is straightforward to calculate cross sections of the DEA (using the asymptotic form of the solution, see equation (13)) as well as cross section of the VE. The T-matrix element for $\nu_i \to \nu_f$ reads [4]

$$T(k_f, \nu_f; k_i, \nu_i) = \int \mathrm{d}r\mathrm{d}\rho \zeta_f(\rho, r) V_{dk_f}(\rho, r) \chi_E(\rho, r). \tag{3.2}$$

Here $\zeta_f(\rho, r)$ is the final-state vibrational wave function of the neutral molecule, ν_f and ν_i represent the sets of vibrational quantum numbers corresponding to the final and initial state, $V_{dk_f}(\rho, r)$ is the capture amplitude as described in the paper above, the subscript f corresponds to the momentum k_f of the free electron leaving the excited molecule and enters the capture amplitude via the correction factor (14), k_i is the initial momentum of the free projectile before entering the collision region. The information about the initial vibrational state of the molecule is included in the solution $\chi_E(\rho, r)$ of equation (6). Corresponding VE cross section can be calculated using the formula [4]

$$\sigma_{\nu_f \nu_i}(E) = \frac{4\pi^3}{k_i^2} \left| T(\mathbf{k}_f, \nu_f; \mathbf{k}_i, \nu_i) \right|^2 . \tag{3.3}$$

The prefactors in this formula depend on the normalization of the scattering states. We assume energy-normalized scattering states for electrons and nuclei. Therefore, knowledge of the nuclear scattering wave function allows us to calculate the corresponding T-matrix as well as the DEA cross sections. However, to calculate the integral (3.2) we need the values of $\chi_E(\rho, r)$ in the region where $\zeta_f(\rho, r)$ is non-zero, while for calculation of the DEA cross section the asymptotic form is sufficient.

It was found in the paper above that the two-dimensional model gives higher DEA cross sections than the one-dimensional models which reproduce the experimental results due to Mann and Linder [36]. The one-dimensional models employed the resonance width function fitted to these experiments. In our two-dimensional calculations this function was extended to two dimensions. However, this model-like extension can be

a reason of the increase in the DEA cross sections. Therefore, we decided to calculate the cross sections for the VE of CF_3Cl using the two-dimensional model and acoording to the results obtained to adjust the two-dimensional extension of the resonance width function.

Using the expansion (8) of $\chi_E(\rho, r)$ in the basis of the vibrational eigenfunctions of the CF_3 fragment, we can write the $T - matrix$ (3.2) in the following form:

$$T(\mathbf{k}_f, \nu_f; \mathbf{k}_i, \nu_i) = \int \mathrm{d}r\mathrm{d}\rho \sum_\nu \zeta_f(\rho, r) V_{dk_f}(\rho, r)\psi_\nu(\rho)\phi_\nu(r) = \int \mathrm{d}\rho \sum_\nu \kappa_{f\nu}(\rho)\psi_\nu(\rho), \tag{3.4}$$

where

$$\kappa_{f\nu}(\rho) = \int \mathrm{d}r \zeta_f(\rho, r) V_{dk_f}(\rho, r)\phi_\nu(r). \tag{3.5}$$

As it is explained in the article above, the inhomogeneous system of ordinary differential equations (9) with corresponding boundary conditions (12) was solved using the predictor-corrector integration method for homogeneous systems and subsequent determination of factors relating the solutions of homogeneous and inhomogeneous systems in the asymptotic region (see equations (13), (17) and (18)). Although this method would be applicable for determination of functions $\psi_\nu(\rho)$ in the regions important for VE, we decided to use other method and we solved system (9) using the exterior complex scaling (ECS) method [37]. The reason was that ECS is more tractable for this class of problems and does not require some approximations necessary to use the predictor-corrector method used in the paper above (quasiclassical approximation to start the integration, restricted number of closed channels). In addition, use of the ECS technique enabled us to test whether all the approximations used in the article presented here are suitable for this problem.

Our tests with calculations of the DEA cross sections using the ECS method showed that it gives the same results as the technique described in the paper above. Therefore, this suggests that both methods are suitable for this problem and interval of scattering energies. All the results were well converged and the differences in the cross sections calculated were smaller than 1%. After these tests we performed a preliminary calculations of the VE and compared the results with previously published experimental works and calculations. The results corresponding to particular excitations from the ground vibrational state are plotted in Figure 3.1 and in Figure 3.2. The first figure shows

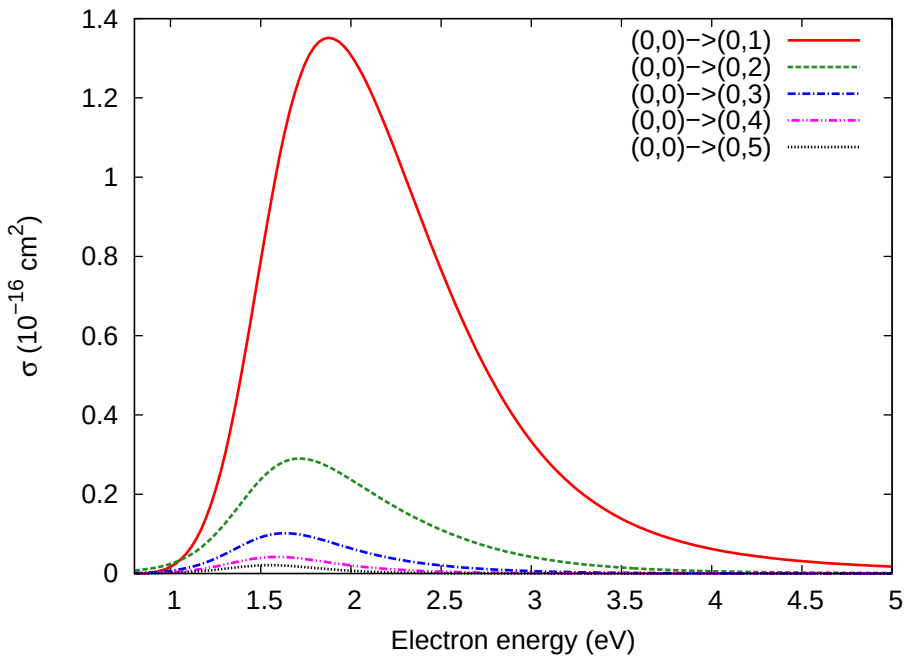

Figure 3.1: VE cross sections obtained from the two-dimensional LCP calculation. The notation of the vibrational transitions is $(\nu_3, \nu_2) \rightarrow (\nu_3', \nu_2')$. All the transitions plotted in this figure correspond to pure excitation of the umbrella mode (the C-Cl stretching mode remains in the ground final state).

the cross sections of the VE from the ground state of CF_3Cl to the ground vibrational state of the C-Cl stretching mode and different excited states of the CF_3 umbrella mode. As can be seen, the cross sections decrease rapidly with increasing vibrational quantum number of the final-state umbrella mode and shows clear peaks in the energy interval 1.5–2 eV. Figure 3.2 shows the VE cross sections corresponding to the lowest excited final vibrational state of the C-Cl stretching mode and different final vibrational states of the umbrella mode. Also these cross sections are subsequently decreasing with raising vibrational quantum number of the umrella mode and show well pronounced peaks in the energy interval 1.5–2 eV.

In order to allow for comparison of our results with previously published non-local one-dimensional calculationof the VE [32], it is necessray to establish the correspondence of the vibrational states of the target in our model with the vibrational states considered in the paper [32]. As the one-dimensional treatment [32] does not distinguish different umbrella states of the CF_3 radical, it is reasonable to assume that in the one-dimensional model all the final umbrella states contribute to the VE cross section equally. Therefore, the results for particular vibrational transition $(\nu_3 = 0) \rightarrow (\nu_3' = 1)$ presented in [32]

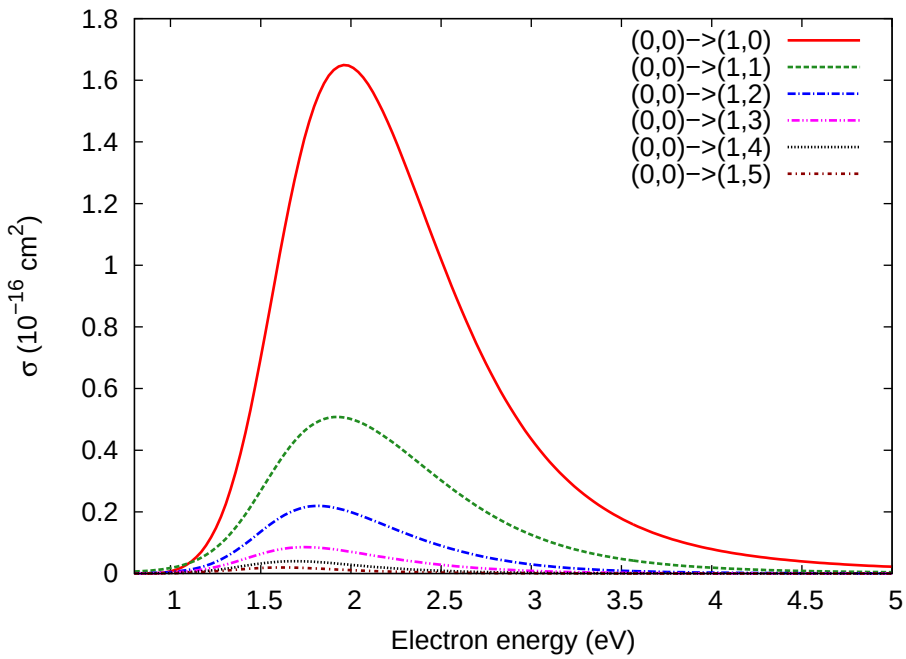

Figure 3.2: VE cross sections obtained from the two-dimensional LCP calculation. The notation of the vibrational transitions is $(\nu_3, \nu_2) \rightarrow (\nu_3', \nu_2')$. All the transitions plotted in this figure correspond to different excitations of the umbrella mode and excitation of the C-Cl stretching mode to its lowest excited state.

corresponds to sum of the VE cross sections corresponding to transitions $(\nu_3 = 0, \nu_2 = 0) \rightarrow (\nu_3' = 1, \nu_2' = n)$. Here n denotes the ground and all the excited final states of the umbrella mode. As can be seen in Figure 3.2, this sum converges very fast and final states with $n > 5$ have negligible contribution to the sum. Comparison of these results is plotted in Figure 3.3. This comparison shows that our sum of the cross sections gives very good agreement with corresponding one-dimensional results taken from [32] for energies below 1.7 eV. There is a discrepancy at higher energies, although both peaks are at approximately the same position. Mann and Linder [36] are able to distinguish different vibrational modes in their experiments. Their results corresponding to pure excitation of the C-Cl stretching mode into its lowest excited state are showed in the same figure. The experimental VE cross sections are in very good agreement with the one-dimensional results of Wilde et al. [32]. This can be explained by the construction of the non-local model which was adjusted to reproduce these data. On the other hand, our calculated VE cross section corresponding to the vibrational transition $(0, 0) \rightarrow (1, 0)$ shows a substantial decrease for all energies when compared with the experimental results

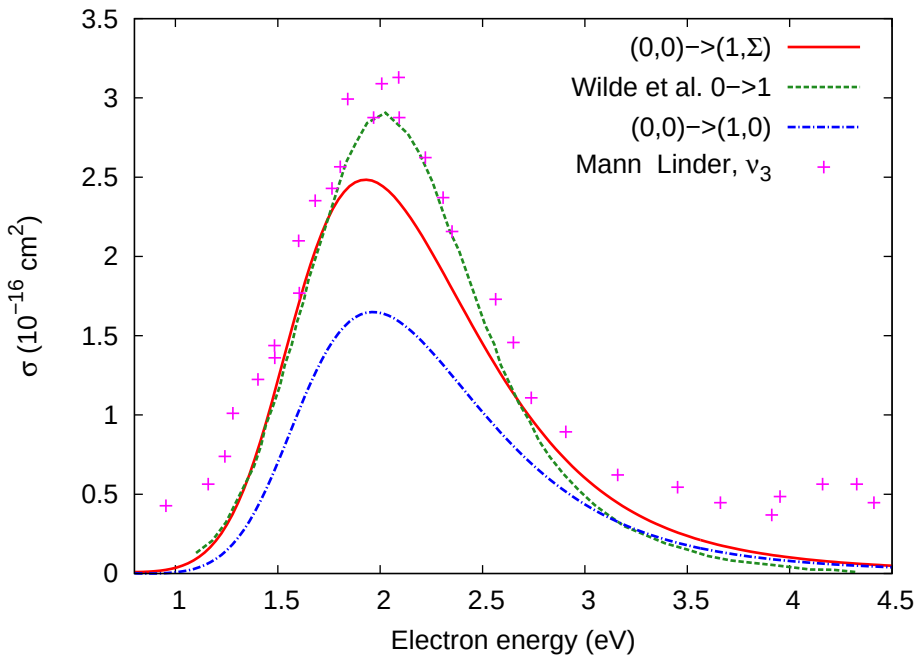

Figure 3.3: Sum of the calculated VE cross sections corresponding to the excitation from the ground state to the lowest excited state of the C-Cl stretching mode (Σ stands for summation over different final umbrella states) is compared with non-local one-dimensional results of Wilde et al. [32] and with corresponding experimental results due to Mann and Linder [36]. Calculated VE cross section $(0,0) \rightarrow (1,0)$.

of Mann and Linder [36]. We explain this observation as well as the discrepancy between our cross sections and the one-dimensional curves taken from [32] by the model-like extension of the resonance width function mentioned above and in the paper included in this chapter. Figure 3.4 shows the comparison of our calculated VE cross section $(0,0) \rightarrow (0,1)$ with corresponding experimental results [36]. The discrepancy which occurs in this comparison can also be attributed to the extension of the width function Γ to two dimensions.

The preliminary calculations of the VE cross sections showed above suggest that the research should be concetrated on the width function. Therefore, the prospect of our forthcomming work is to improve the adjustment of this function in two dimensions. It will lead to an improved LCP model and it will allow for better explanation of the temperature dependence of the DEA cross section mentioned above. In order to make this study complete, we aim to perform the R-matrix fixed-nuclei calculations, obtain independent complex potential energy surfaces and using them calculate the DEA and

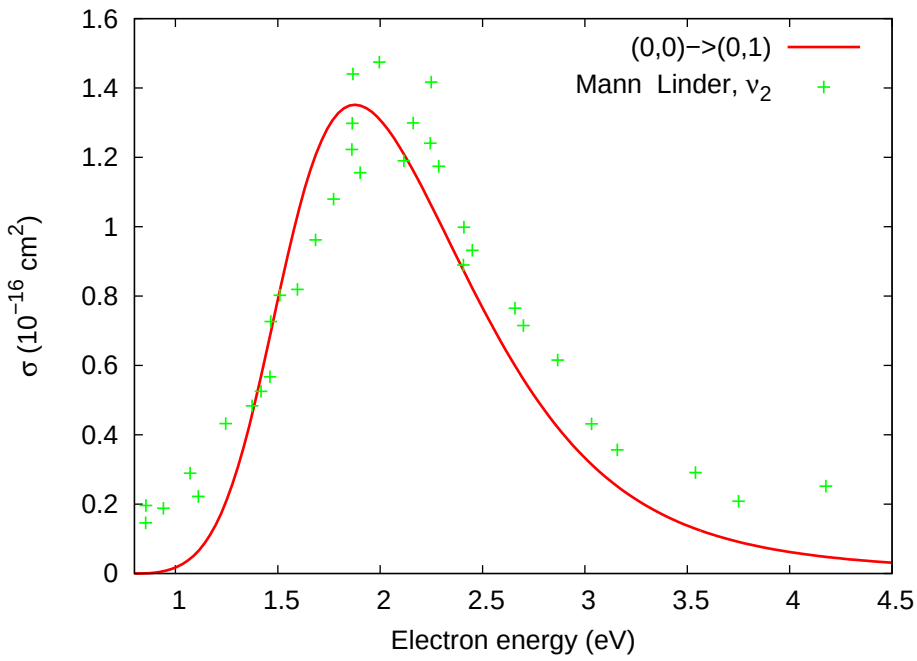

Figure 3.4: Calculated VE cross section $(0,0) \rightarrow (0,1)$ is compared with corresponding results of Mann and Linder [36].

VE cross sections.

Chapter 4

Conclusions

In this work we were dealing with resonant processes in electron scattering off small molecules. We presented four original articles covering the fields of fixed-nuclei scattering calculations (using R-matrix theory) and nuclear dynamics of the DEA and resonant VE (using the LCP approach).

In the first paper presented in this work we are dealing with the role of electron correlation in the fixed-nuclei elastic electron scattering off F_2. It is well-known that F_2 is difficult system with respect to the electron correaltion treatment. Since the internuclear separation at which the anion becomes stable against autodetachment is located very close to the equilibrium geometry of the neutral molecule, the small changes of the position and width of the electronic resonance caused by different electron-correlation treatment lead to rapid changes in the DEA and VE cross sections. The paper included in this work is dealing with R-matrix calculations using the most advanced CI model used for F_2 so far. In addition, it shows the abilities of the Bonn R-matrix codes used to treat the correlation on the SD-MRCI level beyond the widely used SEP approximation. Using this advanced CI model, we calculated all the quantitites (using the FFR approach) necessary for construction of the NRM and calculation of the DEA and VE.

Next two works included here are dealing with R-matrix calculations of electron collisions with lithium dimer. This system represents a challenge for the fixed-nuclei scattering methods since its ground-state and excited-states wave functions have quite large spatial extent. Thus, the unusually large R-matrix sphere was necessary what complicated the representation of the continuum in the inner region. Li_2 has a huge polarizability which complicates the convergence of the CC expansion in the inner region.

In the second article presented here, we emplyed a molecular R-matrix with pseudo-states (MRMPS) method originally developed for treatment of electron-molecule collisions at intermediate energies. However, our application shows that this method is suitable for improved representation of the target leading to better treatment of the polarization effects in the inner region. The results of this work are in very good agreement with the next work included here, where we use larger R-matrix sphere and different representation of the target in the inner region. This suggests that all the features found in the scattering cross sections, are physical and not an artifact of the insufficient representation of the scattering continuum or target. In addition, we confirmed a presence of the low-lying $^2\Sigma_g$ virtual state which was expected to be a resonance in previously published works and which was considered the main channel of DEA to Li_2. In our work we suggested reconsideration of these mechanisms.

The last article included in this work is dealing with the DEA and VE of CF_3Cl using the LCP approximation with emphasis on the effects of two vibrational modes. To our best knowledge, this is the largest molecule treated using the LCP model with more than one vibrational degree of freedom included so far. We found that the DEA to CF_3Cl is an efficient way how to produce vibrationally excited CF_3 fragments and we explained a mechanism of this excitation via final-state interaction during the motion of the system on the anionic surface in the region, where it is not bound. In addition, we performed preliminary calculations of the VE and using the results we aim to improve the construction of the LCP model in order to explain the temperature dependence of the DEA cross sections observed experimentally.

Bibliography

[1] M.A. Huels, J.A. Fedchak, R.L. Champion, L.D. Doverspike, J.P. Gauyacq, and D. Teillet-Billy. Electron detachment in low-energy collisions of halogen anions with atomic hydrogen. *Phys. Rev. A*, 49:255–264, 1994.

[2] A. Chutjian, A. Garscadden, and J. M. Wadehra. Electron attachment to molecules at low electron energies. *Phys. Rep.*, 264:393–470, 1996.

[3] K. Rohr and F. Linder. Vibrational excitation of polar molecules by electron impact. I. Threshold resonance in HF and HCl. *J. Phys. B: At. Mol. Phys.*, 9:2521–2537, 1976.

[4] W. Domcke. Theory of resonance and threshold effects in electron-molecule collisions: The projection-operator approach. *Phys. Rep.*, 208:97–188, 1991.

[5] J.N. Bardsley, A. Herzenberg, and F. Mandl. Vibrational excitation and dissociative attachment in the scattering of electrons by hydrogen molecules. *Proc. Phys. Soc.*, 89:321–340, 1966.

[6] J.N. Bardsley, A. Herzenberg, and F. Mandl. Electron resonances of the H_2^- ion. *Proc. Phys. Soc.*, 89:305–319, 1966.

[7] M. Čížek. *Resonant Processes in Atomic Collisions - Theoretical Considerations and Calculations.* PhD thesis, Charles University Prague, 1999.

[8] P.G. Burke and K.A. Berrington, editors. *Atomic and Molecular Processes: An R-matrix Approach.* IOP Publishing, Bristol, 1993.

[9] E.P. Wigner and L. Eisenbud. Higher angular momenta and long range interaction in resonance reactions. *Phys. Rev.*, 72:29–41, 1947.

[10] B.I. Schneider and T.N. Rescigno. Complex Kohn variational method: Application to low-energy electron-molecule collisions. *Phys. Rev. A*, 37:3749–3754, 1988.

[11] K. Takatsuka and V. McKoy. Extension of the Schwinger variational principle beyond the static-exchange approximation. *Phys. Rev. A*, 24:2473–2480, 1981.

[12] K. Takatsuka and V. McKoy. Theory of electronically inelastic scattering of electrons by molecules. *Phys. Rev. A*, 30:1734–1740, 1984.

[13] P.G. Burke and J. Tennyson. R-matrix theory of electron molecule scattering. *Mol. Phys.*, 103:2537–2548, 2005.

[14] K. Pfingst, B.M. Nestmann, and S.D. Peyerimhoff. An *R*-matrix approach for electron scattering off polyatomic molecules. *J. Phys. B: At. Mol. Opt. Phys.*, 27: 2283–2296, 1994.

[15] J.N. Cooper, E.A.G. Armour, and M. Plummer. The importance of an accurate target wavefunction in variational calculations for (e^+–H_2) scattering. *J. Phys. B: At. Mol. Opt. Phys.*, 41:245201 (8pp), 2008.

[16] L. A. Morgan, C. J. Gillan, J. Tennyson, and X. Chen. R-matrix calculations for polyatomic molecules: electron scattering by N_2O. *J. Phys. B: At. Mol. Opt. Phys.*, 30:4087–4096, 1997.

[17] T. Helgaker, P. Jorgensen, and J. Olsen. *Molecular Electronic-Structure Theory.* Wiley, 2000.

[18] J. Tennyson. A new algorithm for hamiltonian matrix construction in electron - molecule collision calculations. *J. Phys. B: At. Mol. Opt. Phys.*, 29:1817–1828, 1996.

[19] R. Buenker and S. Peyerimhoff. Individualized configuration selection in CI calculations with subsequent energy extrapolation. *Theor. Chim. Act.*, 35:33–58, 1974.

[20] R. Buenker and S. Peyerimhoff. Energy extrapolation in CI calculations. *Theor. Chim. Act.*, 39:217–228, 1975.

[21] R. Buenker, S. Peyerimhoff, and W. Butscher. Applicability of multi-reference double-excitation CI (MRD-CI) method to calculation of electronic wavefunctions and comparison with related techniques. *Mol. Phys.*, 35:771–791, 1978.

[22] M. Hanrath and B. Engels. New algorithms for an individually selecting MR-CI program. *Chem. Phys.*, 225:197–202, 1997.

[23] V. Brems, T. Beyer, B. Nestmann, H.D. Meyer, and L.S. Cederbaum. Ab initio study of the resonant electron attachment to the F_2 molecule. *J. Chem. Phys.*, 117: 10635–10647, 2002.

[24] L.A. Morgan and C.J. Noble. Elastic scattering of electrons by fluorine molecules. *J. Phys. B: At. Mol. Opt. Phys.*, 17:L369–L373, 1984.

[25] B. Nestmann. Characterization of metastable anionic states within the *R*-matrix approach. *J. Phys. B: At. Mol. Opt. Phys.*, 31:3929–3948, 1998.

[26] L. Piela. *Ideas of Quantum Chemistry.* Elsevier, 2007.

[27] T.J. Gil, B.H. Lengsfield, C.W. McCurdy, and T.N. Rescigno. Ab-initio complex Kohn calculations of dissociative excitation of methane - close-coupling convergence studies. *Phys. Rev. A*, 49:2551–2560, 1994.

[28] A. Kazansky. A model study of dissociative attachment of slow electrons to the carbon dioxide molecule. *J. Phys. B: At. Mol. Opt. Phys.*, 28:3987–4004, 1995.

[29] D.J. Haxton, Z. Zhang, H.-D. Meyer, T.N. Rescigno, and C.W. McCurdy. Dynamics of dissociative attachment of electrons to water through the B_{12} metastable state of the anion. *Phys. Rev. A*, 69:062714, 2004.

[30] J. Royal and A.E. Orel. Dissociative attachment to ClCN and BrCN. *J. Chem. Phys.*, 125:214307, 2006.

[31] S.T. Chourou and A.E. Orel. Dissociative electron attachment to acetylene. *Phys. Rev. A*, 77:042709, 2008.

[32] R.S. Wilde, G.A. Gallup, , and I.I. Fabrikant. Semiempirical R-matrix theory of low energy electron-CF_3Cl inelastic scattering. *J. Phys. B: At. Mol. Opt. Phys.*, 32: 663–673, 1999.

[33] T. Beyer, B.M. Nestmann, and S.D. Peyerimhoff. Resonant features of inelastic electron scattering off CF_3Cl in the low-energy region. *J. Phys. B: At. Mol. Opt. Phys.*, 34:3703–3716, 2001.

[34] I. Hahndorf, E. Illenberger, L. Lehr, and J. Manz. Temperature effects of dissociative electron-attachment to CF_3Cl. *Chem. Phys. Lett.*, 231:460–466, 1994.

[35] S. Roszak, W. S. Koski, J. J. Kaufman, and K. Balasubramanian. Structure and energetics of CF_3Cl^-, CF_3Br^-, and CF_3I^- radical anions. *J. Chem. Phys.*, 106: 7709–7713, 1997.

[36] A. Mann and F. Linder. Low-energy electron scattering from halomethanes. III. e-CF_3Cl. *J. Phys. B: At. Mol. Opt. Phys.*, 25:1621–1632, 1992.

[37] C.W. McCurdy, M. Baertschy, and T.N. Rescigno. Solving the three-body coulomb breakup problem using exterior complex scaling. *J. Phys. B: At. Mol. Opt. Phys.*, 37:R137–R187, 2004.